https://technobius.kz/

e-ISSN
2789-7338

Technobius

A peer-reviewed open-access journal

Technobius, LLP *Volume 5, No. 4, 2025*

Technobius

Volume 5, No. 4, 2025

A peer-reviewed open-access journal registered by the Ministry of Culture and Information of the Republic of Kazakhstan, Certificate № KZ26VPY00087928 dated 21.02.2024

ISSN (Online): 2789-7338
Thematic Directions: Construction, Materials Science
Publisher: Technobius, LLP
Address: 2 Turkestan street, office 116, 010000, Astana, Republic of Kazakhstan

Contacts:
Website: https://technobius.kz/
E-mail: technobius.research@gmail.com

CONTENTS

Technobius, 2025, 5(4), 0089, DOI: https://doi.org/10.54355/tbus/5.4.2025.0089

Technobius

https://technobius.kz/

e-ISSN 2789-7338

Article

Fine-grained self-compacting concrete with polyfunctional additive and enhanced performance properties

Zhanar Zhumadilova, Assel Kanarbay, Daniyar Akhmetov*, Assel Aldigaziyeva

Satbayev University, Almaty, Republic of Kazakhstan
*Correspondence: d.a.akhmetov@satbayev.university

Abstract. The results of experimental studies aimed at improving the strength characteristics of cement stone and fine-grained self-compacting concrete through the use of polyfunctional modifying additives based on nano-silicon dioxide (nano-SiO_2) and micro-dispersed mineral components are presented. It was established that the introduction of 0.03% nano-SiO_2 by weight of cement increases the compressive strength of cement stone by up to 32%, which is associated with the intensification of clinker mineral hydration processes, the formation of an additional amount of low-base calcium hydrosilicates, and an increase in the number of crystallization centers in the early stages of hardening. The effectiveness of the combined use of nano-SiO_2 with microsilica and micro-calcite, which are similar in composition to cement but differ in structure and functional activity, has been experimentally confirmed. The use of two-component systems made it possible to increase the flexural strength of cement stone by up to 29% compared to the reference samples. The greatest effect was achieved by adding a polyfunctional three-component additive, including nano-SiO_2, microsilica, and micro-calcite, to the composition of fine-grained self-compacting concrete. The use of this system increased the compressive strength of concrete by 44% (to class B60) and the flexural strength by up to 12.5 MPa (an increase of 53.7% relative to the reference composition). It was additionally established that the complex of additives contributes to the acceleration of self-organization processes in the early stages of hardening by increasing the density of crystallization centers and a more uniform distribution of hydration products in the cement matrix volume.
Keywords: fine-grained self-compacting concrete, strength, calcium hydrosilicates, cement hydration, additives.

1. Introduction

Fine-grained self-compacting concrete (SCC) is a promising area in the field of building materials, focused on creating compositions with improved processability and performance characteristics. Such concretes eliminate the need for mechanical compaction during laying, ensure high fluidity of the mixture, uniformity of structure, and surface quality without additional labor costs. However, in the production of fine-grained SCC, a number of key issues remain unresolved, including insufficient flexural strength, a tendency to delamination, increased water demand, and cement consumption, leading to increased shrinkage and reduced durability of the material. One potential solution for that is the use of fibers of various compositions and structures [1]. Experience with fiber-reinforced concrete [2] shows that the rational areas of application for such concrete are a specific range of monolithic and precast concrete products, as well as the manufacture of impact-resistant and bendable structures using fiber to eliminate the use of additional reinforcement.

Compliance with requirements for achieving high operational quality indicators for concrete and reducing material and energy costs in the production of concrete mixtures and products based on them makes research in the field of obtaining modern types of concrete, such as high-performance concrete according to [3], relevant. The use of such concretes makes it possible to simultaneously reduce the costs of production and operation of load-bearing structures and ensure high reliability of buildings or structures regardless of external environmental conditions. The main quality indicators

of such concrete should be increased strength (over 55 MPa), durability, and mobility (P5-P6) at a water-cement ratio (W/C) not exceeding 0.4 [4].

Problems of structural instability and porosity, characteristic of fine-grained self-compacting concrete systems, are particularly relevant when using fine aggregates and a low water-cement ratio. Sedimentation pores and capillary structure have a significant impact on water permeability, frost resistance, and resistance to external aggressive influences. In addition, the uneven distribution of mixture components and high water mobility in fresh concrete lead to the formation of a surface layer with an increased water-cement ratio, which impairs the mechanical and operational properties of the hardened material [5].

Current research in the field of self-compacting concrete focuses on finding effective solutions aimed at optimizing the structure of cement stone and reducing the volume of free water. One such solution is the use of polyfunctional modifying additives, including active mineral and nanodispersed components, as well as the latest generation of superplasticizers. These additives not only improve the rheological properties of the concrete mix but also contribute to the intensification of hydration processes, the formation of a denser structure, and a reduction in permeability. Particular attention is paid to triple systems combining microsilica, nanosilica, and chemical additives capable of initiating the formation of low-base calcium hydrosilicates and minimizing the content of free calcium hydroxide [6].

The emergence of special cements on the market, such as low water demand (LWD) binders and other types of cements, played an important role in the creation of high-strength concretes, initiating the possibility of obtaining concretes with high strength and other new qualitative operational characteristics [7].

In [8], the term “Reactive Powder Concrete” (RPC) was used for the first time, the main principle of which is to ensure a uniform concrete structure by replacing coarse aggregate in mixtures with fine-grained aggregate, compacting the mixture by optimizing the granulometric composition of the aggregate, using finely dispersed fillers and complexes of modifying additives, as well as using intensive methods of hardening the concrete mixture, which allows obtaining concrete with high performance characteristics (strength of 60-120 MPa, high durability of hardened concrete, frost resistance of at least F 400 and above, water resistance of at least W12). The component composition of such concrete is: Portland cement, microsilica (15-20% of the cement mass), fine-grained sand with a fraction of 0.3 mm (40-50% of the cement mass), and superplasticizer (2-3%) at W/(C+Microsilica) 0.12-0.15. The disadvantage of such concrete is that its strength largely depends on the hardening conditions and the high consumption of superplasticizer.

Despite significant progress in this area, the complex effect of nano- and micro-dispersed additives on the structure and properties of fine-grained cement-based mixtures, as well as the mechanisms of strength characteristic formation in the early stages of hardening, remains insufficiently studied. Special attention should be paid to evaluating the effectiveness of such modifying systems under conditions of minimal cement and water consumption, which is important for improving the energy efficiency of construction production.

This study is aimed at developing and substantiating the composition of fine-grained self-compacting concrete using polyfunctional additives based on microsilica, nano-SiO_2, and other active components that provide a comprehensive improvement in physical, mechanical, and technological properties.

2. Methods

The research methodology is based on the systematic application of scientific approaches focused on the development and optimization of concrete compositions for various functional purposes. At the initial stage, a working hypothesis was formulated, and a review and critical analysis of literary sources was carried out, which made it possible to justify the choice of micro- and nanoscale modifying components that are chemically compatible with cement hydration products, as

well as to form a detailed plan for experimental work. Nano-silicon dioxide (nano-SiO_2) was selected as the basic nano-sized modifier. Studies were conducted on its effect on the processes of structure formation and the physical and mechanical characteristics of cement stone. Based on the data obtained, the choice of micro-dispersed mineral additives (microsilica, micro-calcite) for the formation of complex (two-component) modifying systems was justified. The compositions of polyfunctional additives, including nano-SiO_2 in combination with micro-dispersed fillers, providing a complex effect on the structure and properties of the cement matrix, have been developed and scientifically substantiated. Taking into account the results of physical-mechanical and physical-chemical tests, a multi-level modifying system for fine-grained self-compacting concrete has been proposed. An algorithm for selecting the composition of the modifying system has been developed, taking into account the influence of components on key performance indicators, and tests have been carried out to determine strength, density, and other characteristics, confirming the effectiveness of the proposed system. To study the effect of complex additives on the structure and properties of cement stone, concrete mixtures, and concrete, Portland cement CEM I 42.5 N produced by Alacem LLP (Almaty, Kazakhstan) was used [9]. The characteristics, properties, chemical, and mineralogical composition of the cement used, as provided by the manufacturer's data, are presented in Tables 1-4.

Table 1 – Chemical composition of clinker, %

SiO_2	Al_2O_3	Fe_2O_3	CaO	MgO	SO_3	Alkalis	Other impurities
20.9	4.7	3.3	61.9	3.8	2.7	up to 0.8	1.9

Table 2 – Mineralogical composition of clinker, %

C_3S	C_2S	C_3A	C_4AF	CaO
68.9	12.9	6.2	11.3	0.7

Table 3 – Physical properties of cement

Residue on sieve 0.08, %	Normal consistency, %	Specific surface area, cm^2/g	Particle size, μm	Setting time, min		Losses during ignition, %
				Start	End	
9.7	27.5	3100	10-25	140	270	3.0

Table 4 – Mechanical properties of cement

Strength at normal hardening			
Bending		Compression	
3 days	28 days	3 days	28 days
6.8	7.9	36.4	53.6

Gravel with a particle size of 5-10 mm from the Kentas deposit (Almaty, Kazakhstan), which meets the requirements of [10], [11], was used as the coarse aggregate. The main physical and mechanical characteristics of the gravel aggregate are given in Tables 5-6.

Table 5 – Particle size distribution of gravel aggregate

Passing through a sieve	Sieve mesh size, mm			
	15	10	5	2.5
Total residue, %	100	88.78	11.22	-

Table 6 – Physical and mechanical properties of gravel aggregate

Brand by crushability	Content of plate-shaped and needle-shaped grains, %	Content of dust and clay particles, %	Clay content in lumps, %	Density, kg/m^3	
				Natural	Bulk
1000	12.5 (I group)	0.5	0	2660	1470

Natural quartz sand from the Arna deposit in the Almaty region, which meets the requirements [12], was used as a fine aggregate. The characteristics of the sand are presented in Table 7.

Table 7 – Properties of sand

Gravel content, %	Total residue, % on sieves, mm					Dust and clay particle content, %	Modulus of coarseness	Density, kg/m^3	
	2.5	1.25	0.63	0.32	0.16			Natural	Bulk
-	0.8	1.6	33.0	61.0	96.3	2.1	2.44	1395	2610

Nano-silicon dioxide (nano-SiO_2) synthesized using the plasma arc method was used as a nano-modifier in concrete mixtures. The technological scheme of the experimental setup for obtaining silicon dioxide nano-powder is based on the sublimation process of solid-phase raw materials under the influence of low-temperature arc discharge plasma, followed by the condensation of the vapor phase and the formation of nanoparticles of the target product. The extremely high temperatures of the plasma discharge (up to 5000 K) enable the use of a wide range of materials as raw materials, including natural mineral components [13]. In this work, diatomite from the Utesai deposit in the Aktobe region was used as raw material for obtaining nano-powder.

As can be seen in Figure 1, silicon dioxide nanoparticles with a polydisperse size distribution have a distinctive spherical shape and are represented in the form of agglomerates. The properties of the nano-modifiers used in the work are presented in Table 8.

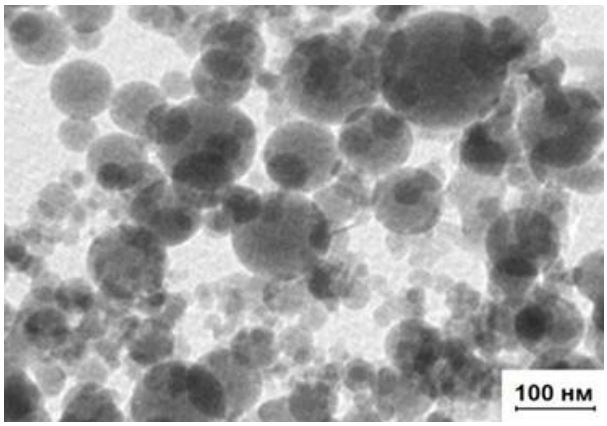

Figure 1 – Micrograph of SiO_2 nano-powder

Table 8 – Properties of nano-modifiers

Label	Specific surface area, m^2/g	Average particle size, nm
H74	282	73.7
H62	392	62.6
H44	511	44.5
H23	740	22.6

Condensed microsilica MCU-95, obtained from the Ferroalloy Plant (Tau-Ken Temir) in Karaganda, was used as the active, finely dispersed component of the modifying additive. According to [14], the annual output of this plant reaches 20,000 tons. The chemical composition and physical and technical properties of microsilica are presented in Tables 9 and 10.

Table 9 – Chemical composition of microsilica

Oxide content, %							
SiO_2	Al_2O_3	Fe_2O_3	CaO	MgO	Na_2O+K_2O	SiC	SO_2
95.5	1.4	0.8	1	0.2	0.3	up to 3	up to 0.09

Table 10 – Physical and technical properties of microsilica

Bulk density, kg/m^3	Natural density, kg/m^3	Particle size, μm	Specific surface area, m^2/g	Humidity, %
270	2200	0.1-1.0	2.5	2

Figure 2 presents the electron microscope image of microsilica.

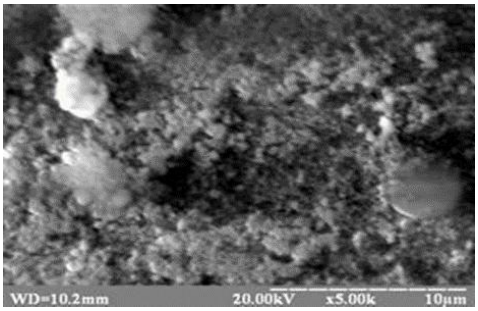

Figure 2 – Electron microscope image of microsilica

Figure 2 shows that the composition of microsilica is predominantly a homogeneous fraction. Microsilica interacts with cement hydration products, forming additional hydrate phases and acting as a gel binder. Microsilica particles, which are 0.5-0.05 μm in size, are capable of filling the voids between cement and aggregate particles, thereby increasing the strength and reducing the delamination of the concrete mixture.

The work used micro-dispersed mineral powder, a waste product formed during the crushing of MK-5 marble, complying with [15], at a quarry of Tekeli-Mramor LLP (Tekeli, Almaty, Kazakhstan). Finely ground marble is a white powder with a crystalline structure. It is characterized by a high calcium carbonate content of at least 95-98%. The physical and chemical properties of micro-calcite are presented in Table 11.

Table 11 – Physical and chemical properties of microcalcite

Chemical composition and properties	
$CaCO_3$, %	96–97
MgO, %	not more than 0.5
SiO_2, %	not more than 0.4
Fe_2O_3, %	not more than 0.2
Mass fraction of fugitive substances, %	not more than 0.15
Mass fraction of water-soluble substances, %	not more than 0.2
Mass fraction of substances soluble in 15% hydrochloric acid solution, %	not more than 97
pH of the aqueous suspension	10.1
Physical properties	
Specific surface area, m^2/g	1.6
Density, kg/m^3	2725
Refractive index	1.6
Hardness on the Mohs scale	3
Humidity, %	not more than 1

The composition of microcalcite is mainly CaCO3 (96-97%), and it also contains impurities of iron oxide, sulfur, magnesium, graphite, and aluminum in an amount of 1-3%.

A polycarboxylate plasticizer for construction materials based on cement binders AR124 manufactured by Arirang Group in Astana (Kazakhstan), was selected as a plasticizer for self-compacting concrete mix. The additive effectively disperses the cement paste in the concrete mixture, plasticizes the concrete mixture, reduces its water demand, and improves the mobility and homogeneity of concrete mixtures. The AR124 additive complies with [16].

The effect of nano-modifiers was studied on samples – 20×20×20 mm cubes made of normal-density cement paste with different additive ratios. The nano-SiO_2 additive content ranged from 0.01 to 0.05% of the cement mass. Silicon dioxide nano-modifiers with different specific surface areas ranging from 280 to 740 m^2/g were used for the studies. Two options were investigated to determine the most efficient method of adding additives: 1) The additive was pre-mixed with the mixing water; 2) The additive was mixed with cement until homogeneous, after which it was mixed with water.

The samples were cured under normal conditions (T = 18–20°C, RH = 90–100%) after molding. The compressive strength of the samples was evaluated after 28 days of curing. At least 5 samples were prepared for each composition. The strength value was determined as the arithmetic mean of the 5 samples, with a coefficient of variation of no more than 5%.

To study the deformation characteristics of hardened concrete, samples measuring 70×70×70 mm were tested for compressive strength in a hydraulic testing machine.

The frost resistance of concrete samples was determined according to [13]. The water resistance of concrete was determined using an accelerated method following [17]. The average density of samples was determined following [18]. The compressive strength of reference and modified samples was determined according to [19].

X-ray phase analysis (XPA) was used to study the phase composition of cement stone and determine its degree of hydration. Samples of finely dispersed cement stone powder were prepared after 28 days of hardening. XPA is used to identify the minerals that make up each sample. Each mineral has a specific set of peaks with its own intensity, and a multicomponent cement stone sample includes the sum of the X-ray diffraction patterns of individual minerals. The phase composition of the samples was studied using a D2PHASER diffractometer (Bruker, USA). The phase composition analysis was performed using DIFFRAC.EVA and DIFFRAC.TOPAS software.

Electron microscopic analysis and analysis of the elemental composition of additives were performed using a JEOL JSM 520 scanning electron microscope in backscattered electron and elemental analysis modes.

The specific surface area and average particle size of the powders were measured using a PSH-12 instrument.

3. Results and Discussion

To evaluate the influence of the structural characteristics of nano-SiO_2, methods of obtaining nanoscale particles, the rational ratio in the “cement-nanoadditive” system, conditions for uniform distribution of nanoparticles in the cement paste volume, and the stability of the obtained characteristics, experimental studies were conducted, the results of which are presented in Table 12.

Table 12 – Characteristics of cement stone with nano-SiO_2

Sample No.	Sample label	Additive content, % of cement mass	W/C	28 days compressive strength, MPa	
				Saturated	Dry
1	Reference	0.00	0.270	68.1	68.1
2	Cement+H74	0.01	0.275	76.0	77.0
3	Cement+H74	0.02	0.280	75.0	81.0
4	Cement+H74	0.03	0.280	64.9	83.0
5	Cement+H74	0.04	0.285	77.0	83.9
6	Cement+H74	0.05	0.290	78.0	84.0
7	Cement+H62	0.01	0.280	64.6	77.0
8	Cement+H62	0.02	0.285	72.3	77.2
9	Cement+H62	0.03	0.285	75.2	77.3
10	Cement+H62	0.04	0.285	75.0	79.0
11	Cement+H62	0.05	0.290	76.0	81.0
12	Cement+H44	0.01	0.265	66.0	68.0
13	Cement+H44	0.02	0.265	70.0	72.0
14	Cement+H44	0.03	0.265	68.0	73.0
15	Cement+H44	0.04	0.275	65.0	69.0
16	Cement+H44	0.05	0.275	64.9	67.0
17	Cement+H23	0.01	0.270	68.0	71.0
18	Cement+H23	0.02	0.270	69.0	73.0
19	Cement+H23	0.03	0.270	69.9	73.3
20	Cement+H23	0.04	0.280	71.1	74.5
21	Cement+H23	0.05	0.285	73.0	74.9

Analysis of the data presented in Table 12 shows that all types of silicon nano-dioxide (nano-SiO_2) studied in this work contribute to an increase in the strength of cement stone on the 28th day of hardening in the range from 3 to 37% compared to the reference sample. The magnitude of the effect is determined by a combination of variable factors. It has been established that increasing the nano-SiO_2 content from 0.01% to 0.05% of the cement mass provides a strength increase of up to 32% relative to the reference composition, However, a further increase in concentration does not lead to a significant improvement in performance, which is due to an increase in the water demand of the system and corresponds to the results obtained in previous studies [6]. In this regard, subsequent experiments were conducted using the specified percentage range of the nano-modifier.

It has also been established that the effectiveness of modification largely depends on the method of additive introduction. The most pronounced increase in strength (up to 38% compared to the reference composition) was recorded when nano-SiO_2 was pre-mixed with cement. With the alternative method of introduction, agglomeration of nanoparticles is observed, which prevents their uniform distribution in the volume of the binder matrix and significantly reduces the strengthening effect.

Thus, analysis of the results obtained from studying the influence of the characteristics of silicon nanodioxid (nano-SiO_2), methods of its synthesis and introduction into cement paste, as well as the dosage of additives on the properties of the binder system, made it possible to determine the rational content of nanoscale particles in the cement matrix, which is 0.01-0.05% of the cement mass. Within this range, the increase in the strength of cement stone reaches 32%, which determined the choice of this dosage for further research. The data obtained are consistent with the results of [20], where it is noted that excessive introduction of silica nanoparticles can cause “oversaturation” of the system, slowing down the processes of hydration and hardening, which is also confirmed in several works [21].

This effect is explained by the high chemical activity and reactivity of nano-silicon dioxide, which promotes the binding of a significant portion of the mixing water into poorly soluble crystallohydrate compounds. This leads to a deficiency of free moisture necessary for the hydration of clinker minerals and, as a result, a slowdown in structure formation. To identify the mechanisms and patterns of formation of the composition, structure, and properties of cement stone, a series of physical and chemical studies of reference and modified samples was performed.

Comparative X-ray phase analysis of the hydration products of reference cement and cement with H74 (Figure 3) confirms the formation of new crystalline phases in modified cement stone.

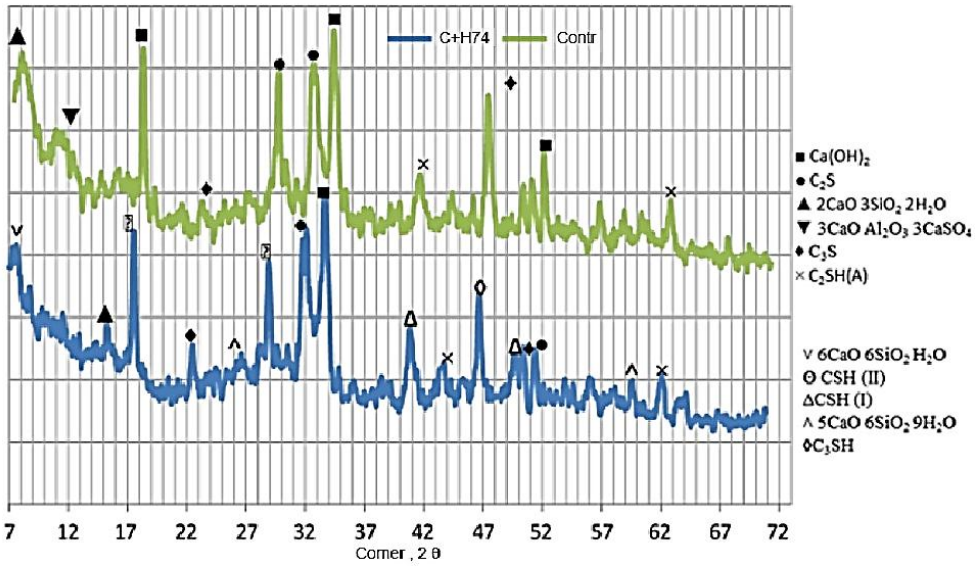

Figure 3 – X-ray images of the reference sample of SCC and SCC with nanomodifier H74

According to X-ray phase analysis data, the introduction of the modifying additive H74 contributes to the intensification of calcium hydroxide binding, which is accompanied by an increase in the content of low-base calcium hydrosilicates C–S–H (d/n = 4.93; 2.91; 2.19; 2.07; 1.99; 1.81×10^{-10} m), the formation of which probably determines the increase in the strength of the cement stone. A significant decrease in the amount of free calcium hydroxide is confirmed by diffractograms showing an increased background in the small-angle region and a decrease in the intensity of the diffraction peaks of the crystalline phases $Ca(OH)_2$ (d/n = 4.9; 2.64; 1.8; 1.49×10^{-10} m), which correlates with the hydration reactions of cement clinker minerals.

The results of studies on the effect of silicon nano-dioxide with different specific surface areas and concentrations on the behavior of cement systems suggest that the chemical interaction mechanism is only realized if the composition of the nanoparticles corresponds to the hydration products of cement minerals, which ensures their inclusion in the reaction of secondary hydrate phase formation. These conclusions are consistent with the results presented in [22]. Thus, the experimental results confirm the effectiveness of modifying the structure of cement stone by introducing silicon dioxide nanoparticles.

The polyfunctional additive (PA) was made by mixing the components in a high-speed mixer at a working speed of 60 rpm. The components were loaded in stages, starting with the largest fraction (micro-calcite), followed by the introduction of microsilica and nano-modifier H74. The total mixing time was 20 minutes. During mixing, additional grinding of the coarse fraction particles took place, accompanied by their joint mechanical activation with micro-dispersed and nano-dispersed components, which ensured uniform distribution of the modifying components in the system and intensified interaction with the cement matrix. Table 13 shows the elemental composition of the additive components.

Table 13 – Additive component composition

Name	Microsilica	Microcalcite	H74
SiO_2	+	+	+
CaO	-	+	-
Al	+	-	-
C	+	+	-
MgO	+	+	-

The data presented in Table 13 show that the elemental composition of all components of the complex additive (i.e., PA) is qualitatively the same.

Comparative data from electron microscopic analysis of the structure of the reference cement stone and the modified complex additive PD and nano-SiO_2 are presented in Figures 4 and 5.

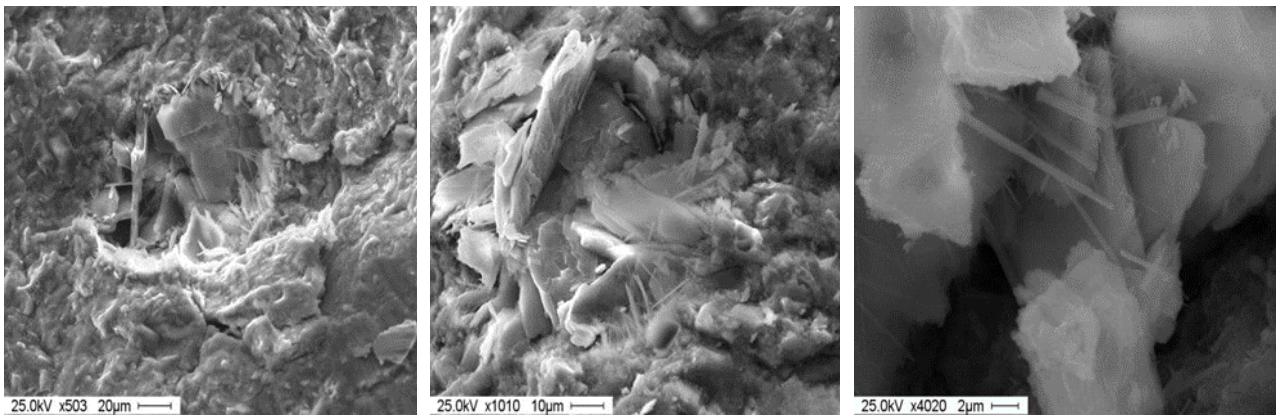

a) ×440 b) ×2000 c) ×4000

Figure 4 – Electron microscope image of a reference cement stone

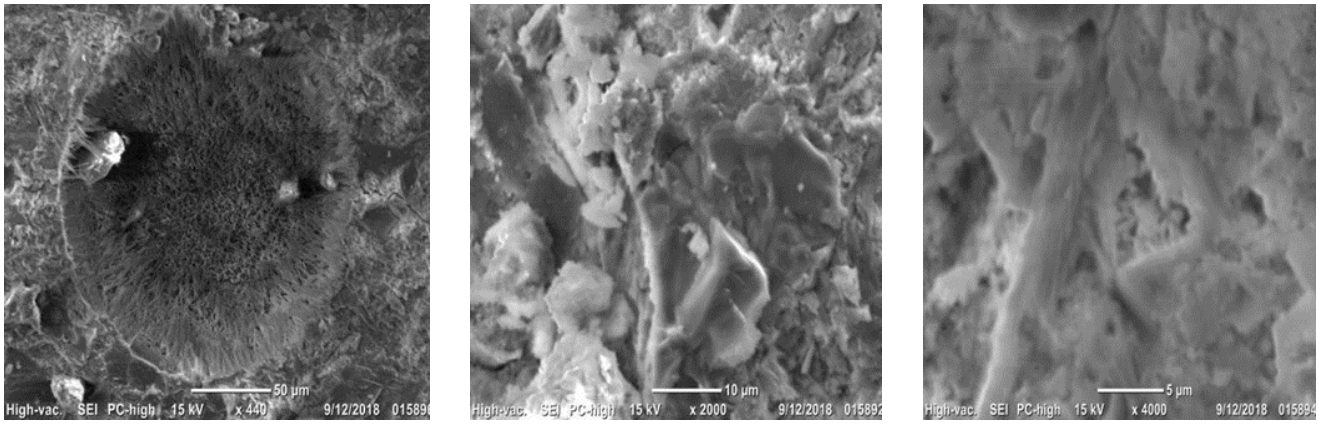

a) ×440 b) ×2000 c) ×4000

Figure 5 – Electron microscope image of cement stone modified with a complex additive of PA and nano-SiO_2

Analysis of microstructural data (Figures 4 and 5) shows that cement stone samples modified with a complex additive (polyfunctional system and nano-SiO_2) are characterized by a denser and more homogeneous structure compared to the reference samples. The structure of the reference sample (Figure 4) shows pronounced heterogeneity, a significant volume of open pores, and the presence of needle-like crystalline formations characteristic of ettringite. Only insignificant amounts of portlandite are fixed on the surface of the modified sample, while the formation of a layered structure of low-base calcium hydrosilicates (herringbone morphology) is observed.

The pore space of the modified cement stone is almost completely filled with growing hydrosilicate crystals, which ensures the compaction of the structure and the formation of additional substrates for crystallization centers. Such "clogging" of pores contributes to increased water resistance and frost resistance of concrete, which is confirmed by [23].

Given that the specific surface area of the N74 nanomodifier significantly exceeds that of the polyfunctional additive (PA) and cement, the mechanism of their combined effect on the system is determined by the sequence of adsorption on the surface of cement particles and the nature of the physicochemical interaction of the components. During the preparation of construction mixtures, adsorption shells are formed when N74 particles evenly cover the surfaces of cement and PA. The resulting adsorption contacts between the sorbent and the adsorbate act as crystallization centers, which significantly accelerates the processes of hydration and structure formation of cement stone, especially in the initial stages of hardening [24].

Table 14 shows quantitative (oxide) analysis of electron microscopic studies.

Table 14 – Quantitative (oxide) analysis of electron microscopic studies (mass fraction, %)

No.	MgO	Al_2O_3	SiO_2	SO_3	Fe_2O_3	CaO
001	1.27	5.54	15.11	4.9	4.72	67.66
002	-	7.55	51.2	10.83	-	30.45
003	-	6.6	51.3	5.7	-	36.4

To verify the results obtained by electron microscopic analysis, Table 14 shows the quantitative oxide composition of the cement stone sample modified by the PD + H74 system at three points under investigation (001, 002, and 003; see Figure 5). Analysis of the data presented allows us to conclude that low-base calcium hydrosilicates belonging to tobermorite-like phases are predominantly formed in the pore space of cement stone (Figure 5). Points 002 and 003 are characterized by a CaO/SiO_2 ratio < 1.5, which confirms the predominance of low-base calcium hydrosilicates in the composition of the formed phases.

Additionally, Figure 6 shows the results of bending tests on modified cement stone, performed in comparison with the reference composition, which allows us to evaluate the contribution of the complex additive to the improvement of strength characteristics.

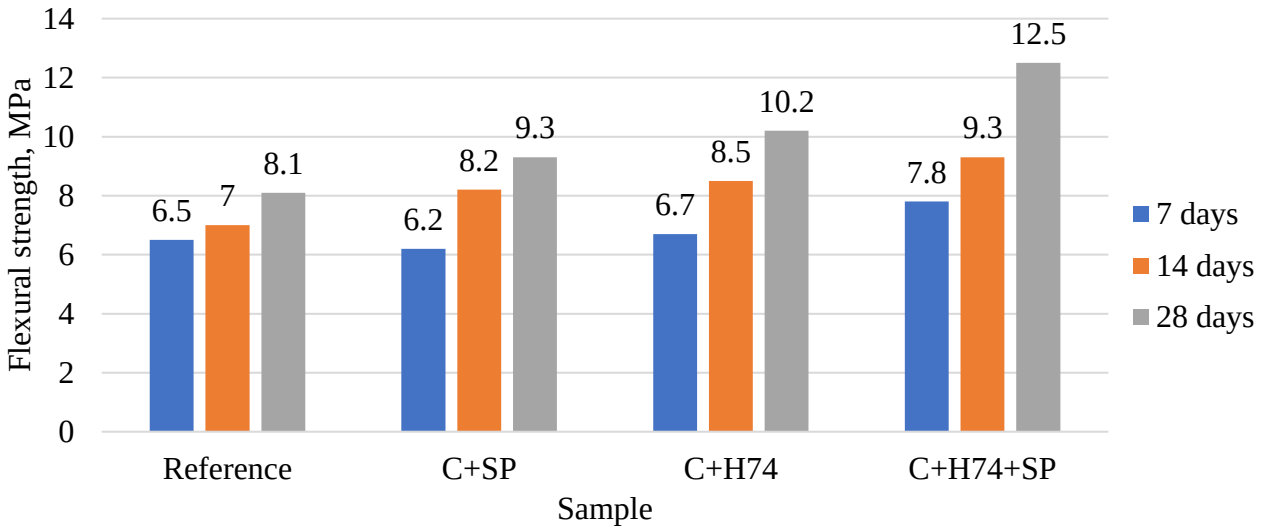

Figure 6 – Flexural strength of modified cement stone

Thus, the use of a complex additive comprising a polyfunctional system (PA) and nanomodifier N74 increased the flexural and compressive strength of cement stone by 29% and 45%, respectively, as well as a reduction in the water demand of the mixture, which is associated with the hydrophobic-hydrophilic properties of the PA components. The achieved effect may be due not only to the modification of rheological characteristics, but also to the participation of the additive in the processes of cement stone structure formation. The pore space of the matrix is filled with growing calcium hydrosilicates, which form a compact structure and additional crystallization centers, which is consistent with the results presented in [25].

The structure of a concrete mix can be represented as a homogeneous mixture of aggregate grains of various fractions and cement paste used to fill the voids between the aggregate grains and coat them. The thickness of the cement paste coating on the aggregate grains h is an input parameter. The value of the thickness of the cement paste coating of aggregate grains h can be determined as the amount of cement paste V_c minus the volume of intergranular voids V_v, relative to the surface area of the aggregate grains, S:

$$h = \frac{V_c - V_v}{S} \quad (1)$$

Taking into account expression (1) and based on the equation of absolute volumes used in calculating the composition of concrete mix, the following system of equations is formed, allowing the consumption of components per 1 m^3 of concrete mix to be determined:

$$1 = V_g^{hard} + V_c^{void} + V_c^{paste} \quad (2)$$

$$V_g^{hard} = \frac{m_1}{q_1^n} + \frac{m_2}{q_2^n} + \cdots \frac{m_n}{q_n^n} \quad (3)$$

$$V_c^{paste} = h \cdot S_{sa} \cdot \mathrm{M} \quad (4)$$

$$\mathrm{M} = m_1 + m_2 + m_n \quad (5)$$

$$V_c = V_c^{void} + V_c^{paste} = C \cdot (W/C), \quad (6)$$

where: V_g^{hard} – объем зерен заполнителей, м3; V_c^{void}– volume of cement paste filling the voids in the aggregate, m^3; V_c^{paste}– volume of cement paste enveloping aggregate grains, m^3; m_i – consumption of the i-th filler per 1 m^3 of concrete mix, kg; ρ^n– natural density of grains of the i-th aggregate, kg/m^3; V_p – volume of voids, m^3; V_f– total volume occupied by the aggregate mixture, m^3; h – effective thickness of the cement paste film enveloping the aggregate grains, μm; S_{sa} – specific surface area of the aggregate mixture, kg/m^2; ρ_c – natural density of cement, kg/m^3; m_i – mass fraction of the i-th filler; W/C − water-cement ratio.

Depending on the task at hand, the proposed system of equations can be used to determine various parameters of the concrete mix. By setting target indicators for the properties of the concrete

mix and concrete, such as mobility and strength, and using mathematical calculation methods, it is possible to obtain more accurate and reliable predictive values for the strength of the material [26].

In particular, with fixed values of the water-cement ratio, mass fractions of each aggregate, and thickness of the cement shell on the surface of the aggregate grains, the system allows determining the consumption of all components included in the mixture to obtain concrete with specified physical and mechanical characteristics [26].

Two types of cement paste were used in the concrete composition: 1) reference; 2) developed (cement + polyfunctional additive (PA) in the amount of 5% of the cement mass). The initial value of the thickness of the cement paste coating on the grains is conventionally taken as 10 μm.

To verify the convergence of the calculated and experimental data on the compositions of fine-grained self-compacting concrete, a series of tests was carried out on laboratory samples to determine their main physical and mechanical characteristics. The initial compositions of the concrete mixtures used in the studies are presented in Table 15.

Table 15 – Compositions of concrete mixtures per 1 m^3

Composition No.	Crushed stone of 5-10 mm, kg	Sand, kg	Cement, kg	W/C	PA, kg	Superplasticizer, l	Slump flow, cm	Design strength of concrete, 28 days, MPa
1 (reference)	1000	670	545	0.36	-	-	60	46
2	1100	560	555	0.33	-	2.23	63	49
3	950	690	550	0.35	26.85	2.41	64	65
4	1150	590	525	0.32	26.05	2.56	66	67

10×10×10 cm cubic samples were prepared for testing. At least 20 samples were prepared for each composition. Strength was determined as the arithmetic mean of the test results for five samples for each control hardening period, with a coefficient of variation not exceeding 5%.

In concrete production, not only are the proportions of the modifying additives important, but also the algorithm for their introduction into the mixture. The polyfunctional additive (PA) should be introduced into the cement matrix at the mixing stage before the addition of fine and coarse aggregates, which ensures uniform distribution of the modifier in the volume of the cement stone. Violation of the sequence and addition of MA after the cement has been combined with the aggregates leads to uneven distribution of the components, which reduces the effectiveness of the modification. The superplasticizer was added to the finished mixture together with the mixing water.

The strength characteristics of the concrete samples were determined at 3, 7, 28, and 120 days of hardening. Figure 7 shows the comparative results of strength gain over time for the tested compositions.

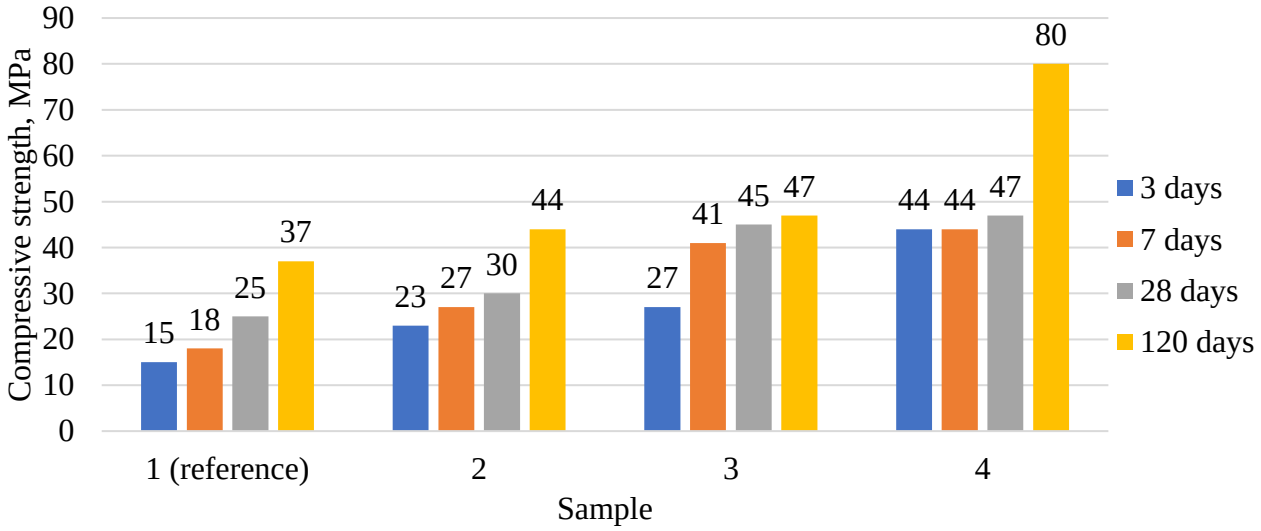

Figure 7 – Strength development kinetics of fine-grained self-compacting concrete

Analysis of the experimental data in Figure 7 shows that the introduction of a polyfunctional additive and the determination of the optimal ratio of dispersed components in the concrete mixture (composition 3) provide an increase in the compressive strength of fine-grained self-compacting concrete at different hardening times compared to the reference samples (composition 1). At 3 days – by 92%, at 7 days – by 64%, at 28 days – by 41%, at 120 days – by 38%. The addition of a plasticizer, together with PD (compositions 3 and 4), contributes to an increase in strength indicators: in 3 days – by 81%, in 7 days – by 54%, in 28 days – by 44%, in 120 days – by 48% compared to the reference (composition 1).

Compositions 3 and 4 were selected based on strength and mobility indicators, and further research was conducted on them. Thus, the water resistance of the reference and modified concrete samples was determined using the AGAMA-2 device. It has been established that modified concrete samples are characterized by a significant increase in water impermeability (grade W16) compared to reference compositions (grade W8). The increase in water resistance is explained by the formation of a denser material structure due to the rational selection of the mixture composition and a reduction in the open porosity of the cement stone.

When exposed to low temperatures accompanied by alternating freeze-thaw cycles, the greatest danger to concrete is the presence of “free water” in the pore space. When it freezes in the pores, internal pressure is formed, and repeated cycles of phase transitions associated with an increase in water volume by approximately 9% lead to progressive destruction of the pore structure. Water penetrating into the resulting microcracks contributes to the expansion of damage and the development of internal destruction in the concrete structure.

The amount of “free water” in the pore space can be reduced by using modifying additives that decrease the open porosity of the cement stone and form a denser concrete structure with increased water resistance and resistance to cyclic exposure to frost and heat.

The frost resistance of the reference and modified concrete samples was determined using the third accelerated method with multiple freeze-thaw cycles in accordance with the methodology [27]. The tests were carried out in accordance with the requirements of [27], with the reference and modified samples being pre-saturated with a 5% sodium chloride solution before testing and subsequent strength determination.

During the experiment, samples were selected for evaluation at several cycles corresponding to the intermediate frost resistance grade (with fixed mass changes of no more than 2%, which meets the requirements of [27]), as well as after the maximum number of cycles at which a decrease in the strength characteristics of the concrete was observed. The processing of the test results for determining the frost resistance grade of concrete was carried out in full compliance with the requirements of [27]. As a result, the reference concrete samples withstood 5 cycles of frost resistance testing using the third accelerated method, which corresponds to the F1200 grade, while the modified concrete with a polyfunctional additive (PA) demonstrated resistance to 27 cycles, corresponding to the F1700 grade. The results obtained confirm that the improvement in the performance properties of fine-grained self-compacting concretes is achieved by the formation of a homogeneous and compacted structure of cement stone and concrete matrix at various scale levels. This effect is due to the rational selection of the component composition of the concrete mix – from the grain composition of aggregates to microparticles of modified binder – and the application of a developed algorithm for designing the composition of self-compacting fine-grained concrete, taking into account the structural and technological characteristics of micro-dispersed components.

Table 16 – Comparative data on the physical and mechanical characteristics of fine-grained SCC

Composition	Slump flow, cm	Design strength of concrete, 28 days, MPa	Experimental concrete strength, 28 days, MPa	Water resistance, (MPa) grade	Frost resistance	Density, kg/m^3
Reference	60	49	53 (B40)	(0,8) W8	F1200	2373
Modified	67	67	77.1 (B60)	(1,6) W16	F1700	2384

Thus, the complex of physical and mechanical studies confirmed the effectiveness of the proposed method for designing the composition of fine-grained self-compacting concrete using the developed polyfunctional additive. Analysis of the experimental data obtained (Table 16) demonstrates that the use of this additive and the proposed approach to designing the composition of fine-grained self-compacting concrete ensures the production of concrete with increased strength, water resistance, and frost resistance.

4. Conclusions

1. It has been established that the introduction of nano-silicon dioxide (nano-SiO_2) with a particle size of up to 40 nm in an amount of 0.03% of the cement mass provides an increase in the compressive strength of cement stone by up to 32% (90 MPa) relative to the reference samples. This effect is due to the formation of an additional amount of high-strength low-base calcium hydrosilicates, an increase in the number of crystallization centers in the early stages of cement hydration, and the initiation of structure formation processes in the "nano-SiO_2 – micro-dispersed component – cement" system.

2. Complex (two-component) modifying additives based on nano-silicon dioxide, microsilica, and micro-calcite have been developed. Their influence on the processes of regulating the structure and physical and mechanical characteristics of cement stone and fine-grained self-compacting concrete has been experimentally investigated.

3. An algorithm for designing the composition of fine-grained concrete has been developed, taking into account the structural and technological parameters of micro-dispersed components and the thickness of the cement shell on the surface of the aggregate grains. The application of this algorithm ensures the formation of a homogeneous and compacted structure of fine-grained concrete with high-performance properties. The calculated values of the mixture composition showed satisfactory convergence with the experimental data.

4. The developed fine-grained concrete compositions with a multi-level polyfunctional additive (PA) in the amount of 5% of the cement mass ensure high performance characteristics: strength class B60, flexural strength 12.5 MPa, frost resistance up to F1700, and water resistance up to W16.

Acknowledgments

This research was funded by the Science Committee of the Ministry of Science and Higher Education of the Republic of Kazakhstan (Grant No. AP27511185).

References

[1] F. Sanchez and A. Borwankar, "Multi-scale performance of carbon microfiber reinforced cement-based composites exposed to a decalcifying environment," *Materials Science and Engineering: A*, vol. 527, no. 13–14, pp. 3151–3158, May 2010, doi: 10.1016/j.msea.2010.01.084.

[2] L. A. Suleymanova, Pogorelova I.A., A. S. Slepuhin, and S. I. Plehova, "To the question of condition survey of the civil buildings," *Bulletin of Belgorod State Technological University named after. V. G. Shukhov*, vol. 1, no. 9, pp. 63–66, 2016.

[3] "GOST 25192-2012 Concretes. Classification and general technical requirements," Moscow: Standardinform, 2012, p. 10.

[4] J. Newman and B. S. Choo, "Advanced Concrete Technology," Amsterdam, Netherlands: Elsevier, 2003, p. 280. doi: 10.1016/B978-0-7506-5686-3.X5246-X.

[5] A. V. Fedorov and V. N. Aksenov, "To the question of the use of high-strenght concrete in compressed of tall buildings," *Engineering Journal of Don*, vol. 50, no. 3, p. 102, 2018.

[6] A. I. Karlina, Y. I. Karlina, and V. A. Gladkikh, "Analysis of Experience in the Use of Micro- and Nanoadditives from Silicon Production Waste in Concrete Technologies," *Minerals*, vol. 13, no. 12, p. 1525, Dec. 2023, doi: 10.3390/min13121525.

[7] S. V. Makarenko, "Cements with low water demand as an alternative type of binding mixture used in ready-mixed concrete," *Izvestiya vuzov. Investitsii. Stroitelstvo. Nedvizhimost*, vol. 13, no. 1, pp. 58–63, Nov. 2023, doi: 10.21285/2227-2917-2023-1-58-63.

[8] P. Richard and M. Cheyrezy, “Reactive Powder Concretes With High Ductility and 200 - 800 Mpa Compressive Strength,” in *“SP-144: Concrete Technology: Past, Present, and Future,”* Farmington Hills, MI: American Concrete Institute, 1994, pp. 507–518. doi: 10.14359/4536.
[9] “GOST 31108-2020 Common cements. Specifications,” Moscow: Standardinform, 2020, p. 29.
[10] “GOST 8267-93 Crushed stone and gravel of solid rocks for construction works. Specifications,” Moscow: Standardinform, 1993, p. 21.
[11] “GOST 26633-2015 Normal-weight and sand concretes. Specifications,” Moscow: Standardinform, 2015, p. 15.
[12] “GOST 8736-2014 Sand for construction works. Specifications,” Moscow: Standardinform, 2014, p. 21.
[13] P. V. Kosmachev, “Poluchenie nanorazmernogo dioksida kremniya plazmenno-dugovym metodom iz vysokokremnezemistogo prirodnogo syrya,” Tomsk, Russia: TGASU, 2018, p. 141.
[14] “GOST 58894-2020 Silica fume for concretes and mortars. Specifications,” Moscow: Standardinform, 2020, p. 19.
[15] “GOST R 56775-2015 Microcalcite. for construction materials. Specifications,” Moscow: Standardinform, 2015, p. 12.
[16] “GOST 30459-2008 Admixtures for concretes and mortars. Determination and estimate of the efficiency,” Moscow: Standardinform, 2008, p. 18.
[17] “GOST 12730.5-2018 Concretes. Methods for determination of water tightness,” Moscow: Standardinform, 2018, p. 26.
[18] “GOST 12730.1-2020 Concretes. Methods of determination of density,” Moscow: Standardinform, 2012, p. 18.
[19] “GOST 10180-2012 Concretes. Methods for strength determination using reference specimens,” Moscow: Standardinform, 2012, p. 36.
[20] E. V. Korolev, “Nanotechnology in material science. Analysis of chievements and current state,” *Construction Materials*, pp. 47–78, 2014.
[21] A. V. Nomoev, V. T. Lygdenov, L. A. Urkhanova, and S. A. Lkhasaranov, “Fine-grained cement concrete with nanodispersed modificator,” *Nanotehnologii v stroitel'stve*, vol. 2, no. 4, pp. 42–52, 2010.
[22] Y. Qing, Z. Zenan, K. Deyu, and C. Rongshen, “Influence of nano-SiO_2 addition on properties of hardened cement paste as compared with silica fume,” *Constr Build Mater*, vol. 21, no. 3, pp. 539–545, Mar. 2007, doi: 10.1016/j.conbuildmat.2005.09.001.
[23] T. V. Kuznecova and C. B. Samchenko, “Mikroskopiya materialov cementnogo proizvodstva,” Moscow: MIKHiS, 2007, p. 304.
[24] M. Zaichenko, S. Lakhtaryina, O. Yegorova, V. Gubar, and A. Sokolova, “Optimization of cement stone composition with microsilicasuspension additive and SIKA VISCOCRETE SUPERPLASSIFIER 5 NEW ST,” *Modern industrial and civil construction*, vol. 14, no. 1, pp. 5–12, 2018.
[25] I. A. Iochinskaya, *Vliyanie kompleksnyh dobavok na processy gidratacii i tverdeniya portlandcementa: Avtoreferat dis. kand. tehn. nauk: 05.23.05*. Moscow, 1974.
[26] Yu. M. Bazhenov, “Concrete Technology,” Moscow: ACB, 2011, p. 528.
[27] “GOST 10060-2012. Concretes. Methods for determination of frost-resistance,” Moscow: Standardinform, 2018, p. 24.

Information about authors:

Zhanar Zhumadilova – PhD, Associate Professor, Deputy Director, Institute of Architecture and Civil Engineering, Satbayev University, Almaty, Republic of Kazakhstan, z.zhumadilova@satbayev.university
Assel Kanarbay – MSc, Assistant, Department of Engineering Systems and Networks, Institute of Architecture and Civil Engineering, Satbayev University, Almaty, Republic of Kazakhstan, a.kanarbay@satbayev.university
Daniyar Akhmetov – Doctor of Technical Sciences, Professor, Department of Civil Engineering and Building Materials, Institute of Architecture and Civil Engineering, Satbayev University, Almaty, Republic of Kazakhstan, d.a.akhmetov@satbayev.university
Assel Aldigaziyeva – MSc, Assistant, Department of Civil Engineering and Building Materials, Institute of Architecture and Civil Engineering, Satbayev University, Almaty, Republic of Kazakhstan, a.aldigaziyeva@satbayev.university

Author Contributions:

Zhanar Zhumadilova – concept, methodology, resources, interpretation, drafting.
Assel Kanarbay – data collection, testing, modeling.
Akhmetov Daniyar – editing, funding acquisition.
Assel Aldigaziyeva – analysis, visualization.

Conflict of Interest: The authors declare no conflict of interest.

Use of Artificial Intelligence (AI): The authors declare that AI was not used.

Received: 10.08.2025
Revised: 25.10.2025
Accepted: 26.10.2025
Published: 28.10.2025

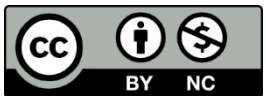

Technobius, 2025, 5(4), 0090, DOI: https://doi.org/10.54355/tbus/5.4.2025.0090

Technobius

https://technobius.kz/

e-ISSN 2789-7338

Vibro-pressed concrete for wall blocks based on lightweight expanded clay aggregate obtained with the addition of oil sludge

Roza Narmanova[1]*, Kylyshbai Bissenov[2], Nargul Saktaganova[2], Sergiy Lyubchyk[3], Nurlybek Kelmagambetov[4]

[1]Laboratory of Engineering Profile "Physical and Chemical Methods of Analysis", Korkyt Ata Kyzylorda University, Kyzylorda, Kazakhstan
[2]Institute of Engineering and Technology, Korkyt Ata Kyzylorda University, Kyzylorda
[3]DeepTechLab, Faculty of Engineering, Lusófona University, Lisbon, Portugal.
[4]Department of Engineering and Logistics, Kyzylorda Bolashak University, Kyzylorda, Kazakhstan
*Correspondence: roza_an@mail.ru

Abstract. This study develops lightweight expanded clay aggregate (LECA) from local low-expanding loams using an oil-sludge-based fuel-containing additive and evaluates its use in vibro-pressed lightweight aggregate concrete (LWAC) wall blocks. LECA was produced by granulation and firing, then characterized by bulk density, water absorption, and compressive strength. LWAC blocks were manufactured via a semi-dry vibro-pressing route and tested for density, compressive strength, thermal conductivity, and freeze-thaw resistance. The LECA incorporating oil sludge showed a strength increase from 1.38 MPa to 2.8-3.1 MPa with a moderate density rise (316 to 350-400 kg/m^3) while maintaining ~25.8% water absorption. Blocks achieved 800-950 kg/m^3 density and 10-12 MPa compressive strength, with 0.75-0.8 W/(m·K) thermal conductivity and 50-75 freeze-thaw cycles. XRD pattern fitting indicated silicate- and spinel-type crystalline phases, though some matches require verification. Overall, the raw material and processing route enable structural wall units with improved thermal performance. The future work should prioritize moisture-related durability under higher saturation.

Keywords: expanded clay aggregate, oil sludge additive, vibro-pressing, lightweight aggregate concrete, thermal insulation wall blocks.

1. Introduction

Improving the energy efficiency of buildings remains a major driver of innovation in wall and envelope materials, because heat losses through external walls strongly affect operational energy demand and life-cycle impacts of the building stock [1]. In many cold and continental climates, the envelope must simultaneously provide (i) adequate load-bearing capacity, (ii) low thermal conductivity, and (iii) long-term durability under freeze-thaw action and moisture exposure. A common approach is to use multilayer systems where a structural wall (e.g., masonry or concrete) is combined with an external insulation system. However, such solutions introduce additional interfaces, workmanship sensitivity, and serviceability/fire-safety considerations that motivate continued interest in single-layer wall units with improved thermophysical performance [2], [3], [4]. Consequently, the development of structural-thermal insulating wall blocks based on lightweight concrete remains an actual research and engineering task.

Lightweight aggregate concrete (LWAC) is widely recognized as an effective route to reduce density and improve thermal performance compared with normal-weight concrete, while retaining sufficient mechanical strength for many structural or semi-structural applications [5]. Among manufactured lightweight aggregates, lightweight expanded clay aggregate (LECA) is particularly important due to its relatively stable production technology and favorable combination of low density, internal porosity, and chemical compatibility with cement matrices [6]. The porous shell-core microstructure of LECA decreases thermal conductivity and can also provide internal curing effects, while the overall performance of LECA concrete depends strongly on aggregate grading, water absorption/pre-wetting practice, and the quality of the interfacial transition zone [5], [6], [7], [8]. Recent studies and overviews show that concretes with expanded clay aggregates can achieve strength levels suitable for structural elements and can contribute to lowering heat transfer through building envelopes, provided that mixture design and moisture control are properly managed [6], [7], [8], [9], [10]. For wall blocks, these considerations are especially important because thermal performance, density class, and water absorption must be balanced against compressive strength and production feasibility.

At the same time, the properties of LECA itself depend on raw material mineralogy and on additives used during firing that affect bloating, pore formation, and the resulting phase composition and microstructure [11], [12]. This is relevant for regions where local low-expanding loams/clays are available but may require formulation adjustments to achieve stable expansion and target density. An additional motivation is sustainability: the incorporation of industrial wastes as pore-forming agents or fuel-containing additives during ceramic processing has been actively explored to reduce environmental burden and potentially improve performance. For example, oily wastes and petroleum/oil-sludge-type residues have been investigated as additives in fired clay ceramics, showing that they can influence firing behavior, porosity development, and final properties when used in controlled dosages [12], [13]. Related work has also demonstrated the feasibility of using waste engine oil (a fuel-rich waste) as an expansive additive in the production of expanded clay aggregates and has evaluated the effects of such aggregates on the physical and mechanical properties of lightweight concretes [14]. These findings support the broader idea that oil-derived wastes can be valorized in fired clay/ceramsite-type products, but the optimal dosages and processing routes remain highly system-specific and must be validated for the targeted wall products.

A further practical dimension is the manufacturing route of wall blocks. In industrial practice, many masonry and wall units are produced using low-slump or semi-dry mixtures under vibro-pressing/vibro-compaction (simultaneous vibration and pressing), because this method enables fast demolding, dimensional stability, and high productivity [15], [16], [17]. However, the compaction regime, moisture content, and grading are known to significantly affect density, pore connectivity, and consequently both strength and thermophysical properties of the final blocks [15], [16], [17], [18]. While a substantial body of research addresses cast LWAC (including self-compacting variants) [9], fewer studies provide a clear linkage between (i) locally produced expanded clay aggregate characteristics (including phase composition), (ii) semi-dry vibropressed block production parameters, and (iii) the resulting strength-density-thermal conductivity balance required for energy-efficient wall blocks.

Within this context, the present study is important because it targets an applied but scientifically grounded task: developing and experimentally validating vibro-pressed structural-thermal insulating wall blocks made with LECA produced from local raw materials (including low-expanding loam) with the use of an oil-sludge-type additive acting as a fuel-containing/pore-forming component during aggregate production. The goal of the work is to substantiate whether such a combination of local loam-based expanded clay aggregate and vibro-pressed cementitious mixtures can yield wall blocks that meet the required mechanical and thermophysical criteria. To achieve this goal, the study focuses on: characterizing the expanded clay aggregate (including mineral/phase features relevant to firing and performance); producing vibro-pressed expanded-clay concrete blocks using a semi-dry technology consistent with industrial practice; and evaluating key properties (density

class, compressive strength, water absorption, and thermal performance indicators) needed to justify the feasibility of the proposed wall unit concept for energy-efficient construction.

2. Methods

The research objects were LECA and experimental samples of thermal insulation-structural wall blocks produced by semi-dry vibro-pressing from a blend of LECA, M400 cement, and dune sand. The determination of the physical, mechanical, and thermal properties of the blocks was carried out in accordance with [19]. The following raw materials were used: M400 cement as binder complying with [20], dune sand from Kyzylorda deposit (Kyzylorda region, Kazakhstan) as fine aggregate complying with [21], and LECA from Kyzylorda deposit (Kyzylorda region, Kazakhstan) as coarse aggregate complying with [22] with a maximum particle size not exceeding 20 mm. LECA was produced from low-expanding loams using oil sludge as a fuel-containing bloating/pore-forming reagent, based on our previous experience [23], [24]. To facilitate the incorporation of the bloating component, an "oil sludge-dune sand" conglomerate was prepared at a 1:3 proportion, using oil sludge from JSC "PetroKazakhstan Kumkol Resources" (Kyzylorda, Kazakhstan) and the aforementioned dune sand. A pilot batch of 10 m^3 of the LECA has been prepared at the "Stroykombinat" LLP (Uralsk, Kazakhstan) and tested along with conventional LECA (existing in the market), to obtain their physical and mechanical properties according to [22].

For manufacturing the LWAC blocks, the concrete mixture composition (per 1 m^3) consisted of cement – 250 kg, expanded clay (10-20 mm fraction) – 660 kg, sand – 340 kg, and water – 95-100 liters. The average percentage proportion of the biner-aggregates was: cement – 20%, sand – 27%, and LECA – 57%. Before pilot production, mixture compositions were simulated at laboratory scale to obtain effective physical, mechanical, and thermophysical performance, based on prepared samples. Reduced-density thermal insulation-structural blocks of standard size of 390×190×188 mm were then manufactured on the "Mastek-Meteor" molding/vibro-pressing complex (Figure 1) produced by ZAO "Monolit" (Zlatoust, Russia).

Figure 1 – LWAC blocks manufacture using the "Mastek-Meteor" molding/vibro-pressing complex

In production, the reagents were weighed and loaded into the mixer of the "Mastek-Meteor" unit, where water was added, and the mixture was blended to obtain a semi-dry homogeneous mass. The mixture was then transferred to the unit hopper-doser, portioned, and supplied to the mold matrix. Shaping was performed by vibrocompression, forming a level and dense layer of expanded clay particles, water, and cement; three blocks were produced simultaneously, after which the molded blocks were manually removed with pallets and transported for natural curing.

The thermal conductivity of the samples was determined using an ITP-MG-4 “ZOND” thermal conductivity meter (SKB StroyPribor, Chelyabinsk, Russia). X-ray diffraction (XRD) of LECA and LWAC samples was performed using a Rigaku MiniFlex 600 diffractometer (Rigaku Corporation, Akishima-shi, Tokyo, Japan) with CuKα radiation in the 2θ range from 3° to 120°, and the collected data were processed using the PDF-5+ 2024 database.

3. Results and Discussion

Table 1 shows that the proposed LECA formulation improves aggregate strength while maintaining a broadly similar firing regime.

Table 1 – Effect of the developed formulation on LECA properties (pilot-industrial batch)

LECA type	Firing temperature, °C	Compressive strength, MPa	Bulk density, kg/m^3	Water absorption, %
Conventional	1200	1.38	316	25.85
Proposed	1150-1200	2.8-3.1	350-400	25.8

In Table 1, the most important change is compressive strength: it increases from 1.38 MPa to 2.8-3.1 MPa, which suggests the proposed formulation produces granules that are less prone to crushing during handling and concrete mixing. Bulk density also increases from 316 to 350–400 kg/m^3, indicating a trade-off toward a denser aggregate, which often accompanies higher strength in expanded clay systems. This direction is consistent with the general LECA overview that strength and density are strongly controlled by formulation and firing outcomes, including the balance between shell densification and internal porosity [6]. Water absorption remains essentially unchanged (25.85% vs. 25.8%), meaning the pore network accessible to water is not materially reduced. That is important for later concrete production, because high absorption typically requires moisture control or water adjustment to avoid variability in workability and matrix quality.

Table 2 summarizes the key performance envelope of the developed LWAC blocks as a structural-thermal material.

Table 2 – Physical, mechanical, and thermal properties of LWAC

Thermal conductivity, W/(m·K)	Density, kg/m^3	Water absorption, %	Compressive strength, MPa	Frost resistance, cycles
0.75-0.8	800-950	23-25	10-12	50-75

The reported density of 800-950 kg/m^3 confirms that the product is in the lightweight range, which is consistent with using expanded clay aggregate and with the general aim of reducing unit weight in wall elements [5]. The compressive strength of 10-12 MPa indicates that the blocks are positioned for load-bearing or at least structurally relevant masonry applications rather than purely insulating units, and this strength level is in line with the expectation that expanded-clay lightweight concretes can be designed to reach structural grades when mixture design and moisture management are controlled [6]. Thermal conductivity of 0.75-0.8 W/(m·K) suggests that the blocks provide a thermophysical improvement compared with dense concretes, but the value is still relatively high for a “single-layer” wall solution, so in practice the blocks may serve best as structural units with improved thermal performance rather than as a stand-alone high-insulation material. This is consistent with the fact that thermal conductivity in cementitious materials is strongly influenced by density and pore structure [7]. Water absorption of 23-25% is high, which implies an open pore network and highlights the importance of moisture-related durability, because higher absorption can increase susceptibility to freeze-thaw damage if saturation occurs. Therefore, the reported frost resistance of 50-75 cycles is an important supporting result for serviceability in cold climates.

Figure 2 presents the XRD diffractogram of the fired expanded clay (i.e., proposed LECA). The red curve is the measured diffraction pattern, while the colored reference markers correspond to the phases selected by the identification software/database and used to fit the experimental peaks. The legend also reports the phase fractions obtained from the software’s semi-quantitative evaluation.

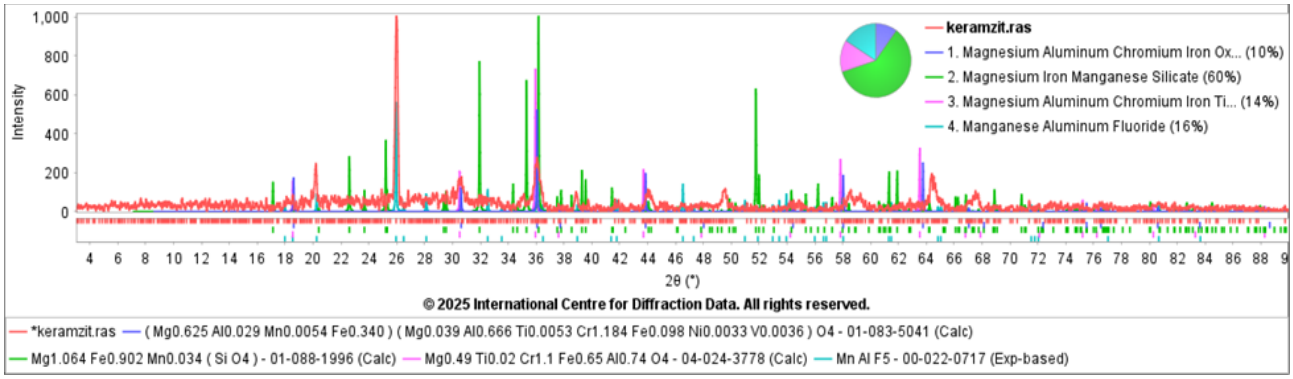

Figure 2 – Diffractogram of LECA

The pattern indicates that the expanded clay is not purely glassy; it contains a clear crystalline fraction. The dominant contribution in Figure 1 is the magnesium–iron–manganese silicate phase, reported as about 60%, because many of the strongest peaks align with that reference pattern. Two cubic spinel-type mixed oxides (Al–Cr–Fe–Mg–O with minor Ti) are also present and together account for a noticeable part of the fitted intensity (reported as 10% and 14%). These spinel-type phases are consistent with high-temperature firing, where Al- and Fe-bearing components of the raw clay can transform into stable mixed oxides. The diffractogram also reports a manganese aluminum fluoride contribution (about 16%). This identification is possible in peak-matching terms, but it is unusual for clay-derived LECA unless a fluorine source exists, so it should be treated as provisional until supported by chemistry or repeated fitting with alternative candidates.

Table 3 lists the phases identified in LECA and provides their crystallographic descriptors.

Table 3 – Phase identification results from XRD pattern fitting of LECA

No.	Compound name	Chemical formula	Crystal system	a (Å)	b (Å)	c (Å)	Unit-cell volume V (Å³)	Z	Space group	X-ray density ρ (g/cm³)
1	Magnesium aluminum chromium iron oxide (spinel)	$Al_{0.695}Cr_{1.184}Fe_{0.438}Mg_{0.664}O_4$	Cubic	8.25	–	–	561.74	8	Fd-3m	8.25
2	Magnesium aluminum chromium iron titanium oxide (spinel)	$Al_{0.74}Cr_{1.10}Fe_{0.65}Mg_{0.49}Ti_{0.02}O_4$	Cubic	8.28	–	–	567.27	8	Fd-3m	4.46
3	Magnesium iron manganese silicate	$(Fe_{0.902}Mg_{1.064}Mn_{0.034})_2SiO_4$	Orthorhombic	4.79	10.34	6.04	299.49	4	Pbnm	3.77
4	Manganese aluminum fluoride	$MnAlF_5$	Orthorhombic	9.54	9.85	3.58	336.41	–	Amam	–

Table 3 confirms that phases 1 and 2 are cubic spinels (space group Fd-3m) with very similar lattice constants (a about 8.25–8.28 Å), which supports the interpretation that they represent a family of closely related high-temperature mixed oxides. In practice, such phases are generally chemically stable and can contribute to the aggregate's mechanical integrity. Phase 3 is an orthorhombic (Pbnm) magnesium-iron-manganese silicate with a, b, c values consistent with an olivine-type silicate. This matches the fact that it is the dominant phase in Figure 2 and is a plausible high-temperature product of silicate systems after firing. Phase 4 is reported as AlF_5Mn (orthorhombic, Amam). Because fluorides are not typical products of firing ordinary loams, this phase comes from database matching and requires confirmation. Overall, Figure 2 and Table 3 together support a fired LECA structure composed of a crystalline assemblage dominated by silicates with a secondary fraction of spinel-type oxides, which is consistent with a thermally treated clay-based ceramic aggregate rather than an amorphous material.

Figure 3 shows the XRD pattern of the LWAC. The red curve is the measured intensity versus 2θ, and the colored reference lines/markers correspond to the phases selected during pattern fitting. The pie chart in the figure reports the software-estimated phase fractions for the fitted set.

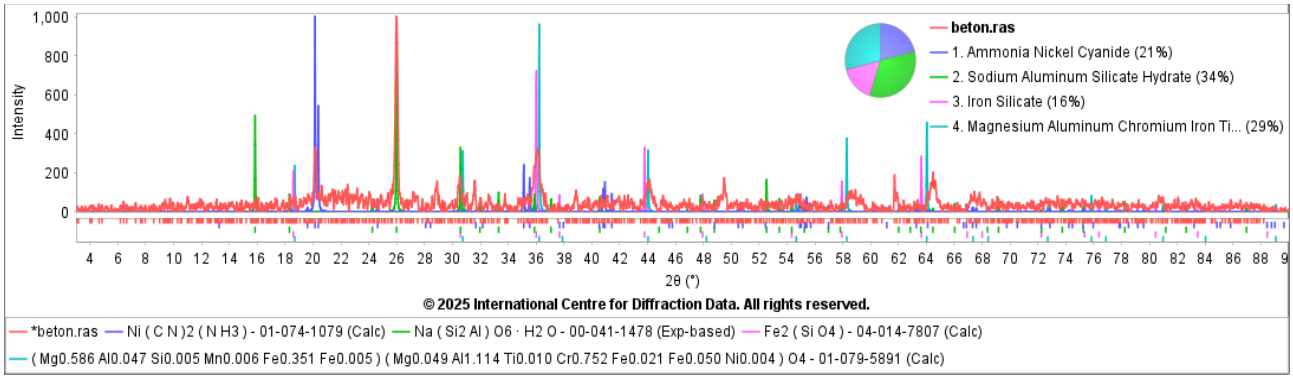

Figure 3 – Diffractogram of LWAC

From Figure 3, the LWAC sample is clearly not fully amorphous. Several sharp peaks indicate distinct crystalline contributions. The fitted phase set is dominated by a "sodium aluminum silicate hydrate" component (reported as 34%) and a spinel-type mixed oxide phase (reported as 29%). Such aluminosilicate-bearing phases are plausible in a system containing fired clay-based aggregate, since fired LECA commonly contains stable crystalline silicate constituents formed during high-temperature processing [6]. The spinel-type oxide contribution is also consistent with the idea that high-temperature firing of clay-based raw materials can yield stable mixed-oxide phases that remain present when the aggregate is incorporated into concrete [11]. Figure 3 also assigns about 16% to "iron silicate" and about 21% to a Ni-C-N phase ("ammonia nickel cyanide" in the figure legend). That last identification is unusual for cement/LECA-based concrete unless there is a credible nickel source, so it should be treated as a tentative match rather than a confirmed reaction product.

Table 4 lists the phases identified in LWAC and provides their crystallographic descriptors.

Table 4 – Phase identification results from XRD pattern fitting of LWAC

No.	Compound name	Chemical formula	Crystal system	a (Å)	b (Å)	c (Å)	Unit-cell volume V (Å³)	Z	Space group	X-ray density ρ (g/cm³)
1	Nickel cyanamide (as reported; requires verification)	$NiCN_2$	Tetragonal	7.22	–	17.42	908.58	8	I41/amd	1.86
2	Iron silicate (spinel-type, fayalite-related notation fixed)	Fe_2SiO_4	Cubic	8.26	–	–	564.46	8	Fd-3m	4.79
3	Magnesium aluminum chromium iron titanium oxide (spinel)	$Al_{1.161}Cr_{0.752}Fe_{0.427}Mg_{0.635}Ti_{0.01}O_4$	Cubic	8.22	–	–	555.19	8	Fd-3m	4.18
4	Analcime	$NaAlSi_2O_6·H_2O$	Cubic	13.71	–	–	2575.13	16	Ia-3d	2.27

Table 4 indicates that two of the identified phases are cubic spinel-structured oxides (Fd-3m) with lattice parameters around 8.22-8.26 Å. This supports the interpretation that a portion of the crystalline signal in LWAC comes directly from the fired aggregate, because spinel-type mixed oxides are typical high-temperature products in clay-derived ceramics and can persist unchanged in the concrete composite [11]. Analcime is a crystalline sodium aluminosilicate hydrate (a zeolite). Its presence could be consistent with an aluminosilicate framework phase in a system containing clay-derived components and alkaline pore solutions, but the manuscript cannot claim a formation mechanism from XRD fitting alone. The $NiCN_2$ assignment remains the weakest point: it is difficult to reconcile with the intended raw materials of LWAC, so it should be flagged as needing verification against alternative database matches, especially because cementitious systems often contain crystalline hydrates (for example, portlandite or ettringite) that may be missed or misassigned if the fitting is constrained. This matters for interpretation because the reviewed literature emphasizes that

performance in LWAC depends strongly on mixture design, moisture control, and microstructure rather than on any single unusual crystalline phase [5].

4. Conclusions

Lightweight expanded clay aggregate (LECA) produced from local low-expanding loams with an oil-sludge-based fuel-containing additive provided a clear mechanical advantage: its compressive strength increased from 1.38 MPa to 2.8-3.1 MPa, while bulk density rose moderately (316 to 350-400 kg/m^3) and water absorption stayed nearly unchanged (~25.8%). Using this LECA in vibro-pressed lightweight aggregate concrete (LWAC) wall blocks resulted in a lightweight density of 800-950 kg/m^3 and compressive strength of 10-12 MPa, with 0.75-0.8 W/(m·K) thermal conductivity and 50-75 freeze-thaw cycles, confirming applicability as structural wall units with improved thermal performance. XRD-based phase fitting indicates the presence of mainly spinel-type and silicate-related crystalline phases in LECA/LWAC; however, several identified matches should be treated as provisional and verified by complementary analyses. Future work should primarily address moisture sensitivity (high water absorption), including optimization of curing/conditioning and durability testing under higher saturation and service-relevant exposure regimes.

References

[1] L. Pérez-Lombard, J. Ortiz, and C. Pout, "A review on buildings energy consumption information," *Energy and Buildings*, vol. 40, no. 3, pp. 394–398, 2008, doi: 10.1016/j.enbuild.2007.03.007.

[2] M. Niziurska, M. Wieczorek, and K. Borkowicz, "Fire Safety of External Thermal Insulation Systems (ETICS) in the Aspect of Sustainable Use of Natural Resources," *Sustainability*, vol. 14, no. 3, p. 1224, Jan. 2022, doi: 10.3390/su14031224.

[3] B. Zhou, H. Yoshioka, T. Noguchi, and T. Ando, "Experimental study of expanded polystyrene (EPS) External Thermal Insulation Composite Systems (ETICS) masonery façade reaction-to-fire performance," *Thermal Science and Engineering Progress*, vol. 8, pp. 83–92, Dec. 2018, doi: 10.1016/j.tsep.2018.08.002.

[4] M. C. Juárez, M. P. Morales, P. Muñoz, and M. A. Mendívil, "Influence of horizontal joint on the thermal properties of single-leaf walls with lightweight clay blocks," *Energy and Buildings*, vol. 49, pp. 362–366, June 2012, doi: 10.1016/j.enbuild.2012.02.033.

[5] K.-C. Thienel, T. Haller, and N. Beuntner, "Lightweight Concrete - From Basics to Innovations," *Materials*, vol. 13, no. 5, p. 1120, Mar. 2020, doi: 10.3390/ma13051120.

[6] A. M. Rashad, "Lightweight expanded clay aggregate as a building material – An overview," *Construction and Building Materials*, vol. 170, pp. 757–775, May 2018, doi: 10.1016/j.conbuildmat.2018.03.009.

[7] K.-H. Kim, S.-E. Jeon, J.-K. Kim, and S. Yang, "An experimental study on thermal conductivity of concrete," *Cement and Concrete Research*, vol. 33, no. 3, pp. 363–371, Mar. 2003, doi: 10.1016/S0008-8846(02)00965-1.

[8] K. S. Chia and M.-H. Zhang, "Water permeability and chloride penetrability of high-strength lightweight aggregate concrete," *Cement and Concrete Research*, vol. 32, no. 4, pp. 639–645, Apr. 2002, doi: 10.1016/S0008-8846(01)00738-4.

[9] J. A. Bogas, A. Gomes, and M. F. C. Pereira, "Self-compacting lightweight concrete produced with expanded clay aggregate," *Construction and Building Materials*, vol. 35, pp. 1013–1022, Oct. 2012, doi: 10.1016/j.conbuildmat.2012.04.111.

[10] S. Real, J. A. Bogas, M. D. G. Gomes, and B. Ferrer, "Thermal conductivity of structural lightweight aggregate concrete," *Magazine of Concrete Research*, vol. 68, no. 15, pp. 798–808, Aug. 2016, doi: 10.1680/jmacr.15.00424.

[11] M. Bernhardt, H. Justnes, H. Tellesbø, and K. Wiik, "The effect of additives on the properties of lightweight aggregates produced from clay," *Cement and Concrete Composites*, vol. 53, pp. 233–238, Oct. 2014, doi: 10.1016/j.cemconcomp.2014.07.005.

[12] S. N. Monteiro and C. M. F. Vieira, "Effect of oily waste addition to clay ceramic," *Ceramics International*, vol. 31, no. 2, pp. 353–358, Jan. 2005, doi: 10.1016/j.ceramint.2004.05.002.

[13] J. D. Martínez, S. Betancourt-Parra, I. Carvajal-Marín, and M. Betancur-Vélez, "Ceramic light-weight aggregates production from petrochemical wastes and carbonates (NaHCO3 and CaCO3) as expansion agents," *Construction and Building Materials*, vol. 180, pp. 124–133, Aug. 2018, doi: 10.1016/j.conbuildmat.2018.05.281.

[14] C. Burbano-Garcia, A. Hurtado, Y. F. Silva, S. Delvasto, and G. Araya-Letelier, "Utilization of waste engine oil for expanded clay aggregate production and assessment of its influence on lightweight concrete properties," *Construction and Building Materials*, vol. 273, p. 121677, Mar. 2021, doi: 10.1016/j.conbuildmat.2020.121677.

[15] Z. Xing, C. Djelal, Y. Vanhove, and H. Kada, "Wood Waste in Concrete Blocks Made by Vibrocompression," *Environ. Process.*, vol. 2, no. S1, pp. 223–232, Nov. 2015, doi: 10.1007/s40710-015-0104-4.

[16] E. Widayanto, A. Soehardjono, W. Wisnumurti, and A. Zacoeb, "The effect of vibropressing compaction process on the compressive strength based concrete paving blocks," *AIMS Materials Science*, vol. 7, no. 3, pp. 203–216, 2020, doi: 10.3934/matersci.2020.3.203.
[17] L. Dvorkin, V. Zhitkovsky, and Y. Ribakov, "Design of Technological Parameters for Vibrocompression of Gypsum Concrete," *Materials*, vol. 18, no. 16, p. 3902, Aug. 2025, doi: 10.3390/ma18163902.
[18] F. Zhang, T. H. Tan, S. S. Sinoh, C.-C. Hung, and K. H. Mo, "Interaction of various parameters on the properties of semi-dry gypsum-based blocks produced by compression forming method," *Construction and Building Materials*, vol. 411, p. 134479, Jan. 2024, doi: 10.1016/j.conbuildmat.2023.134479.
[19] *GOST 33126-2014 Expanded clay concrete blocks. Specifications*. Moscow, Russia: Standardinform, 2015.
[20] *GOST 31108-2016 Common cements. Specifications*. Moscow, Russia: Standardinform, 2019.
[21] *GOST 8736-2014 Sand for construction works. Specifications*. Moscow, Russia: Standardinform, 2019.
[22] *GOST 32496-2013 Fillers porous for light concrete. Specifications*. Moscow, Russia: Standardinform, 2014.
[23] K. A. Bisenov, S. A. Montaev, R. A. Narmanova, and N. O. Appazov, "Ekologo-ekonomicheskie perspektivy ispolzovaniya nefteshlamov v sostave keramzita," *Science News of Kazakhstan*, vol. 132, no. 2, pp. 79–89, 2017.
[24] K. A. Bisenov, R. A. Narmanova, S. A. Montaev, and N. O. Appazov, "Resursosberegayushie tehnologii effektivnoj utilizacii othodov neftedobychi," *Oil and Gas*, vol. 99, no. 3, pp. 128–138, 2017.

Information about authors:
Roza Narmanova – Candidate of Technical Sciences, Docent, Laboratory of Engineering Profile "Physical and Chemical Methods of Analysis", Korkyt Ata Kyzylorda University, Kyzylorda, Kazakhstan, roza_an@mail.ru
Kylyshbai Bissenov – Doctor of Technical Sciences, Professor, Institute of Engineering and Technology, Korkyt Ata Kyzylorda University, Kyzylorda, Kazakhstan, bisenov_ka@mail.ru
Nargul Saktaganova – PhD, Institute of Engineering and Technology, Korkyt Ata Kyzylorda University, Kyzylorda, amanovna.75@mail.ru
Sergiy Liubchik – PhD, DeepTechLab, Faculty of Engineering, Lusófona University, Lisbon, Portugal, p6349@ulusofona.pt
Nurlybek Kelmagambetov – Candidate of Technical Sciences, Department of Engineering and Logistics, Kyzylorda Bolashak University, Kyzylorda, Kazakhstan, nkelmagambetov@mail.ru

Author Contributions:
Roza Narmanova – resources, data collection, editing, drafting, funding acquisition
Kylyshbai Bisenov – concept, methodology.
Nargul Saktaganova – testing, interpretation.
Sergiy Lyubchyk – analysis.
Nurlybek Kelmagambetov – modeling, visualization.

Conflict of Interest: The authors declare no conflict of interest.

Use of Artificial Intelligence (AI): The authors declare that AI was not used.

Received: 17.07.2025
Revised: 13.12.2025
Accepted: 14.12.2025
Published: 16.12.2025

Technobius, 2025, 5(4), 0091, DOI: https://doi.org/10.54355/tbus/5.4.2025.0091

Technobius

https://technobius.kz/

e-ISSN 2789-7338

Article

Low thermal conductivity silica ceramics based on diatomite modified with loam

Azamat Taskaliev*, Bekbulat Shakeshev, Kanat Narikov, Beksultan Idrisov, Kamar Dzhumabaeva

West Kazakhstan Innovation and Technological University, Uralsk, Republic of Kazakhstan
*Correspondence: taskalievazamat@mail.ru

Abstract. This study investigates diatomite-based silica ceramics designed for low thermal conductivity, using diatomite from the Utesai deposit (Aktobe region, Kazakhstan) and loam from the Romanovskoye deposit (West Kazakhstan region, Kazakhstan) as a modifying additive. The raw diatomite is characterized by high porosity and low thermal conductivity, while the ground fraction shows favorable technological behavior for ceramic processing, including low drying sensitivity. Calcination at 950 °C increases density and thermal conductivity, indicating partial densification. Silica-ceramic specimens were produced by plastic and semi-dry molding and fired at 950 °C, both from pure diatomite and from a diatomite-loam composition. The results show that 10% loam addition improves the fired structure: density and strength increase, whereas water absorption and total shrinkage decrease, with only minor changes in thermal conductivity. The combined trends demonstrate the feasibility of producing lightweight silica ceramics with improved integrity while maintaining heat-insulating performance.
Keywords: diatomite, silica ceramics, loam additive, thermal conductivity, water absorption.

1. Introduction

Diatomite is a biochemical rock belonging to the group of siliceous stones [1], consisting of minerals of the silicon oxide group - opal - amorphous silica [2]. Diatomite deposits are stratiform in shape, and in some cases, they have the form of flattened lenses with a relatively consistent thickness [3]. Diatomite can be characterized as a loose or cemented siliceous rock, white or light gray in color, consisting of more than 50% of diatom shells, containing 70-98% silica, with high porosity up to 75% and low bulk density from 420 to 1250 kg/m^3 [4]. It is used as a hydraulic additive for the production of Portland cement, lightweight concrete, ceramic and thermal insulation products, filler for the production of plastics, rubber, and paints [5].

The construction industry is currently focused on expanding its raw material base through the use of low-plasticity clays, loams, opal-cristobalite, and other silica-containing rocks [6]. In this regard, the industrial use of diatomite is based on a number of its physical and chemical properties that allow it to be used as a multi-purpose raw material, such as sound and heat conductivity, resistance to chemical reactions, and fire resistance [7].

[8] studied the effect of firing temperatures of 900, 1000, and 1100 °C on the transformation of the silicon dioxide phase during the manufacture of ceramic products from diatomite. Diffractometry results confirm the suitability of diatomite for the production of ceramic, construction, and thermal insulation materials. According to [9], the effect of the elastic modulus of diatomite on porosity varies in the range from 240 to 50 MPa when the porosity of the medium changes from 20 to 60%, and the tensile strength of the material changes by ≈ 10 MPa with a change in porosity.

To obtain porous silica ceramics with firing temperatures of 1000, 1150, and 1300 °C, [10] used diatomite with an additive of boric acid in an amount of up to 2 %, which had a positive effect

on pore distribution. Studies of modified samples [11] of silica ceramics using clay, diatomite, and boric acid additives showed that the resulting materials had a low Young's modulus, which means they can be deformed under forces that negatively affect their strength.

According to [12], silica ceramics obtained at a firing temperature of 1000 °C had a compressive strength of 20.96 MPa and a thermal conductivity coefficient of 0.29 W/(m·K). In other studies, the strength was 35 MPa with a thermal conductivity coefficient of 0.16 W/(m·K) [13] and 50 MPa [14].

While previous studies have made progress in the physical and mechanical properties of silica ceramics, they mainly used firing temperatures of 1000 °C and above, which leaves a potential for reducing energy losses, an important aspect currently. Therefore, this research aims to develop a technology for the production of silica ceramics designed to minimize heat exchange between the environment and the interior of buildings and structures, with low heating and ventilation costs. The research results are important for the application of diatomite, a unique natural material, in providing high-quality building materials for civil and industrial buildings and structures.

2. Methods

This study incorporated a diatomite from the Utesai deposit (Aktobe region, Kazakhstan) as a main siliceous raw material, and a loam from the Romanovskoye deposit (West Kazakhstan region, Kazakhstan) as a modifying additive.

To determine the physical properties of the diatomite rock, cubic specimens (100 mm edge length) were prepared by sawing from diatomite pieces. The average density [15] was determined by weighing using ACS electronic scales (HUADE Ltd., Shanghai, China). Thermal conductivity [16] was measured using an ITP-MG-4 ZOND device ("Special Design Bureau Stroypribor" LLC, Chelyabinsk, Russia). For ceramic-technology studies, diatomite pieces were ground to obtain a fraction with particle sizes <2 mm (Figure 1) using an MShL-1 laboratory ball mill (NPK Mekhanobr-Technika, St. Petersburg, Russian Federation). To evaluate the effect of high-temperature treatment on diatomite properties, the <2 mm diatomite fraction was fired at 950 °C in an EKPS 50/1300 electric furnace (Smolensk SKTB SPU, Smolensk, Russia), producing calcined diatomite (i.e., thermolite).

Figure 1 – Finely ground (left) and fired (right) diatomite

Silica-ceramic laboratory specimens were produced as Ø50 mm × 50 mm cylinders. For forming and testing operations, an LO-257 mold (RNPO RusPribor LLC, St. Petersburg, Russia) and a PGM-50MG4 press (SKB Stroipribor LLC, Chelyabinsk, Russia) were used (Figure 2). Two forming routes were used [17]: plastic molding and semi-dry molding. Specimens were produced from (i) 100% diatomite and (ii) a mixture of 90% diatomite + 10% loam (by mass). After shaping, specimens were dried in an SNOL 67/350 unit (Smolensk SKTB SPU, Smolensk, Russia) and then fired at 950 °C in an EKPS 50/1300 electric furnace.

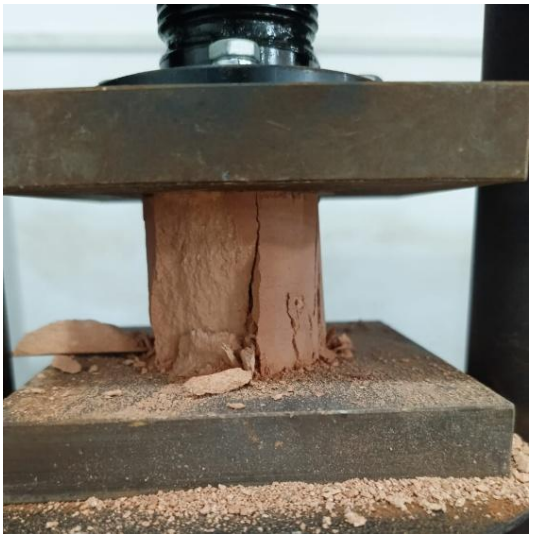

Figure 2 – Compression test of samples

For diatomite, the following properties were determined [18]: average density and thermal conductivity (rock cubes), bulk density, thermal conductivity, plasticity coefficient, adhesion (stickiness), and drying sensitivity coefficient (ground fraction).

For thermolite (calcined diatomite), bulk density and thermal conductivity were determined after firing at 950 °C.

For fired silica-ceramic specimens, the following properties were determined: average density, compressive strength, thermal conductivity, water absorption, and total shrinkage for both forming routes (plastic and semi-dry) and for both compositions (0% and 10% loam).

3. Results and Discussion

The diatomite rock shows (Table 1) a consistently low average density (~950 kg/m³) coupled with low thermal conductivity (~0.132 W/(m·K)) and very high porosity (~64%). Such a combination is characteristic of highly porous siliceous materials: the pore network reduces heat transfer, while also limiting mechanical load-bearing capacity. The small spread between replicate samples indicates stable properties for the studied diatomite source.

Table 1 – Physical properties of diatomite (100 mm rock cubes)

Sample	Average density, kg/m^3	Thermal conductivity, W/(m·K)	Porosity, %
1	948	0.131	64.1
2	952	0.133	63.9
3	950	0.132	64.0
Average value	950	0.132	64.0

For ceramic processing, the diatomite fraction (<2 mm) remains lightweight (bulk density ~410 kg/m³) and shows very low thermal conductivity (~0.098 W/(m·K)), consistent with its highly porous structure (Table 2). The plasticity coefficient (~5.88), low adhesion (~8.8 g/cm²), and very low drying sensitivity (~0.173) indicate that this diatomite fraction is weakly adhesive and relatively insensitive to drying, which is technologically favorable (less risk of drying cracks and less sticking to tooling). In contrast, loam is much denser (1425 kg/m³) and much more thermally conductive (0.84 W/(m·K)). It also has a substantially higher plasticity coefficient (15.6) and adhesion (22.3 g/cm²), meaning it can function as a binder/plasticizing component. However, its high drying sensitivity coefficient (1.8) implies that loam-rich bodies would be more prone to drying defects if drying is not controlled. Therefore, using loam as a limited additive is logically consistent: it can improve shaping/green strength and firing behavior without fully inheriting the drying risks of loam.

Table 2 – Comparison of average technological properties: diatomite vs loam

Material	Bulk density, kg/m^3	Thermal conductivity, W/(m·K)	Plasticity coefficient	Adhesion, g/sm^2	Drying sensitivity coefficient
Diatomite	410	0.098	5.88	8.8	0.173
Loam	1425	0.84	15.6	22.3	1.8

After firing the diatomite fraction at 950 °C, the bulk density increases markedly to ~725 kg/m³, while thermal conductivity rises to ~0.11 W/(m·K), as shown in Table 3. This increase is expected: firing reduces the open porosity and increases solid-phase connectivity (densification and/or partial sintering), which improves heat conduction through the solid skeleton. In practical terms, calcination shifts the material from an extremely porous powder to a denser, thermally more conductive product.

Table 3 – Bulk density and thermal conductivity of thermolite (calcined diatomite at 950 °C)

Sample	Bulk density, kg/m^3	Thermal conductivity, W/(m·K)
1	725	0.11
2	726	0.12
3	724	0.10
Average value	725	0.11

Table 4 shows the properties of silica ceramics produced by plastic molding.

Table 4 – Physical and mechanical properties of plastic-molded silica ceramics

Composition	Average density, kg/m^3	Strength, MPa	Thermal conductivity, W/(m·K)	Water absorption, %	Complete shrinkage, %
Diatomite	918.5	100	0.11	55	5.6
Diatomite (90%) and loam (10%)	1015.5	110	0.112	45	4.2

As is seen from Table 5, for plastic-molded silica ceramics fired at 950 °C, ceramics based on 100% diatomite show an average density of 918.5 kg/m³ and thermal conductivity of ~0.11 W/(m·K). Water absorption is high (55%), indicating a significant fraction of open pores, which is consistent with the raw diatomite's porous nature. Introducing 10% loam increases density (to 1015.5 kg/m^3) and strength (from 100 to 110), while reducing water absorption (from 55% to 45%) and total shrinkage (from 5.6% to 4.2%). The direction of these changes is internally consistent: loam likely promotes stronger particle bonding and a more continuous fired structure (better packing and/or formation of binding phases during firing), which reduces the volume of interconnected open pores. Thermal conductivity increases only slightly (from 0.11 to 0.112), which is expected when density increases and porosity decreases.

Table 5 shows the properties of silica ceramics produced by semi-dry molding.

Table 5 – Physical and mechanical properties of semi-dry molded silica ceramics

Composition	Average density, kg/m^3	Strength, MPa	Thermal conductivity, W/(m·K)	Water absorption, %	Complete shrinkage, %
Diatomite	1014.2	75	0.11	48	6.7
Diatomite (90%) and loam (10%)	1086.5	83	0.112	42	4.8

As is seen from Table 5, semi-dry molded ceramics show higher densities than plastic-molded ones for both compositions (1014.2 vs. 918.5 kg/m^3 for pure diatomite; 1086.5 vs. 1015.5 kg/m³ for the loam-containing mix). Correspondingly, water absorption is lower (48% vs. 55% for pure diatomite; 42% vs. 45% for the loam mix), which aligns with the denser structure. However, strength is lower for semi-dry molded samples than for plastic-molded samples (75 vs. 100 for pure diatomite; 83 vs. 110 for the loam mix), and total shrinkage is higher (6.7 vs. 5.6; 4.8 vs. 4.2). Interpreting these results together suggests that higher "bulk density" from semi-dry molding does not automatically

translate into higher mechanical performance; likely because strength is influenced not only by density but also by how uniformly particles bond and whether defects (e.g., lamination planes, incomplete interparticle contact, microcracking from constrained shrinkage) form during forming/drying/firing. Plastic molding can provide more uniform particle rearrangement and bonding, which may explain the higher measured strengths despite slightly lower densities. As in plastic molding, adding 10% loam improves the semi-dry results: density increases (from 1014.2 to 1086.5), strength rises (from 75 to 83), and water absorption drops (from 48% to 42), while shrinkage decreases (from 6.7% to 4.8). This supports the same functional role of loam as a reinforcing/structure-forming additive in fired bodies.

Across all datasets, the key controlling factor is porosity: the raw diatomite's very high porosity explains its low thermal conductivity, but it also leads to high water absorption in fired ceramics unless the structure is partially densified. Calcination increases density and thermal conductivity, indicating pore reduction and stronger solid connectivity.

For fired silica ceramics at 950 °C, the 10% loam addition consistently improves performance in both forming routes: it increases density and strength while reducing water absorption and shrinkage. This combination is technologically important because it indicates that small loam contents can enhance the integrity of the fired structure without causing a large penalty in thermal conductivity (only a slight increase is observed).

When comparing forming routes, semi-dry molding produces denser bodies with lower water absorption, but the measured strength is lower, and shrinkage is higher than for plastic molding. For applications where mechanical reliability is critical, the plastic-molding route appears more favorable based on the strength results reported, while semi-dry molding may be more suitable when lower water absorption (via higher density) is prioritized, especially when combined with a loam additive.

4. Conclusion

The investigated Utesai diatomite is a highly porous siliceous raw material (porosity ≈64%), which explains its low thermal conductivity (≈0.132 W/(m·K)) at a relatively low average density (≈950 kg/m³). In ground form (<2 mm), diatomite remains lightweight (bulk density ≈410 kg/m³) and thermally efficient (≈0.098 W/(m·K)) while showing low drying sensitivity, indicating good technological suitability for ceramic processing. Firing at 950 °C converts the diatomite into a denser, thermally more conductive product (thermolite: bulk density ≈725 kg/m³; thermal conductivity ≈0.11 W/(m·K)), consistent with partial densification and reduced open porosity.

Silica ceramics fired at 950 °C demonstrate that both the forming route and composition govern the balance between strength and moisture-related properties. Adding 10% loam to diatomite consistently improves performance in both plastic and semi-dry molding: density increases (by ~7-11%), strength rises (by ~10-11% as reported), water absorption decreases (by ~12-18%), and total shrinkage reduces (by ~25-28%), while thermal conductivity changes only slightly (from ≈0.11 to ≈0.112 W/(m·K)). Comparing forming routes, semi-dry molding yields higher density and lower water absorption, whereas plastic molding provides higher strength for the studied compositions. Overall, a diatomite-based body with a limited loam addition (10%) is the most balanced option among those tested, enabling low thermal conductivity alongside improved structural integrity and reduced water uptake.

References

[1] T. B. Zdorik, V. V. Matias, I. N. Timofeev, and L. G. Feldman, "Mineraly i gornye porody SSSR," Moscow, Russia: Mysl, 1970, p. 439.

[2] P. V. Smirnov *et al.*, "Diatomites and opoka from western Kazakhstan deposits: lithogeochemistry, structural and textural parameters, potential of use," *Bulletin of the Tomsk Polytechnic University. Geo Assets Engineering*, vol. 334, no. 7, pp. 187–201, July 2023, doi: 10.18799/24131830/2023/7/4046.

[3] M. N. Baranova, S. F. Korenkov, and N. G. Chumachenko, "The History of Development of Siliceous Rocks," *Stroitel'nye Materialy*, no. 8, pp. 4–7, 2011.

[4] A. S. Avramenko, M. V. Cherepanova, V. S. Pushkar', and S. B. Yarusova, "Diatom characteristics of the Far East siliceous organogenic deposits," *Russian Geology and Geophysics*, vol. 56, no. 6, pp. 947–958, June 2015, doi: 10.1016/j.rgg.2015.05.010.
[5] R. V. Sadakova, "Use of diatomite in agriculture," *Youth and science*, no. 2, p. 49, 2015.
[6] A. Yu. Stolboushkin, "Perspective Direction of Development of Building Ceramic Materials From Low-Grade Stock," *Stroitel'nye Materialy*, vol. 758, no. 4, pp. 24–28, 2018, doi: 10.31659/0585-430X-2018-758-4-24-28.
[7] M. A. Smirnov, "Penodiatomitovyj kirpich, osobennosti i primenenie," in *Proceedings of the IV Mezhdunarodnyj studencheskij stroitelnyj forum*, Tver, Russia: Tver State Technical University, 2019, pp. 331–334.
[8] A. Šaponjić *et al.*, "Porous ceramic monoliths based on diatomite," *Ceramics International*, vol. 41, no. 8, pp. 9745–9752, Sept. 2015, doi: 10.1016/j.ceramint.2015.04.046.
[9] M. Kokunesoski *et al.*, "Macroporous monoliths based on natural mineral sources, clay and diatomite," *Sci Sintering*, vol. 52, no. 3, pp. 339–348, 2020, doi: 10.2298/SOS2003339K.
[10] Skvortsov A. A., Nikolaev V. K., Luk'yanov M. N., and Chebeneva I. E., "On the issue of deformation and destruction of porous ceramics based on diatomite," *Physics of the Solid State*, vol. 65, no. 1, p. 120, 2023, doi: 10.21883/PSS.2023.01.54985.485.
[11] C. Nnaji, B. Afangideh, and C. Ezeh, "Performance evaluation of clay-sawdust composite filter for point of use water treatment," *Nig. J. Tech.*, vol. 35, no. 4, p. 949, Sept. 2016, doi: 10.4314/njt.v35i4.33.
[12] Kazan National Research Technological University, L. N. Nazharova, T. R. Shakirov, and Kazan National Research Technological University, "Ceramic materials with adjustable thermal insulation properties," *Herald of Technological University*, vol. 26, no. 12, pp. 107–113, 2023, doi: 10.55421/1998-7072_2023_26_12_107.
[13] E. I. Dudina and A. R. Smagina, "Izgotovlenie diatomitovogo penolegkoves," in *Proceedings of the XIII Mezhdunarodnyj molodezhnyj forum*, Belgorod, Russia: Belgorod State Technological University named after V.G. Shukhov, 2021, pp. 1590–1594.
[14] L. N. Nazharova, E. N. Filippovich, A. V. Skvorcov, and A. R. Valiullova, "Vliyanie diatomita i produktov ego pererabotki na obzhigovye svojstva keramicheskih izdelij," *Herald of Technological University*, vol. 15, no. 20, pp. 87–89, 2012.
[15] *GOST 17177-94 Thermal insulating materials and products for building application. Test methods*, IPK Izdatelstvo standartov. Moscow, Russia, 1994.
[16] *GOST 30256-94 Building materials and products. Method of thermal conductivity determination by cylindrical probe*, IPK Izdatelstvo standartov. Moscow, Russia, 1994.
[17] *GOST 530-2012 Ceramic brick and stone. General specifications*, Standartinform. Moscow, Russia, 2013.
[18] *GOST 21216-2014 Clay raw materials. Test methods*. Moscow, Russia: Standardinform, 2015.

Information about authors:

Azamat Taskaliev – Master of Technical Sciences, Lecturer, Department of Architecture and Civil Engineering, West Kazakhstan Innovation and Technological University, Uralsk, Republic of Kazakhstan, taskalievazamat@mail.ru
Bekbulat Shakeshev – Candidate of Technical Sciences, Rector, West Kazakhstan Innovation and Technological University, Uralsk, Republic of Kazakhstan, bekshakeshev@mail.ru
Kanat Narikov – Candidate of Technical Sciences, Lecturer, Department of Architecture and Civil Engineering, Uralsk, Republic of Kazakhstan, knarik1969@mail.ru
Beksultan Idrisov – Master of Technical Sciences, Lecturer, Department of Architecture and Civil Engineering, West Kazakhstan Innovation and Technological University, Uralsk, Republic of Kazakhstan, beksultan.idirisov@mail.ru
Kamar Dzhumabaeva – Master of Technical Sciences, Lecturer, Department of Architecture and Civil Engineering, West Kazakhstan Innovation and Technological University, Uralsk, Republic of Kazakhstan, zhumabaeva12.02.88@gmail.com

Author Contributions:

Azamat Taskaliev – concept, project making, analysis.
Bekbulat Shakeshev – resources, methodology.
Kanat Narikov – project making, editing.
Beksultan Idrisov – data collection, visualization.
Kamar Dzhumabaeva – testing, interpretation.

Conflict of Interest: The authors declare no conflict of interest.

Use of Artificial Intelligence (AI): The authors declare that AI was not used.

Received: 13.10.2025
Revised: 22.12.2025
Accepted: 23.12.2025
Published: 25.12.2025

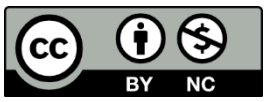

Technobius, 2025, 5(4), 0092, DOI: https://doi.org/10.54355/tbus/5.4.2025.0092

Technobius

https://technobius.kz/

e-ISSN 2789-7338

Article

Utilization of waste glass, ceramic scraps, and slag in manufacturing ceramic building materials

Zhanar Kaliyeva[1], Danara Mazhit[1], Gabit Satmagambetov[2], Kinga Korniejenko[3]

[1]Department of Technology of Industrial and Civil Engineering, L.N. Gumilyov Eurasian National University, Astana, Kazakhstan
[2]G-park, LLP, Astana, Kazakhstan
[3]Faculty of Materials Engineering and Physics, Cracow University of Technology, Cracow, Poland
*Correspondence: danara.08.1998@mail.ru

Abstract. This study examines the potential for reducing the consumption of natural clay raw materials while simultaneously recycling various types of waste in the production of clay ceramic materials. Crushed ceramics, thermal power plant slag, and cullet were used as technogenic components. The compositions were prepared using clay with varying waste content (5-20% by weight relative to clay) and the addition of an alkaline additive, NaOH (10% of the clay weight). After forming cylindrical samples, they were dried and fired at temperatures up to 1000 °C for 1 hour. The chemical composition of the raw materials was studied using XRF/EDS, and the microstructure was studied using SEM. Density, water absorption, linear shrinkage, and compressive strength were determined. The combined introduction of waste has a synergistic effect on the sintering processes and structure formation. Glass cullet acts as a fluxing agent and promotes compaction of the body, ceramic waste acts as an inert filler, reducing the risk of deformation, and slag introduces reactive aluminosilicate components that influence phase formation. An optimal waste content range has been demonstrated: moderate dosages improve performance without compromising processability. The best results were obtained with a composition of 10% glass cullet, 10% ceramic waste, and 5% slag (at 10% NaOH): compressive strength was 16 MPa, water absorption was approximately 7%, and density was approximately 1.32 g/cm^3. The results confirm the potential of integrated waste recycling for producing ceramic materials at lower firing temperatures.
Keywords: clay, glass waste, ceramic brick waste, slag, ceramics.

1. Introduction

The production of ceramic materials consumes a high proportion of natural clay resources, leading to the depletion of non-renewable raw materials, increased production costs, and the industrial waste accumulation. Despite the widespread use of industrial waste in ceramic production, issues such as the instability of the chemical and mineralogical composition of the waste, insufficient understanding of their combined effects in multicomponent systems, and the risk of deterioration in the strength and process properties of ceramics during firing raise many questions [1].

In recent years, a number of studies have focused on the partial or complete replacement of natural clay with man-made raw materials. The works [2], [3] have proven the possibility of using various technogenic materials in the production of ceramic bricks as additives, and in some compositions as the main raw material, partially or completely replacing non-renewable, exhaustible resources of clay rocks. The large volume of ceramic brick production allows the utilization of industrial waste in quantities and a wide range of their composition using traditional technology and equipment [4], [5]. In addition, the creation of raw material compositions using technogenic materials as additives is one of the ways to expand the scale of use of low-grade clay rocks, improve technical properties, and reduce the cost of the resulting ceramic bricks [6].

There is a slight increase in water absorption when the amount of brick powder in the batch increases. It tracks the dynamics of decreasing values for the samples' compressive strength, average density, thermal conductivity coefficient, and total shrinkage. [7] and [8] show that brick waste can be used in the current technology of ceramic brick grades M125 and M150 with a brick powder content of up to 30 weight percent in a two-component batch at a firing temperature of up to 950 °C.

More recent studies have considered alternative waste streams. For example, [9] explores the use of a composite mixture of brick waste powder and ceramic powder as a substitute for clay in brick production. The study shows that approximately 27% of the clay can be replaced with waste while maintaining the same density, porosity, and water absorption capacity as bricks containing 100% clay.

Waste from thermal power plants, particularly ash and slag, is also widely considered as raw materials for ceramic materials. Several studies have shown that these wastes contribute to the formation of a dense structure, a reduction in firing temperature, and an increase in strength properties [10], [11]. For example, adding thermal power plant slag to the ceramic mass, the sintering temperature affected the final materials' porosity. Because a compacted microstructure forms at higher temperatures, porosity decreases. Porosity increased with increasing CaO and Al_2O_3 concentration, porosity decreased with increasing MgO and Fe_2O_3 content, while permittivity and electrical conductivity increased. Firing at 1000-1200 °C yielded samples with a compressive strength of 45-60 MPa. The authors note that fly ash-based ceramics have a dense microstructure and low water absorption [10]. It dropped from sixteen percent to ten percent [11].

Another waste that we used in our work is glass waste, which has a high content of SiO_2, Na_2O, CaO, and Al_2O_3. The addition of crushed glass to clay reduces sintering temperatures, improves phase transformations during firing, and creates a denser microstructure. The authors looked at using leftover glass in red ceramics to replace up to 20% of the sand. Samples were burned at 800, 900, and 1000 °C. Density, flexural strength, and porosity all increased with the addition of 20% glass, reducing water absorption by 8-10% [12], [13].

Only a limited number of studies have addressed the combined use of wastes. In studies [14], [15], ceramic materials were produced from ash, slag, and cullet without the use of clay, achieving a strength of approximately 10 MPa at a firing temperature of approximately 1200 °C. As in our study, chemical and mineralogical analysis of the waste was conducted: X-ray fluorescence (XRF), X-ray diffraction (XRD), and scanning electron microscopy (SEM) to study the morphology and composition. In our work, we used ceramic waste as a third waste material. But the compressive strength results were similar: theirs was 10 MPa, ours was 9 MPa. The chemical composition of both works showed the predominance of the elements aluminum (25.8%) and silicon (53.7%). The most important difference between these works and ours is that we used clay as the main raw material, while they used waste.

In studies [16], [17], binary waste systems (ceramic cullet and glass, or slag and ceramic scrap) were considered; however, a comprehensive assessment of the synergistic effect of multicomponent systems was lacking. As in our work, the technology consisted of the use of ceramic brick waste and glass waste with the addition of clay; firing was carried out at 700-900 °C, and the difference is that they didn't add slag. The granules exhibited low water absorption (<5%) and high resistance to cyclic heating.

According to [17], to create ceramic tiles, they use steel slag and brick waste (ceramic scrap) crushed to powder form. Our material's moderate CaO and MgO content, along with its higher SiO_2 and Al_2O_3 content, ensures more stable sintering and prevents deformation during firing, according to a comparison of our XRF and XRD analysis results with published data. Cullet causes an amorphous glass phase to form, which densifies the structure, lowers porosity, and permits firing temperatures to be lowered to 900-1050 °C without compromising strength. The fact that we use cullet also provides advantages such as compaction of the structure, reduction of porosity, and allows us to reduce the firing temperature to 900-1050 °C while maintaining strength.

Thus, a literature review reveals insufficient study of ceramic materials produced using combined waste streams, particularly in systems where clay is retained as the primary raw material

[12], [14], [15], [16], [17], [18], [19]. The mutual influence of ceramic cullet, thermal power plant slag, and cullet on sintering processes, microstructure formation, and physical and mechanical properties at low firing temperatures remains understudied.

Therefore, the research problem of this study is the lack of optimized ceramic body compositions that would enable the simultaneous recycling of several types of industrial waste, reduce firing temperatures, and maintain stable material performance characteristics.

This study aims to develop and study clay-based ceramic materials using the integrated use of ceramic waste, thermal power plant slag, and glass cullet, as well as to evaluate their phase composition, microstructure, and physical and mechanical properties. It is expected that the combined use of various industrial wastes will achieve a synergistic effect, optimize chemical composition, and improve the environmental and economic efficiency of ceramic product production.

2. Methods

All raw materials, including clay, ceramic cullet, and slag used in this study, were collected from the SG Brick, LLP (Astana, Kazakhstan). Another waste material used was crushed bottle glass obtained from post-consumer glass waste (Astana, Kazakhstan). Caustic soda (NaOH, 98%, China) was used as an alkaline additive. Distilled water was used for the preparation of all mixtures.

The sensitivity of the clay to drying was determined using the Chizhsky method [20] in laboratory conditions. Plates measuring 10×10×1 cm were formed and dried over a heating device at a temperature of 200 °C. The Rutkovsky technique was used to estimate the granulometric composition of clay [20].

The microstructure of the samples was analyzed using a scanning electron microscope (SEM). To make the geopolymer surfaces electrically conductive, a thin layer of gold was applied. The analysis was carried out using a JSM-IT200 scanning electron microscope (JEOL, Tokyo, Japan). mA DII-29010SCTR Smart Coater (JEOL, Tokyo, Japan) was used for gold coating of the samples.

The chemical composition (elemental and oxide) of the specimens was determined using X-ray fluorescence spectroscopy (XRF). The research (Figure 1) was conducted with the EDX-7200 (SHIMADZU EUROPA GmbH, Duisburg, Germany); the PCEDX Navi software (Version: EDX-7000P) was used.

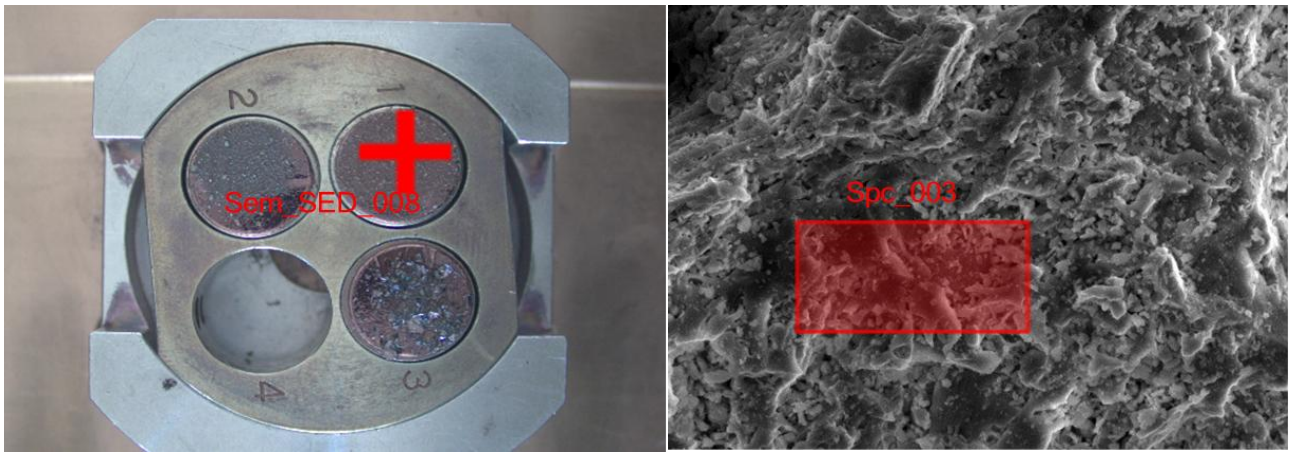

Figure 1 – EDS analysis of the selected point of the clay material

First, all raw materials (clay, crushed glass, ceramic cullet, and slag) were dried to constant mass and ground to the required particle size. The dry components were then mixed according to the designed compositions.

Cylindrical specimens were prepared using clay as the main raw material with the addition of glass waste, ceramic cullet, and slag. The content of each waste component varied individually and in combination, ranging from 5%, 10%, and 20% by weight relative to the clay content. NaOH

(caustic soda) was added to improve the strength of the compositions, 10% from the clay mass. NaOH was dissolved in water and then introduced into the dry mixture.

The prepared mixtures were molded into cylindrical samples with initial dimensions of 5×10 cm. After drying, the dimensions of the samples decreased to approximately 4.8×9.8 cm. Photographs of the dried samples are presented in Figure 2. The samples were dried in the drying machine SHS-80-01 SPU of the NV-LAB (Almaty, Kazakhstan) at 100 °C for 12 hours. The dried samples were fired in a laboratory muffle furnace SNOL 8.2 of the SNOL-TERM (Tver, Russia) at the selected sintering temperatures up to 1000 °C with a holding time of 1 hour, followed by furnace cooling.

Figure 2 – Waste-based ceramic samples after drying

Images of the fired samples after compressive strength testing are shown in Figure 3 to provide visual documentation of the experimental procedure and sample integrity. The tests were carried out on presses from the company "Controls" (Italy).

Figure 3 – Ceramic material tested for compressive strength

Samples were also tested to determine density, water absorption, and linear shrinkage. Water absorption was determined by weighing a dry and water-saturated sample. Bulk density was calculated using the dry mass of the sample divided by its geometrical volume. Linear shrinkage was calculated using the initial and final lengths of the samples before and after firing.

3. Results and Discussion

The results of Chizhsky's method showed that the clay is less sensitive to drying. Table 1 shows the granulometric composition of clay by the Rutkovsky method.

Table 1 – Granulometric composition of clay by the Rutkovsky method

Content of fractions, % by weight		
Sand particles of 1-0.05 mm	Dusty particles of 0.05-0.005 mm	Clay particles, less than 0.005 mm
33.75%	49.79%	16.46%

It was found that the majority of the material consists of silt particles 0.05-0.005 mm in size (49.79%), indicating the predominance of the fine fraction. The content of sand particles larger than 0.05 mm is 33.75%, while the proportion of clay particles smaller than 0.005 mm is 16.46%. According to literature, the predominance of the dust fraction promotes denser particle packing and positively influences the formation of the ceramic body structure during firing, ensuring uniform shrinkage and reducing internal stress [21]. The presence of the sand fraction acts as a leaning component, reducing shrinkage deformations during drying and firing and decreasing the tendency of the products to crack. This clay belongs to the sandy loam type, with a moderate content of sand and dust particles and a relatively low proportion of clay fraction. This ensures satisfactory plasticity during molding and a low tendency to crack during drying. At the same time, the clay content ensures sufficient plasticity of the mass, necessary for molding ceramic products [22].

Air shrinkage was calculated using the findings of measuring the samples' size change upon drying. Table 2 indicates the physical results after firing the clay.

Table 2 – Results after firing

Firing temperature	Average density, g/cm^3	Linear fire shrinkage, %	Volumetric fire shrinkage, %	Linear total shrinkage, %	Volumetric total shrinkage, %
950	1.73	0.30	0.48	3.65	8.65
960	1.75	0.47	1.80	4.1	8.89

According to Table 2, increasing the firing temperature from 950 °C to 960 °C results in an increase in average density from 1.73 to 1.75 g/cm^3. This indicates compaction of the ceramic body. At higher temperatures, diffusion processes are enhanced, leading to denser particle packing and a reduction in pore space. Linear shrinkage during firing increases from 0.30% to 0.47%, while volumetric shrinkage increases from 0.48% to 1.80%. This indicates that volumetric shrinkage is more sensitive to temperature changes. Linear total shrinkage increases from 3.65% to 4.1%, while volumetric shrinkage increases from 8.65% to 8.89%. This suggests that increasing the firing temperature to 960 °C enhances material compaction without causing excessive deformation [23].

Figure 4 shows the clay’s microstructure analysis report by scanning electron microscope.

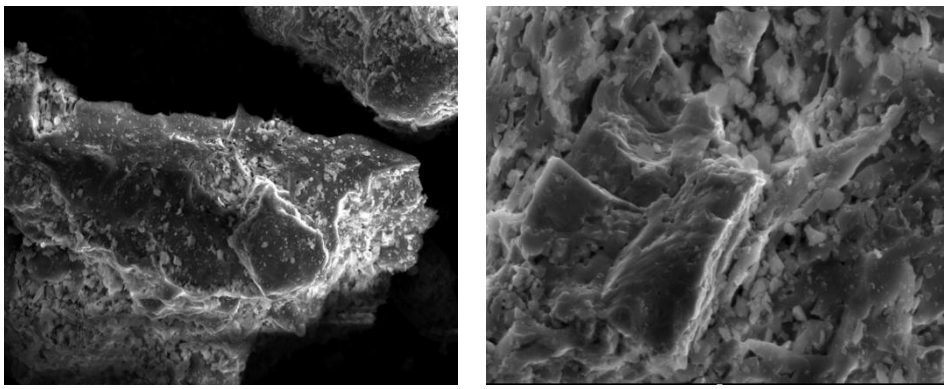

a) Magnification 1000x b) Magnification 3500x

Figure 4 – Micrograph of clay

According to the image at 1000x magnification, particles measuring 20–30 µm in length have a layered, laminar structure with distinct edges and fracture planes characteristic of layered minerals such as kaolinite, montmorillonite, or illite. At 3500x magnification, particles measuring 0.2–1.5 µm with a scaly relief indicate the presence of montmorillonite. It was noticed in [24] too.

The chemical composition of clay by element is shown in Table 3 (Figure 1).

Table 3 – Element-by-element composition of clay, %

O	Mg	Na	Al	Si	K	Fe
45.26	0.95	2.26	16.3	26.21	4.97	4.05

Utilizing energy-dispersive X-ray spectroscopy (EDS), the elemental makeup of the clay sample was ascertained. We were able to determine the primary oxides that make up the material's structure. The spectrum contained the following elements: O, Si, Al, Fe, Mg, Na, and K. Oxygen (O) ensures the stability of the crystal lattice and binds metals to form stable oxides. Silicon (Si) is responsible for hardness, chemical resistance, and the formation of quartz and glassy phases. Aluminum (Al) increases refractoriness and promotes the formation of mullite ($3Al_2O_3$ $2SiO_2$), which provides high strength and fire resistance. Magnesium (Mg) improves heat and chemical resistance and participates in the formation of high-temperature phases. Sodium (Na) and Potassium (K) act as fluxing elements, accelerating the sintering process. They promote the formation of the glassy phase, reduce porosity, and increase mechanical strength [8].

Table 4 displays the findings of the chemical composition of clay by oxides.

Table 4 – Oxide chemical composition of clay, %

Na_2O	MgO	Al_2O_3	SiO_2	K_2O	FeO
2.98	1.54	30.08	54.51	5.81	5.07

Good brick clay contains Al_2O_3 in the range of 20-30%, SiO_2 in the range of 50-60%, CaO in the range of 1-5%, and Fe_2O_3 in the range of 5-6% [25], [26]. SiO_2 determines plasticity, heat resistance, and shrinkage during firing; Al_2O_3 and MgO impart strength, fire resistance, and other oxides reduce the melting temperature and improve sintering [27].

Figure 5 shows the chemical composition of slag obtained by XRF analysis.

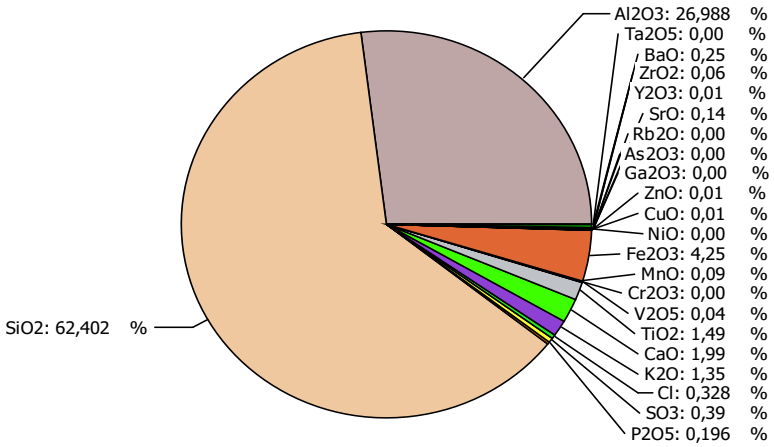

Figure 5 – Chemical composition of slag

SiO_2 and Al_2O_3 make up the majority of these ashes, with trace quantities of Fe_2O_3, K_2O, SO_3, and CaO. Its chemical makeup is comparable to what other writers have described [28], [29]. The high silica content is similar to that found in clays used for ceramic bricks, making the material suitable for replacing part of the clay. Al_2O_3 aids in the synthesis of mullite ($3Al_2O_3$ $2SiO_2$). Both oxides are responsible for the mechanical strength and heat resistance of ceramics. Fe_2O_3 content of

up to 6% ensures normal fusibility without the risk of overfiring [12]. The oxides CaO, MgO, K_2O, TiO_2, and SO_3 are present in small quantities (less than 2%). They primarily reduce the sintering temperature and form a liquid phase.

Figure 6 shows the percentage of oxides in glass waste.

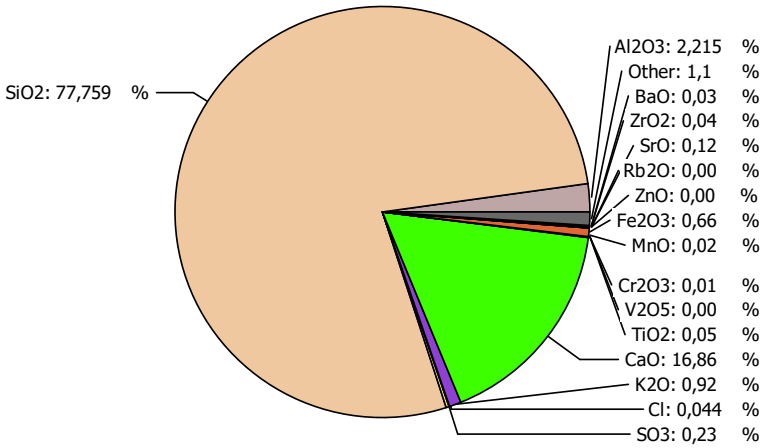

Figure 6 – Chemical composition of glass waste

Silicon dioxide is the main component of glass waste [30]. A SiO_2 content of 70-73% indicates the amorphous nature of the glass, which is capable of forming a stable silicate structure. Calcium oxide acts as a stabilizer for the glass structure. The total content of the remaining oxides does not exceed 3%, so they do not significantly affect the chemical balance of the material. However, they certainly contribute to the formation of a homogeneous microstructure [31].

Figure 7 demonstrates the chemical composition of ceramic broken brick waste.

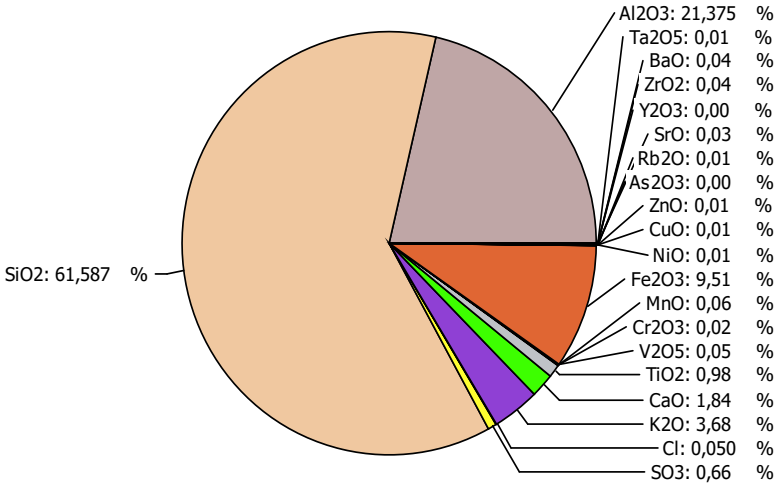

Figure 7 – Chemical composition of broken brick waste

According to X-ray fluorescence (XRF) data from a number of open-source studies [17], ceramic waste is characterized by a predominance of SiO_2, Al_2O_3, and Fe_2O_3, with low contents of CaO, MgO, and Na_2O, which we also observe in our work. These oxides explain the appearance of anorthite/diopside/gehlenite phases in the system during co-sintering with slag. Ceramic waste acts as a structural filler and flux. Together with cullet and slag, it contributes to the compaction of the microstructure. This combination of waste allows for the optimization of the chemical composition of the ceramic material, improving its strength characteristics and reducing energy costs during firing.

10 % glass paint, 10 % ceramic paint, 5 % slag, and 10 % caustic soda were used in quantities to establish the sample's maximum compressive strength of 16 MPa. Glass begins to soften and melt at temperatures of 700-900 °C, filling the pores between clay particles and promoting sintering. This

improves particle adhesion and reduces porosity, which directly increases compressive strength [24]. The total amount of waste was 25%, which is similar to the study where the waste was 25%-30% [8], [9].

Ceramic cullet acts as an inert filler, reducing shrinkage during drying and firing [32]. Slag promotes the formation of additional silicate and aluminosilicate phases [33].

The compressive strength of the material was 16 MPa. The water absorption of the samples was 7%. A reduction in size of 0.2 cm corresponds to approximately 4% shrinkage in diameter and 2% in height. The density of the samples is approximately 1.32 g/cm^3.

4. Conclusions

The present study showed that wastes such as glass, ceramic cullet, and thermal power plant slag are effective at using them in ceramic production. Granulometric analysis of the clay revealed that it is a moderately plastic clay with low drying sensitivity.

The stable functional roles of the components in the multicomponent system were established. Glass cullet acts primarily as a fluxing component: during firing, it promotes the formation of a liquid phase, intensifies sintering, and leads to microstructural compaction. Ceramic waste acts as an inert filler, stabilizing the formation and behavior of the mass during firing by reducing its tendency to excessive shrinkage and deformation.

It has been shown that such a system is characterized by an optimal waste content range: moderate dosages provide a positive (synergistic) effect and improve operationally significant characteristics, whereas excessive replacement of clay with waste can disrupt the sintering balance and lead to the preservation of porosity, which limits strength and increases water absorption. This confirms that the properties of multicomponent mixtures are not simply the sum of the effects of individual additives and require targeted optimization of the composition.

Thus, the integrated use of glass cullet, ceramic waste, and slag in a clay base is a technologically feasible approach for the simultaneous recycling of several types of industrial waste, reducing the consumption of natural clay and potentially reducing firing energy consumption by intensifying sintering processes. Promising areas for further research include assessing durability (including frost resistance), the reproducibility of properties with varying waste composition, and the environmental safety of materials (particularly in terms of leaching properties).

References

[1] S. Javed *et al.*, “Strategies and pathways to improve circularity in ceramic tile production,” *Journal of Cleaner Production*, vol. 517, p. 145788, July 2025, doi: 10.1016/j.jclepro.2025.145788.

[2] I. G. Dovzhenko, “The influence of metallurgical slurries on drying behaviour of ceramic masses for lining brick production,” *Glass and Ceramics*, vol. 86, no. 12, pp. 24–27, 2013.

[3] A. Yu. Stolboushkin, G. I. Berdov, O. A. Stolboushkina, and V. I. Zlobin, “Firing temperature impact on structure forming in ceramic wall materials produced of fine dispersed iron ore enrichment wastes,” *News of higher educational institutions. Construction*, vol. 661, no. 1, pp. 33–41, 2014.

[4] A. G. Tkachev, E. A. Yatsenko, V. A. Smoliy, A. S. Kosarev, and E. B. Dzyuba, “Influence of coal-mining waste on forming, drying and roasting properties of ceramic weight,” *Technique and technology of silicates*, vol. 20, no. 2, pp. 17–21, 2013.

[5] V. Z. Abdrahimov and I. V. Kovkov, “Ekologicheskie, teoreticheskie i tehnologicheskie principy ispolzovaniya fosfornogo shlaka i zoloshlakovogo materiala v proizvodstve vysokomarochnogo keramicheskogo kirpicha,” in *monograph*, Centr Perspektiv. Razvitiya., Samara, Russia, 2009, p. 154.

[6] N. T. Andrianov *et al.*, “Himicheskaya tehnologiya keramiki,” in *Textbook for universities*, Moscow, Russia: Rif Strojmaterialy, 2012, p. 496.

[7] A. I. Fomenko, V. S. Gryzlov, and A. G. Kartyushina, “Waste of ceramic brick as effective component of building composite materials,” *Modern high technologies*, no. 2–2, pp. 260–264, 2016.

[8] A. I. Fomenko, A. G. Kaptyushina, and V. S. Gryzlov, “Expansion of Raw Material Resources Base for Construction Ceramics,” *Construction Materials*, no. 12, pp. 25–27, 2015, doi: 10.31659/0585-430X-2015-732-12-25-27.

[9] A. Khitab *et al.*, “Manufacturing of Clayey Bricks by Synergistic Use of Waste Brick and Ceramic Powders as Partial Replacement of Clay,” *Sustainability*, vol. 13, no. 18, p. 10214, Sept. 2021, doi: 10.3390/su131810214.

[10] R. P. Dos Santos *et al.*, "Coal Fly Ash Ceramics: Preparation, Characterization, and Use in the Hydrolysis of Sucrose," *The Scientific World Journal*, vol. 2014, no. 1, pp. 1–7, 2014, doi: 10.1155/2014/154651.
[11] P. S. Minakova, A. V. Taskin, and I. I. Nadtochiy, "Production of high-strength ceramics from ash and slag waste," *Tendencii razvitiya nauki i obrazovaniya*, vol. 78, no. 2, pp. 105–107, 2021, doi: 10.18411/trnio-10-2021-69.
[12] G. Delaqua *et al.*, "Application of Glass Waste on Red Ceramic to Improve Sintering," *Sustainability*, vol. 14, no. 16, p. 10454, Aug. 2022, doi: 10.3390/su141610454.
[13] L. Barbieri, A. Corradi, and I. Lancellotti, "Bulk and sintered glass-ceramics by recycling municipal incinerator bottom ash," *Journal of the European Ceramic Society*, vol. 20, no. 10, pp. 1637–1643, Sept. 2000, doi: 10.1016/S0955-2219(00)00032-7.
[14] Diana. M. A. Valderrama, J. A. G. Cuaspud, L. Paredes-Madrid, Comprehensive Management of Agro-industrial Productivity and Services GISPA, Santo Tomas University, Tunja, Av. Universitaria, No. 45-202. Tunja, Boyacá, Colombia, Institute for Research and Innovation in Materials Science and Technology, Pedagogical and Technological University of Colombia, Av. Central del Norte, 39-115, Tunja, Boyacá, Colombia, and Faculty of Mechanic, Electronic and Biomedical Engineering, Universidad Antonio Nariño, Tunja 150001, Colombia, "Physical analysis and production-mechanics of glass-ceramic prototypes made by sintering cold-compacted powder samples (10% slag, 70% fly ash and 20% glass cullet)," *AIMS Materials Science*, vol. 8, no. 4, pp. 538–549, 2021, doi: 10.3934/matersci.2021033.
[15] D. M. Ayala Valderrama, J. A. Gómez Cuaspud, J. A. Roether, and A. R. Boccaccini, "Development and Characterization of Glass-Ceramics from Combinations of Slag, Fly Ash, and Glass Cullet without Adding Nucleating Agents," *Materials*, vol. 12, no. 12, p. 2032, June 2019, doi: 10.3390/ma12122032.
[16] E. Siedlecka, J. Siedlecki, B. Bednarski, and S. Białek, "From Waste to Resource: Circular Economy Approaches to Valorize Fine Glass, Ceramic, and Plastic Residues in a Glass Recycling Plant," *Sustainability*, vol. 17, no. 17, p. 7966, Sept. 2025, doi: 10.3390/su17177966.
[17] Y. Ji, E. Li, G. Zhu, R. Wang, and Q. Sha, "Preparation and Performance of Ceramic Tiles with Steel Slag and Waste Clay Bricks," *Materials*, vol. 17, no. 8, p. 1755, Apr. 2024, doi: 10.3390/ma17081755.
[18] G. A. Khater, B. S. Nabawy, A. A. El-Kheshen, M. A.-B. Abdel Latif, and M. M. Farag, "Use of Arc Furnace Slag and Ceramic Sludge for the Production of Lightweight and Highly Porous Ceramic Materials," *Materials*, vol. 15, no. 3, p. 1112, Jan. 2022, doi: 10.3390/ma15031112.
[19] O. Gencel *et al.*, "Recycling industrial slags in production of fired clay bricks for sustainable manufacturing," *Ceramics International*, vol. 47, no. 21, pp. 30425–30438, Nov. 2021, doi: 10.1016/j.ceramint.2021.07.222.
[20] "GOST 21216-2014 Clay raw materials. Test methods," Moscow, Russia: Standardinform, 2015, p. 43.
[21] I. A. Ryb'ev, "Stroitelnoe materialovedenie," in *Uchebnoe posobie dlya stroitelnyh specialnostej vuzov*, Moscow, Russia: Vysshaya shkola, 2003, p. 701.
[22] C. Candeias, I. Santos, and F. Rocha, "Characterization and Suitability for Ceramics Production of Clays from Bustos, Portugal," *Minerals*, vol. 15, no. 5, p. 503, May 2025, doi: 10.3390/min15050503.
[23] S. Karaman, S. Ersahin, and H. Gunal, "Firing temperature and firing time influence on mechanical and physical properties of clay bricks," *Journal of scientific and industrial research*, vol. 65, no. 2, pp. 153–159, 2006.
[24] A. V. Hrachanikau, A. S. Kauchur, P. I. Manak, and I. A. Tsimanov, "Research on the effectiveness of using the additive of break glass in the production of ceramic materials," *Bulletin of Vitebsk State Technological University*, vol. 49, no. 3, pp. 85–96, 2024, doi: 10.24412/2079-7958-2024-3-85-96.
[25] A. Khitab, "Materials of Construction: Classical and Novel," Lahore, Pakistan: Allied Books, 2012.
[26] A. Khitab and W. Anwar, "Classical Building Materials," in *Advanced Research on Nanotechnology for Civil Engineering Applications:*, in Advances in Civil and Industrial Engineering. , Hershey, PA, USA: IGI Global, 2016, pp. 1–27. doi: 10.4018/978-1-5225-0344-6.
[27] X. Gu and Y. Ling, "Characterization and properties of Chinese red clay for use as ceramic and construction materials," *Science Progress*, vol. 107, no. 1, p. 00368504241232534, Jan. 2024, doi: 10.1177/00368504241232534.
[28] C. Argiz, A. Moragues, and E. Menéndez, "Use of ground coal bottom ash as cement constituent in concretes exposed to chloride environments," *Journal of Cleaner Production*, vol. 170, pp. 25–33, Jan. 2018, doi: 10.1016/j.jclepro.2017.09.117.
[29] S. Naganathan, A. Y. O. Mohamed, and K. N. Mustapha, "Performance of bricks made using fly ash and bottom ash," *Construction and Building Materials*, vol. 96, pp. 576–580, Oct. 2015, doi: 10.1016/j.conbuildmat.2015.08.068.
[30] R. M. Khattab, M. A. Marzouk, and H. E. H. Sadek, "Synthesis and characterization of kaolin glass cullet ceramics modified with transition metal oxides for enhanced mechanical and optical properties," *Sci Rep*, vol. 15, no. 1, p. 19337, June 2025, doi: 10.1038/s41598-025-03908-6.
[31] Y. Xin *et al.*, "Recycling Crushed Waste Beer Bottle Glass in Fired Clay Bricks," *Buildings*, vol. 11, no. 10, p. 483, Oct. 2021, doi: 10.3390/buildings11100483.
[32] T. N. Krasnova, "Effect of ceramic mass composition on the preservation of porous ceramic products," *The Heritage Institute journal*, vol. 42, no. 3, pp. 42–47, Aug. 2025, doi: 10.34685/HI.2025.47.95.029.
[33] O. V. Suvorova and D. V. Makarov, "Foam Glass and Foam Materials Based on Ash-Slag Wastes from Thermal Power Plants (Review)," *Glass Ceram*, vol. 76, no. 5–6, pp. 188–193, Sept. 2019, doi: 10.1007/s10717-019-00162-x.

Information about authors:
Zhanar Kaliyeva – Candidate of Technical Sciences, Associate Professor, Department of Technology of Industrial and Civil Engineering, L.N. Gumilyov Eurasian National University, Astana, Kazakhstan, zhanna-080477@mail.ru
Danara Mazhit – PhD Student, Department of Technology of Industrial and Civil Engineering, L.N. Gumilyov Eurasian National University, Astana, Kazakhstan, danara.08.1998@mail.ru
Gabit Satmagambetov – Director, G-Park, LLP, Astana, Kazakhstan, gsatmagambetov@mail.ru
Kinga Korniejenko – Professor, Faculty of Materials Engineering and Physics, Cracow University of Technology, Cracow, Poland, kinga.korniejenko@pk.edu.pl

Author Contributions:
Zhanar Kaliyeva – concept, methodology, funding acquisition.
Danara Mazhit – testing, modeling, interpretation, drafting.
Gabit Satmagambetov – data collection, analysis, visualization.
Kinga Korniejenko – editing, resources, review, specialized technical input.

Conflict of Interest: The authors declare no conflict of interest.

Use of Artificial Intelligence (AI): The authors declare that AI was not used.

Received: 19.10.2025
Revised: 26.12.2025
Accepted: 27.12.2025
Published: 28.12.2025

Technobius, 2025, 5(4), 0093, DOI: https://doi.org/10.54355/tbus/5.4.0093

Technobius

https://technobius.kz/

e-ISSN 2789-7338

Article

A field-validated finite element framework for predicting transient temperature fields in multilayer pavements

Giuseppe Loprencipe[1], Kurmangazy Tileu[2], Koblanbek Aytbayev[2], Adina Ainayeva[2,*], Beksultan Chugulyov[2]

[1]Faculty of Civil and Industrial Engineering, Sapienza University of Rome, Rome, Italy
[2]JSC "Kazakhstan Road Research Institute", Astana, Kazakhstan
*Correspondence: a.ainayeva@qazjolgzi.kz

Abstract. Extreme continental climates in Kazakhstan impose large diurnal and seasonal thermal gradients in pavements, accelerating temperature-related distress. This study develops and validates a two-dimensional finite element model for predicting non-stationary temperature fields in multilayer pavement–subgrade systems from geographic location and climatic inputs. The transient heat-conduction problem with a surface thermal-balance boundary condition was implemented in MATLAB (PDE Toolbox). Validation used hourly temperatures from embedded sensors on the Kyzylorda-Shymkent (at km 2057) and Oskemen-Zyryanovsk (at km 0+075) highways during 1-31 July 2014. Predictions reproduced the attenuation of temperature amplitude with depth and closely matched measurements: coefficients of variation were <0.25 and correlations approached 1.0 at 2.1 m. Root mean square errors ranged from 0.44-7.49 °C and 0.26-5.65 °C for the two sites. The approach supports climate-resilient pavement design using readily available air-temperature data.

Keywords: temperature regime, non-stationary temperature field, numerical methods, finite element method, pavement.

1. Introduction

Highways are complex engineering systems that require consideration of numerous factors during their design, including the temperature regime [1]. In particular, the continental climate of Kazakhstan is characterized by a wide range of temperature fluctuations between winter and summer, low air humidity, and limited precipitation across most of the territory. Additionally, the northern regions experience long and harsh winters accompanied by short summers, whereas in the southern regions, winters are short and summers are prolonged and hot [2].

To enable long-term monitoring of temperature and moisture variations within pavement layers and the subgrade under different climatic conditions, three specialized measurement complexes were installed near Astana in 2010 [3]. These complexes were equipped with temperature and humidity sensors embedded in road sections with asphalt and cement-concrete pavements [4]. Later, in 2013, similar systems were installed near Oskemen, Almaty, Shymkent, and Atyrau [5].

The determination of the transient temperature field within pavement and subgrade layers of roads relies on mathematical modeling methods, which are widely applied worldwide in various forms [6]. All such approaches primarily use air temperature data as input. The determination of pavement surface temperature – essential for defining boundary conditions in mathematical models – is addressed differently by researchers [7]. Typically, the diurnal and seasonal variations in solar radiation intensity are first evaluated, which depend significantly on the geographic latitude of the location [8], [9]. In some cases, average seasonal wind speeds are incorporated, while in others,

empirical relationships for convective heat exchange at the pavement surface are employed [10]. However, the applicability of these models is limited under the climatic conditions of Kazakhstan. Many existing pavement temperature prediction models were developed for regions with moderate climates and relatively stable humidity levels, and they often rely on empirical coefficients calibrated for specific geographic zones. In contrast, Kazakhstan is characterized by a sharply continental climate with extreme seasonal and daily temperature variations, low atmospheric humidity, and significant differences in solar radiation intensity across regions. These factors reduce the accuracy of models that do not explicitly account for regional climatic parameters and local thermophysical properties of pavement materials.

In recent years, approaches have been actively developed that combine the finite element method with climate models for analyzing thermal processes in road structures [11], [12]. These works demonstrate the potential for predicting temperature fields, considering the dynamics of climate change and regional peculiarities of heat exchange. In particular, the integration of data on solar radiation, humidity, and wind loads enhances the accuracy of modeling seasonal temperature fluctuations in road surface temperatures. It shows that the finite element method (FEM) is widely used in solving temperature-related problems for various pavement types [13], [14]. Moreover, FEM is applied to analyze the influence of climatic factors and material properties on pavement temperature and the near-surface thermal environment [15], [16]. The method's universality also makes it possible to combine temperature prediction models with mechanical property analysis for investigating thermally induced mechanistic behavior in pavement structures [17], [18]. Furthermore, FEM enables two- and three-dimensional heat transfer modeling, which is essential for analyzing planar thermal processes within pavement systems [19].

Therefore, this study aims to develop and validate a numerical model for predicting non-stationary temperature fields in multilayer pavement structures based on geographic location and climatic conditions. The model is verified using experimental data obtained from two highway sections: the "Kyzylorda-Shymkent" (km 2057) and "Oskemen-Zyryanovsk" (km 0+075) highways for the period 1-31 July 2014. The calculated results are compared with hourly temperature measurements recorded by embedded sensors.

2. Methods

The proposed model is verified based on the comparison of experimentally measured and numerically computed temperature values within pavement and subgrade layers.

First, the model determines the thermal balance on the road surface. The total heat flux incident on the pavement surface ($q(t)t$) results from the combined influence of various external factors, including the temperature difference between the ambient air and the pavement surface, which induces convective heat exchange between the two media [20], [21]. In general form, the total heat flux acting on the pavement surface (Figure 1) at any given time can be expressed as follows:

$$q(t) = q_k + q_c + q_s + q_a + q_e, \quad (1)$$

where: q_e – latent heat flux associated with moisture evaporation from the pavement surface, kW/m^2.

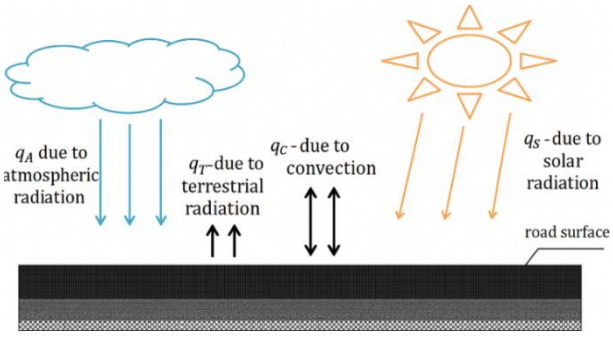

Figure 1 – Schematic representation of the total heat flux formation on the pavement surface

However, when solving the specific problem, the first term in Eq. (1) is excluded, since it is determined by the following expression:

$$q_k = -k\frac{T_d - T}{d}kTdT_d d, \quad (2)$$

where: k – coefficient of conductive heat transfer, W/(m·°C); T – temperature at the pavement surface point to be determined, °C; d – depth of the considered point within the pavement structure, m; T_d – temperature at a certain depth (d), °C.

Consequently, $q_k = 0$, because at the pavement surface $d = 0$ and $T_d = T$. Thus, the total heat flux acting on the pavement surface, which is required for defining the boundary condition of the Cauchy problem, is expressed as follows:

$$q(t) = q_c + q_s + q_a + q_e \quad (3)$$

The transient heat conduction in a plane (2D) solid body is described by a parabolic-type differential equation:

$$K_{xx}\frac{\partial^2 T}{\partial x^2} + K_{yy}\frac{\partial^2 T}{\partial y^2} + Q = \lambda\frac{\partial T}{\partial t}, \quad (4)$$

with the following boundary conditions:

$$K_{xx}\frac{\partial T}{\partial x}l_x + K_{yy}\frac{\partial T}{\partial y}l_y + h_c(T - T_в) + q = 0, \quad (5)$$

where: K_{xx} and K_{yy} – coefficients of conductive heat transfer along the coordinate axes, kW/(m·°C); h_c – convective heat transfer coefficient between the surface of the solid body and the surrounding air, kW/(m²·°C); T – unknown temperature of the body surface where convective heat exchange occurs, °C; Q – internal heat source within the body, kW/m³; T_a – known ambient air temperature, °C; l_x, l_y – directional cosines; q – heat flux intensity, kW/m²; $\lambda = c\rho$, where c is the specific heat capacity, J/(kg·°C), and ρ is the material density, kg/m^3.

The differential equations and boundary conditions used in Eqs. (4) and (5) are based on the classical principles of the theory of unsteady thermal conductivity [22], [23] and implemented using finite element modeling techniques in accordance with [24], [25].

To solve Eq. (4), the variational principle is used, according to which, when the heat transfer process reaches its transient steady state, the amount of heat accumulated by the body at that moment attains its minimum value.

In this work, the method of approximate replacement of the partial time derivative with its finite-difference analog using a central difference scheme is applied. As a result, the differential equation is reduced to a system of linear algebraic equations:

$$\left([K] - \frac{2}{\Delta t}[C]\right)\{T\}_0 - 2\{F\}^*, \quad (6)$$

where: $\{F\}^* = \frac{1}{2}(\{F\}_1 + \{F\}_0)$. Here, the nodal heat load vectors $\{F_0\}$and $\{F_1\}$ correspond to the time moments t and $t + \Delta t$, respectively ($\{T_0\}tt + \Delta t\{T_1\}\{F\}^*$). Assuming that the initial nodal temperature values at time are known, the nodal temperature values at time can be obtained by solving Eq. (6), respectively. The column vector contains known parameters; therefore, it can be calculated before solving Eq. (6).

The calculations were performed in the MATLAB environment using a custom script based on the standard PDE Toolbox libraries. An uneven grid with a depth step of 0.02-0.05 m was used for sampling. The criterion for the convergence of the iterative process was considered to be a change in the temperature of nodes of less than 0.001 °C in neighboring iterations. The correctness of grid independence was monitored by reducing the grid pitch by 50% and checking the stability of the results (< 1% discrepancy).

The proposed method for solving the transient heat conduction problem for a multilayer pavement structure was tested on the “Kyzylorda-Shymkent” highway section, at km 2057, near the city of Turkestan in the Turkestan region, and on the “Oskemen-Zyryanovsk” highway section, at km 0+075, between 1 and 31 July 2014 by comparing the calculated temperatures with experimental data obtained under similar climatic conditions. The validation of the results was performed by statistical analysis, including the estimates of the coefficients of variation, correlation factors, and the indicators

of the root mean square error (RMSE), which together provided an opportunity to assess the reliability of the model and the degree of accuracy of its predicted values.

The "Kyzylorda-Shymkent" highway pavement structure consists of 6 pavement layers, and the "Oskemen-Zyryanovsk" highway – 3, constructed on a soil subgrade (Figure 2), with layer thicknesses and materials' physical, mechanical, and thermophysical properties shown in Table 1.

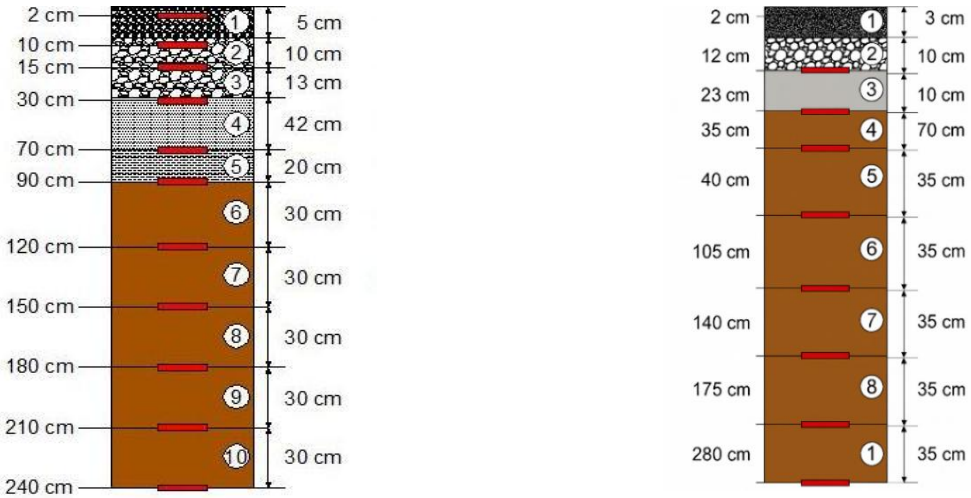

a) Kyzylorda-Shymkent b) Oskemen-Zyryanovsk

Figure 2 – Structure of the highway sections with a layout of temperature and humidity sensors

Table 1 – Characteristics of the layers

Layer No.	Material of the layer	Thickness, m	Thermal conductivity coefficient, W/(m·°C)	Specific heat capacity, J/(kg·°C)	Density, kg/m^3
Kyzylorda-Shymkent highway section					
1	Fine-grained asphalt concrete	0.05	1.40	1650.0	2400
2	Coarse-grained asphalt concrete	0.10	1.25	1650.0	2300
3	Fine-grained asphalt concrete (old layer)	0.13	1.40	1650.0	2400
4	Coarse-grained cold asphalt concrete	0.42	1.25	1650.0	2300
5	Sand-gravel mix (fine)	0.20	1.80	1000.0	1400
6	Sand-gravel mix (coarse)	0.30	1.80	1000.0	1900
7	Subgrade soil (heavy sandy loam)	-	1.62	1450	200
Oskemen-Zyryanovsk highway section					
1	Fine-grained asphalt concrete and bituminous binder	0.03	1.40	1650	2400
2	Cold asphalt concrete	0.10	1.25	1650	2300
3	Sand-gravel mix	0.10	1.80	1000	1900
4	Subgrade soil (heavy sandy loam)	-	1.62	1450	200

The Interpribor Company (Chelyabinsk, Russia) has manufactured temperature and humidity sensors at the order of the JSC "Kazakhstan Road Research Institute". Each sensor, made in the form of a metal capsule, contains an element for measuring temperature based on the effect of thermal resistance and an element for measuring humidity through diamagnetic permeability [5]. The temperature elements of the sensors were calibrated by the manufacturer, and the moisture elements were tested by the JSC "Kazakhstan Road Research Institute" laboratory. Calibration of the sensors was carried out using the soils selected at their installation location.

3. Results and Discussion

The results of comparison between the experimental data and the calculated results obtained using the MATLAB-based program for the "Kyzylorda-Shymkent" and "Oskemen-Zyryanovsk" highway sections, for the period 1-31 July 2014, are presented in Figures 3 and 4.

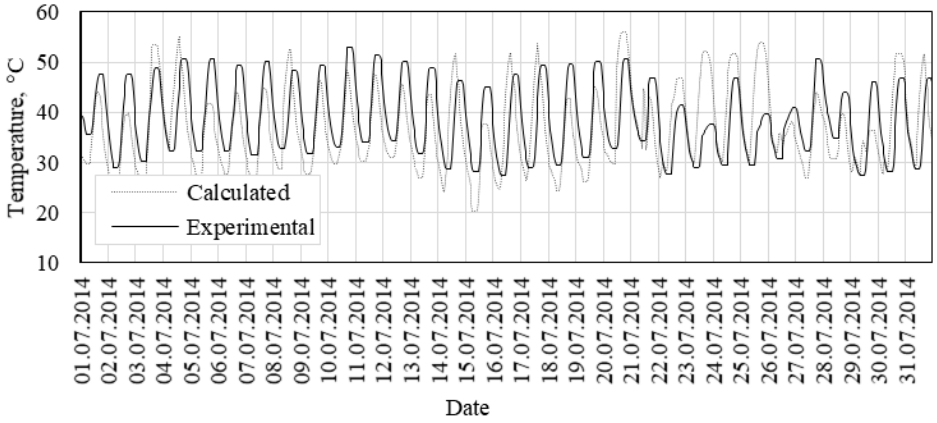

a) At a depth of 0.02 m (pavement surface)

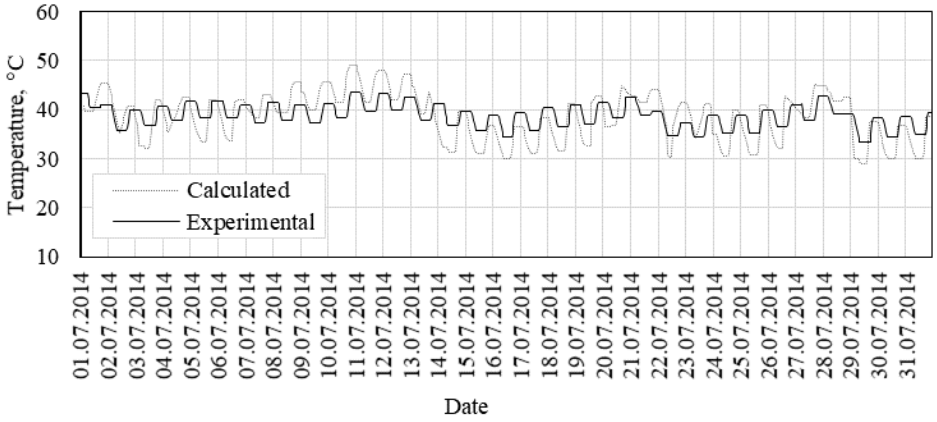

b) At a depth of 0.15 m

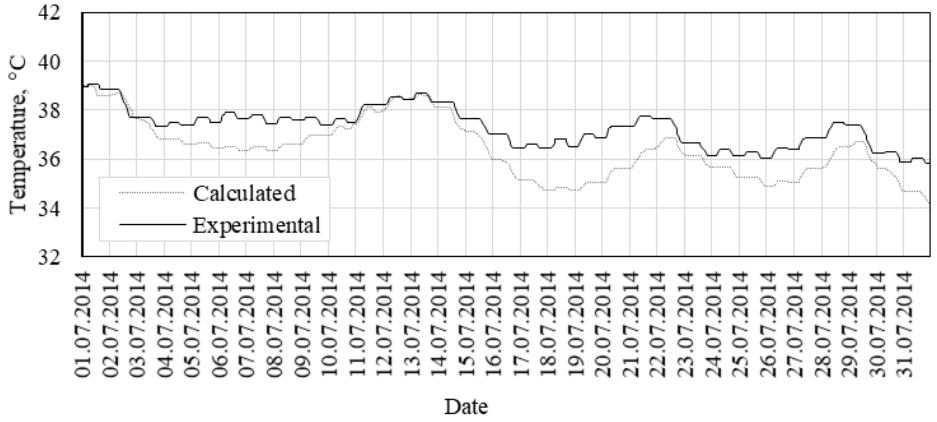

c) At a depth of 0.7 m

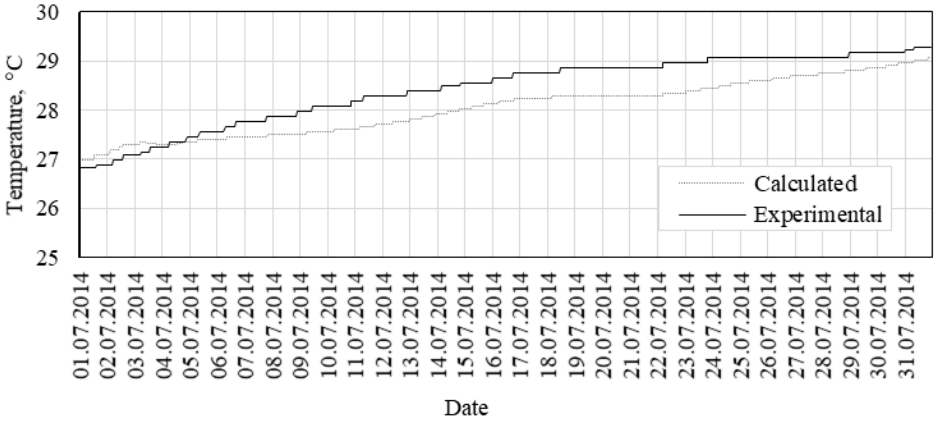

d) At a depth of 2.1 m

Figure 3 – Temperature values for the “Kyzylorda-Shymkent” highway section

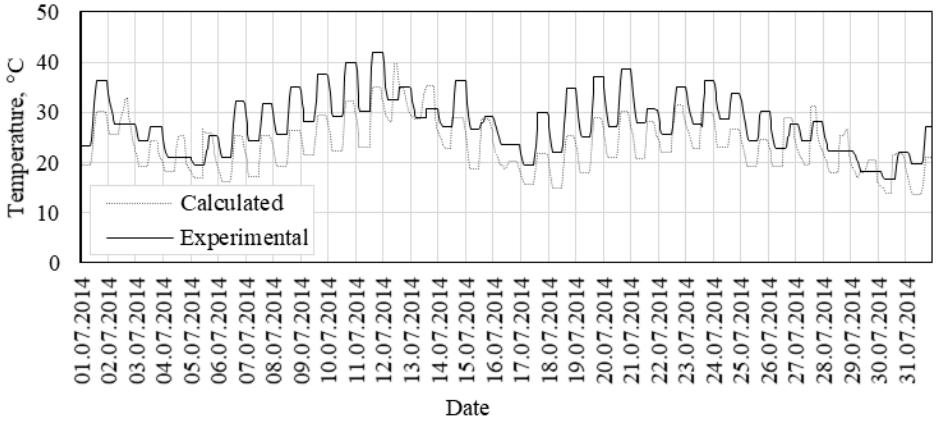

a) At a depth of 0.02 m (pavement surface)

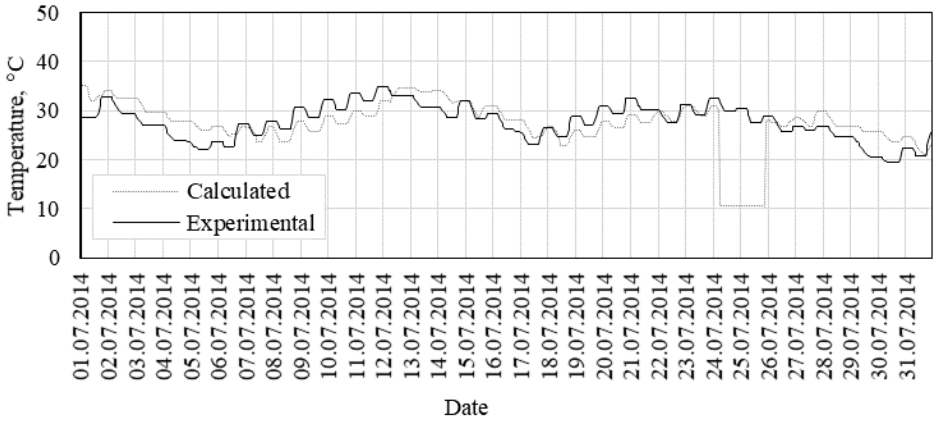

b) At a depth of 0.23 m

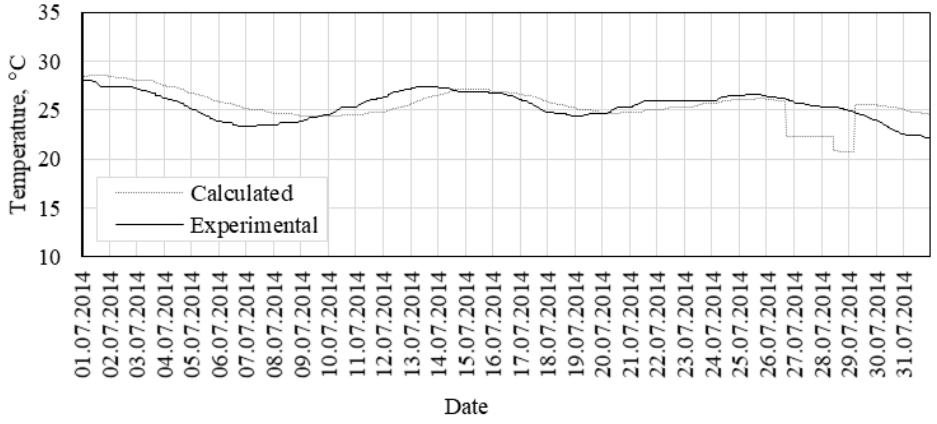

c) At a depth of 0.7 m

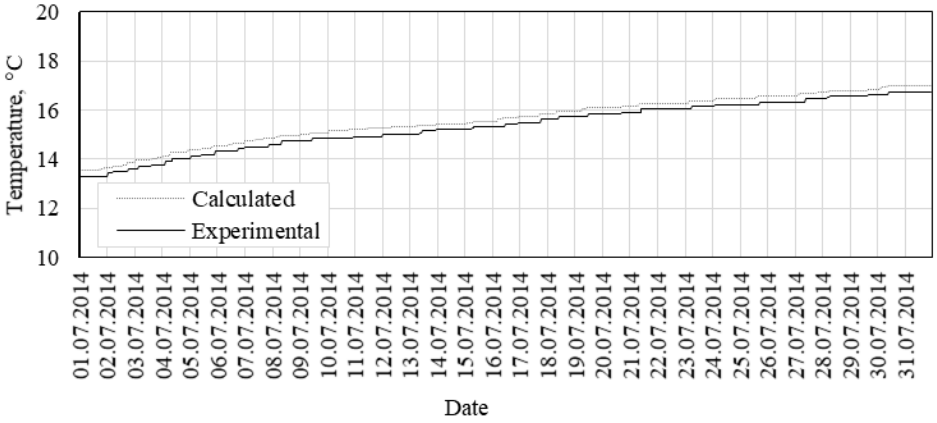

d) At a depth of 2.1 m

Figure 4 – Temperature values for the “Oskemen-Zyryanovsk” highway section

Figures 3 and 4 above demonstrate the temperature fluctuations over 31 days of July 2014 at the various depths between 0.02 and 2.1 m of the highway sections “Kyzylorda-Shymkent” and “Oskemen-Zyryanovsk”, respectively. In both sections, there is a noticeable trend toward a decrease in the amplitude of temperature fluctuations with an increase in measurement depth. It is also seen that the curves representing the calculated values of the temperature are very close to those of experimentally measured ones. The results of the statistical analysis in Figures 5 and 6 present more detailed insights into the significance of this proximity.

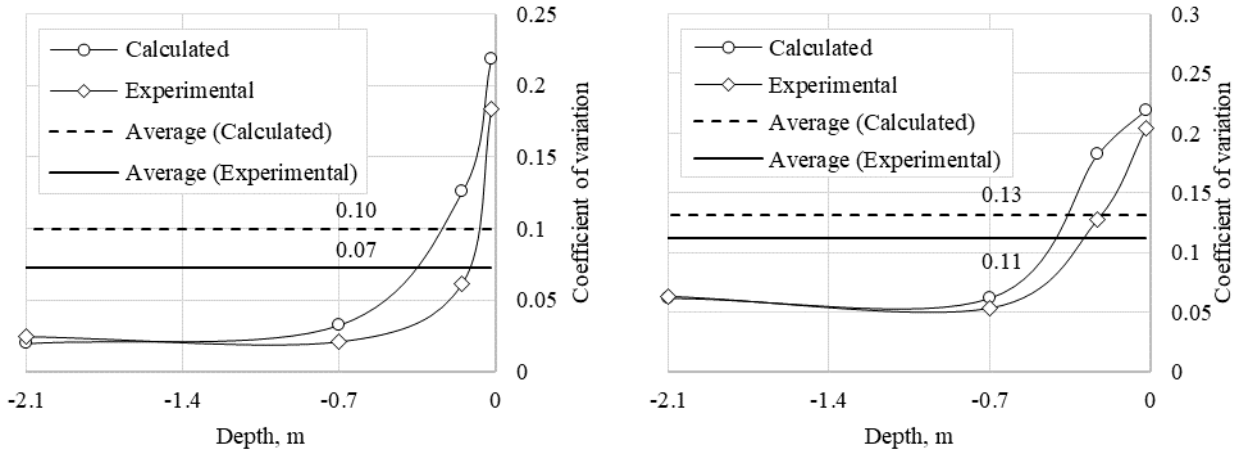

a) Kyzylorda-Shymkent b) Oskemen-Zyryanovsk

Figure 5 – Coefficient of variation

Figure 5 shows the coefficients of variation for the calculated and experimental values of temperature, which reveals the extent of their dispersion. Thus, for both highway sections, the coefficients of variation are less than 0.25, while their average values are at a low level and differ slightly. This may indicate a certain stability in the measurements with sensors (for experimental values) and in the estimates with the model (for calculated values). Overall, the decrease in the values of the coefficients of variation is observed with the increase in depth. To reflect the convergence between the calculated and experimental values, Figure 6 presents the results of correlation factor estimates along with the RMSE.

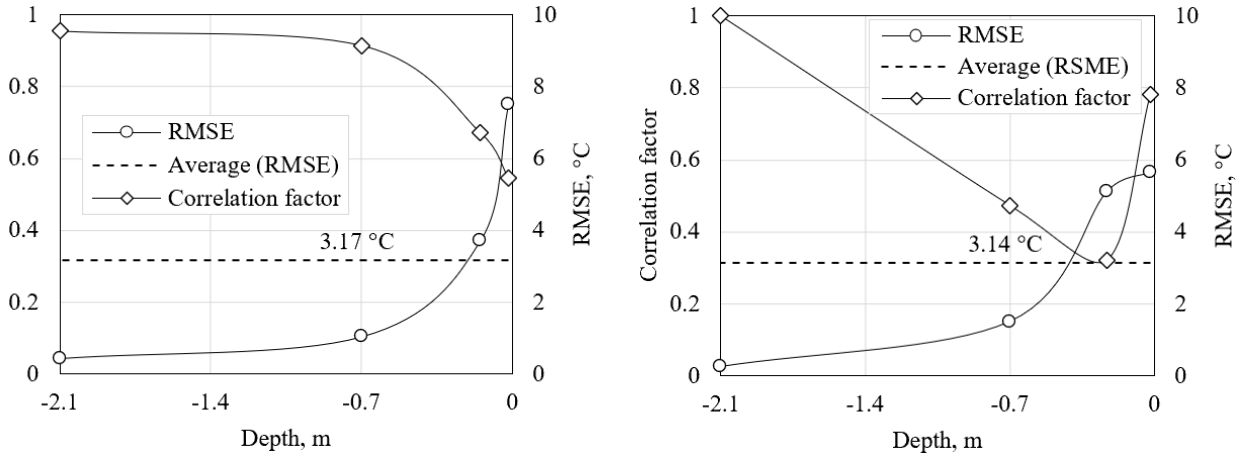

a) Kyzylorda-Shymkent b) Oskemen-Zyryanovsk

Figure 6 – Correlation factor and RMSE

Figure 6 shows that at greater depths, the calculated values of temperature correlate with experimental values for both highway sections. Thus, at a depth of 2.1 m, the correlation factor is really close to 1.0, and at a depth of 0.7 m, the correlation factor is still higher than 0.9 for the “Kyzylorda-Shymkent” highway section, but for the “Oskemen-Zyryanovsk”, it is around 0.5,

decreasing to 0.3 at a depth of 0.23 m and rapidly increasing to 0.8 at a depths of 0.02 m, suggesting the influence of external factors during the run of the model (computer malfunctions, power surges). This pattern is clearly visible in Figures 4b and 4c, where deviant fluctuations of the calculated values of the temperature can be observed at depths of 0.23 and 0.7 m. Despite this occurrence, the RMSE values reflect pretty low ranges of 0.44-7.49 °C for the "Kyzylorda-Shymkent" highway section, and 0.26-5.65 °C for the "Oskemen-Zyryanovsk" highway section, averaging to 3.17 and 3.14 °C, respectively.

Overall, the results of comparing the calculated and experimental temperature values at the nodal points of the studied highway sections indicate the adequacy of the proposed mathematical model for describing the formation of the transient temperature field in the examined multilayer pavement structure. The slight discrepancy between the calculated and experimental results of the transient temperature field in the multilayer pavement structure may be attributed to the assumption regarding the intentional time shift applied when determining the nodal load vector [5].

Thus, the proposed method for solving the transient heat conduction problem makes it possible to determine the non-stationary temperature field in a multilayer pavement structure using only the time-dependent air temperature data for the period of interest, which can be obtained from a meteorological station located near the studied highway section. The developed model makes it possible to predict the temperature field for various road surface structures, taking into account the climatic parameters of the region, which can be used in the design of thermally deformable road surfaces and optimization of the composition of asphalt mixtures.

4. Conclusion

This study developed a two-dimensional finite-element framework to reproduce the non-stationary temperature field in multilayer pavement–subgrade systems using a surface heat-flux boundary condition derived from the pavement thermal balance and time-dependent meteorological input. The model was implemented in MATLAB (PDE Toolbox) with verified convergence and grid-independence controls, enabling stable transient solutions over the analyzed period.

Validation against hourly in-situ sensor records for two highway sections ("Kyzylorda-Shymkent" and "Oskemen-Zyryanovsk") over 1-31 July 2014 showed that the computed temperature profiles closely follow measured trends across depths from 0.02 to 2.1 m, with attenuation of fluctuation amplitude with depth captured consistently. Statistical agreement indicators confirmed the adequacy of the approach: coefficients of variation were below 0.25, correlations improved with depth (approaching 1.0 at 2.1 m), and RMSE values remained within practical bounds (0.26-7.49 °C depending on depth/section).

From an engineering standpoint, the proposed model provides a practical tool for estimating internal pavement temperatures needed for thermally driven performance checks (e.g., material selection, seasonal construction/maintenance planning, and subsequent coupling with mechanistic response analyses). Remaining discrepancies are plausibly linked to input/measurement irregularities and simplifying assumptions in boundary/loading representation. Future work should extend the framework toward coupled heat-moisture processes, improved representation of external climatic actions, and three-dimensional simulations for complex geometries and localized effects.

References

[1] Zh. A. Shakhmov *et al.*, "Case study of the dynamics of thermal expansion of concrete in pavements of South Kazakhstan," *Transportation Engineering*, vol. 19, p. 100298, Mar. 2025, doi: 10.1016/j.treng.2024.100298.

[2] A. Alibayeva, Y. Amirbayev, D. Alizhanov, M. Zhumamuratov, and M. Smagulova, "Sustainable road surfaces: Evaluating eco-friendly additives on bitumen penetration grade," *E3S Web of Conferences*, vol. 614, p. 04013, 2025, doi: 10.1051/e3sconf/202561404013.

[3] M. Pshembayev, "Regulation of the water-heat regime of the subgrade of cement-concrete road," *International Journal of GEOMATE*, vol. 25, no. 111, pp. 145–152, Nov. 2023, doi: 10.21660/2023.111.4035.

[4] M. J. Roshan and A. Gomes Correia, "Multifunctional Cementitious Composites from Fabrication to Their Application in Pavement: A Comprehensive Review," *Applied Sciences*, vol. 15, no. 7, p. 3451, Mar. 2025, doi: 10.3390/app15073451.

[5] B. B. Teltayev and E. A. Suppes, "Temperature and moisture in a highway in the south of Kazakhstan," *Transportation Geotechnics*, vol. 21, p. 100292, Dec. 2019, doi: 10.1016/j.trgeo.2019.100292.

[6] S. Roy, A. Mateos, J. Paniagua, and S. Nassiri, "Improving sensor encapsulation for long-term monitoring of relative humidity and temperature inside concrete pavements," *International Journal of Pavement Engineering*, vol. 26, no. 1, p. 2497463, Dec. 2025, doi: 10.1080/10298436.2025.2497463.

[7] I. Adwan *et al.*, "Asphalt Pavement Temperature Prediction Models: A Review," *Applied Sciences*, vol. 11, no. 9, p. 3794, Apr. 2021, doi: 10.3390/app11093794.

[8] S. Pashiardis, A. Pelengaris, and S. A. Kalogirou, "Geographical Distribution of Global Radiation and Sunshine Duration over the Island of Cyprus," *Applied Sciences*, vol. 13, no. 9, p. 5422, Apr. 2023, doi: 10.3390/app13095422.

[9] M. Ilbeigi, F. Mashhadimohammadzadehvazifeh, M. Salehi Heydari, Z. Hosseini, and F. Khalili, "Optimizing tilt angles for solar energy harvesting on building façades: evidence from Babolsar, Iran," *Architecture, Structures and Construction*, vol. 5, no. 2, p. 46, Dec. 2025, doi: 10.1007/s44150-025-00164-0.

[10] Z. Motamedi, T. Bansal, H. Mattsson, J. Åström, and J. Casselgren, "A dynamic boundary condition finite difference model for predicting pavement profile temperatures: Development and validation," *Transportation Engineering*, vol. 18, p. 100287, Dec. 2024, doi: 10.1016/j.treng.2024.100287.

[11] M. Venkateswar Reddy, B. Hemasunder, S. V. Ramana, P. Ramesh Babu, P. Thejasree, and J. Joseph, "State of art on FEM approach in inverse heat transfer problems for different materials," *Materials Today: Proceedings*, p. S2214785323037227, July 2023, doi: 10.1016/j.matpr.2023.06.323.

[12] E. Badakhshan, J. Vaunat, and G. Veylon, "A finite element model of thermo-hydraulic behavior of vegetation considering soil-atmosphere interactions," *Computers and Geotechnics*, vol. 188, p. 107540, Dec. 2025, doi: 10.1016/j.compgeo.2025.107540.

[13] T. T. T. Tran, H. H. Nguyen, P. N. Pham, T. Nguyen, P. Q. Nguyen, and H. N. Huynh, "Temperature-related thermal properties of paving materials: experimental analysis and effect on thermal distribution in semi-rigid pavement," *Road Materials and Pavement Design*, vol. 24, no. 11, pp. 2759–2779, Nov. 2023, doi: 10.1080/14680629.2023.2170270.

[14] J. Songok, A. Mäkiranta, N. Rapantova, P. Pospisil, and B. Martinkauppi, "Numerical simulation of heat recovery from asphalt pavement in Finnish climate conditions," *International Journal of Thermal Sciences*, vol. 187, p. 108181, May 2023, doi: 10.1016/j.ijthermalsci.2023.108181.

[15] D. Han, C. Li, X. Wei, J. Yang, C. Wu, and Q. Ouyang, "2D temperature field analysis of asphalt pavements with three different types of subgrade structures," *Case Studies in Thermal Engineering*, vol. 54, p. 103964, Feb. 2024, doi: 10.1016/j.csite.2023.103964.

[16] Y. Qin, X. Zhang, K. Tan, and J. Wang, "A review on the influencing factors of pavement surface temperature," *Environmental Science and Pollution Research*, vol. 29, no. 45, pp. 67659–67674, Sept. 2022, doi: 10.1007/s11356-022-22295-3.

[17] D. Saliko, A. Ahmed, and S. Erlingsson, "Development and validation of a pavement temperature profile prediction model in a mechanistic-empirical design framework," *Transportation Geotechnics*, vol. 40, p. 100976, May 2023, doi: 10.1016/j.trgeo.2023.100976.

[18] G. H. Hamedi, A. H. Asadi, and J. Zarrinfam, "Investigating the effect of fundamental properties of materials on the mechanisms of thermal cracking of asphalt mixtures," *Construction and Building Materials*, vol. 411, p. 134426, Jan. 2024, doi: 10.1016/j.conbuildmat.2023.134426.

[19] Y. Sun, Z. Zhang, H. Gong, C. Zhou, J. Chen, and B. Huang, "3D Multiscale Modeling of Asphalt Pavement Responses under Coupled Temperature–Stress Fields," *Journal of Engineering Mechanics*, vol. 148, no. 3, p. 04022010, Mar. 2022, doi: 10.1061/(ASCE)EM.1943-7889.0002089.

[20] W. Hua, L. Jin, M. Bai, and H. Zhang, "Experimental investigation and modeling of heat and moisture transfer beneath asphalt pavements under rainfall conditions," *Case Studies in Thermal Engineering*, vol. 73, p. 106741, Sept. 2025, doi: 10.1016/j.csite.2025.106741.

[21] J. Chen, C. Sun, X. Sun, H. Dan, and X. Huang, "Finite difference model for predicting road surface ice formation based on heat transfer and phase transition theory," *Cold Regions Science and Technology*, vol. 207, p. 103772, Mar. 2023, doi: 10.1016/j.coldregions.2023.103772.

[22] H. S. Carslaw and J. C. Jaeger, "Conduction of Heat in Solids," 2nd ed., Oxford: Clarendon Press, 1959, p. 310.

[23] F. P. Incropera, D. P. DeWitt, T. L. Bergman, and A. S. Lavine, "Fundamentals of Heat and Mass Transfer," 8th ed., Hoboken, NJ: Wiley, 2017, p. 992.

[24] "ISO 8302:1991 Thermal insulation - Determination of steady-state thermal resistance and related properties - Guarded hot plate apparatus," London, UK: ISO, 1991, p. 47.

[25] "GOST 30256-94 Building materials and products. Method of thermal conductivity determination by cylindrical probe," MNTKS, 1994, p. 20.

Information about authors:
Giuseppe Loprencipe – Associate Professor, Faculty of Civil and Industrial Engineering, Sapienza University of Rome, Rome, Italy, giuseppe.loprencipe@uniroma1.it
Kurmangazy Tileu – PhD, Head, Digitalization Department, JSC "Kazakhstan Road Research Institute", Astana, Kazakhstan, k.tileu@qazjolgzi.kz
Koblanbek Aytbayev – Candidate of Technical Sciences, Leading Researcher, Scientific Research Department, JSC "Kazakhstan Road Research Institute", Almaty, Kazakhstan, a.aytbayev@qazjolgzi.kz
Adina Ainayeva – Head, External Communications Service, JSC "Kazakhstan Road Research Institute", Astana, Kazakhstan, a.ainayeva@qazjolgzi.kz
Beksultan Chugulyov – Leading Engineer, Testing Laboratory, JSC "Kazakhstan Road Research Institute", Astana, Kazakhstan, b.chugulyov@qazjolgzi.kz

Author Contributions:
Giuseppe Loprencipe – modeling, analysis, validation, visualization, editing.
Kurmangazy Tileu – concept, supervision, methodology, analysis, editing.
Koblanbek Aytbayev – methodology, resources, interpretation, editing.
Adina Ainayeva – concept, data collection, drafting, communication, editing.
Beksultan Chugulyov – data collection, laboratory testing, visualization, analysis.

Conflict of Interest: The authors declare no conflict of interest.

Use of Artificial Intelligence (AI): The authors declare that AI was not used.

Received: 23.10.2025
Revised: 17.12.2025
Accepted: 28.12.2025
Published: 29.12.2025

Technobius, 2025, 5(4), 0094, DOI: https://doi.org/10.54355/tbus/5.4.2025.0094

Technobius
https://technobius.kz/
e-ISSN 2789-7338

Article

Optimizing sodium sulfonate dosage in non-autoclaved aerated concrete: effects on pore stability, strength, and abrasion resistance

Nurlan Bekkaliev*, Yerlan Sabitov

L.N. Gumilyov Eurasian National University, Astana, Kazakhstan
*Correspondence: nurlan_b-90@mail.ru

Abstract. This study evaluates sodium sulfonate as a structuring surfactant for non-autoclaved aerated concrete to stabilize pore formation and improve performance. A laboratory dosage series (0-0.25% by cement mass, water-to-cement ratio 0.45) and a pilot D700 production verification (GB1-GB4) were performed. At 28 days, the reference mixture reached 1.5-2.0 MPa, while 0.10-0.15% sodium sulfonate increased strength to 2.3-2.7 MPa; higher dosages reduced strength and impaired pore stability. In the pilot series, average density ranged from 610 to 740 kg/m^3 and compressive strength from 2.0 to 2.5 MPa, with GB3 showing the best strength-to-density balance (SQC 0.034). Abrasion improved from 0.84 to 0.71 g/cm^2. The additive improved plasticity and pore uniformity. Overall, 0.10-0.15% is recommended for practical production with minimal process complexity.
Keywords: aerated concrete, sodium sulfonate, non-autoclave hardening, aluminum powder, cellular structure.

1. Introduction

Among the various types of cellular concrete, special attention is paid to non-autoclaved aerated concrete, the production of which does not require expensive autoclave equipment and high-temperature processing. This approach significantly reduces capital costs and simplifies the technological process, making it accessible to a wide range of construction companies [1].

Cellular concrete is currently one of the most sought-after building materials due to its combination of low specific weight, high thermal and sound insulation properties, and sufficient mechanical strength for use in load-bearing and enclosing structures [2]. These materials are characterized by a porous structure, which is formed by introducing a gas generator into the cement-mineral matrix, significantly reducing density and improving thermal insulation characteristics. One of the key technological challenges in the production of non-autoclaved aerated concrete is the stabilization of the gas structure during the hardening period. The pores formed during the chemical decomposition of the gas generator must be evenly distributed and stable until the cement stone has completely set. Failure to comply with this condition leads to the formation of uneven porosity, a decrease in strength, and a deterioration in the thermal insulation characteristics of the material.

To solve this problem, surfactants are often added to the non-autoclaved aerated concrete formula to help stabilize the foam and form a uniform porous structure. Among them, sodium sulfonate (Na-SO_3 compounds) is of particular importance – an anionic surfactant with the unique ability to simultaneously stabilize gas bubbles, improve the distribution of liquid in cement paste, and regulate the size and shape of pores [3]. In addition, sodium sulfonate performs several additional functions in the concrete mix. It can act as a plasticizer, improving the workability and mobility of the fresh mix without increasing the water-cement ratio, as well as a pore structure regulator, allowing a uniform and fine-pored matrix to be obtained. The introduction of such an additive has a positive effect on strength characteristics, reduces shrinkage deformation, and improves the frost resistance of

the finished material. Practical interest in sodium sulfonate is also due to its economic affordability and technological simplicity of application. Experimental studies show that the optimal dosage of this additive depends on the designed density of aerated concrete and can vary between 0.05 and 0.25% of the cement mass, ensuring a balance between strength, density, and stability of the porous structure. In general, the use of sodium sulfonate allows for the production of non-autoclaved aerated concrete with improved performance characteristics that can compete with materials produced using autoclave treatment.

In modern construction, special attention is paid to expanding the raw material base through the use of affordable mineral components and technological additives, such as cements of various compositions, slag products, aluminum powder, and surface-active substances. These materials make it possible to create lightweight, thermally efficient, and durable building products, in particular non-autoclaved aerated concrete, without the use of complex and expensive autoclave equipment [4]. One of the main technological challenges in the production of non-autoclaved aerated concrete is the formation of a stable porous structure. The gas bubbles formed during the reaction of the gas generator with the cement paste must retain their shape and be evenly distributed until the cement stone sets. Failure to comply with this condition leads to uneven porosity, reduced strength, and deterioration of the material's thermal insulation characteristics. Surface-active additives are widely used to stabilize the gas structure. The most promising of these is sodium sulfonate, which simultaneously acts as a foam stabilizer, pore structure regulator, and plasticizer. Its introduction ensures a more uniform distribution of pores, reduces the tendency of the mixture to delaminate, and improves the fluidity of the cement paste. Experiments show that the optimal concentration of sodium sulfonate is 0.05–0.25% of the cement mass, which allows a balance to be achieved between the strength and density of the material.

Previous studies [5] have shown that the addition of sodium sulfonate increases the compressive strength of aerated concrete by 10-20% compared to control samples without additives and simultaneously reduces its density by 5-15%. In addition, stabilizing the porous structure reduces the thermal conductivity of the material to 0.11-0.13 W/m×K, which makes the products more energy efficient and helps reduce the cost of heating and air conditioning buildings. The relevance of developing technologies for the production of non-autoclaved aerated concrete with modifying additives is determined by the need to improve the energy efficiency of buildings and structures. The use of sodium sulfonate allows for the production of lightweight blocks with a uniform porous structure, low thermal conductivity, and satisfactory strength, while reducing energy consumption for technological processes and minimizing operating costs.

This study aims to obtain a non-autoclaved aerated concrete with the addition of sodium sulfonate, providing an optimal combination of strength, density, and thermal insulation properties. The results obtained contribute to the expansion of the raw material base and improve the environmental and economic efficiency of construction technologies [6].

2. Methods

2.1 Materials and experimental design

Non-autoclaved aerated concrete was produced using Portland cement M400 from Caspian Cement, LLP (Aktau, Kazakhstan) as the binder and sodium sulfonate from Damu-Chemistry, LLP (Karaganda, Kazakhstan) as a structuring additive. Quartz sand with a particle size of ≤ 2.5 mm was used as the fine aggregate. The water-to-cement ratio (W/C) was kept constant at 0.45 for the laboratory dosage study. For each composition, at least three specimens were prepared for compressive strength testing and three specimens for abrasion resistance testing. The tests were carried out in the “Building Materials and Building Thermophysics” testing laboratory of the West Kazakhstan Innovation and Technology University (Uralsk, Kazakhstan).

The study consisted of two stages:

- Stage A (laboratory dosage study): sodium sulfonate dosage varied from 0 to 0.25% by cement mass, while cement and sand quantities and W/C were kept constant (Table 1).

- Stage B (pilot/production verification, designed density D700): a plant-scale series (GB1-GB4) produced under production conditions, with a fixed base recipe and stepwise sodium sulfonate dosage (Table 2).

Table 1 – Sample mixtures

Sample	Cement, g	Sand, g	Sodium sulfonate, % of cement weight	W/C
1*	400	1200	0.00	0.45
2	400	1200	0.05	0.45
3	400	1200	0.10	0.45
4	400	1200	0.15	0.45
5	400	1200	0.20	0.45
6	400	1200	0.25	0.45

** Reference sample*

2.2 Mixing and specimen preparation (Stage A)

For each batch, component proportions were calculated for a single mix. Sodium sulfonate was first dissolved in a portion of the mixing water, then combined with the remaining water. Dry materials were mixed in a laboratory mixer for 60-90 s, after which the sulfonate solution was introduced and mixing continued for 2-3 min until a homogeneous mixture was obtained. The mixture temperature and total mixing time were recorded.

Specimens were cast into molds of 100×100×100 mm for compressive strength testing and 70×70×40 mm for abrasion testing. Molds were filled in one or two layers with light tamping (without intense vibration). The surfaces were leveled, covered with plastic film, and kept in molds for 24 ± 4 h at 20 ± 2 °C. After demolding (24-48 h), specimens were cured under natural conditions at 20-25 °C and relative humidity ≥ 50% until testing at 28 days.

2.3. Pilot/production compositions and curing (Stage B, D700)

Pilot compositions (GB1-GB4) were produced under the technological conditions of Batys Story Engineering, LLP (Uralsk, Kazakhstan) for a designed density D700 [7], with sodium sulfonate introduced into the dry mixture as a structure-forming additive, guided by [8]. The fixed base recipe and the sodium sulfonate variation are summarized in Table 2.

Table 2 – Pilot/production compositions (Stage B, designed density D700)

Sample	Sand, kg	Cement, kg	Water, l	Caustic soda, kg	Aluminum powder, kg	Sodium sulfonate content, %
GB1*	403	310	260	3	0.55	-
GB2	403	310	260	3	0.55	10
GB3	403	310	260	3	0.55	20
GB4	403	310	260	3	0.55	30

** Reference sample*

After molding, pilot specimens were subjected to heat treatment in a drying chamber at 60 °C before subsequent testing.

2.4. Compressive strength testing

Compressive strength was determined in accordance with [9] using a hydraulic press (maximum capacity 1000 kN). Before testing, specimen surfaces were cleaned, and dimensions were measured. The load was applied at 0.5-0.8 MPa/s until failure. The compressive strength test setup is shown in Figure 1.

Figure 1 – Testing aerated concrete samples for compressive strength

2.5. Abrasion resistance testing

Abrasion resistance was measured on 70×70×40 mm specimens (Stage A) and, for the pilot study, by mass-change measurements using the IB-1 device. Abrasion testing was conducted in accordance with [10], using a rotating-disc abrasion configuration with quartz sand (0.5-1.0 mm) and an applied load of approximately 294 N (30 kgf). After testing, specimens were cleaned and dried at 105 ± 5 °C to constant mass. Abrasion was quantified by mass loss and, where required, converted to volumetric abrasion using specimen density. The abrasion test setup is shown in Figure 2.

Figure 2 – Testing aerated concrete samples for abrasion resistance

3. Results and Discussion

3.1. Effect of sodium sulfonate dosage in laboratory mixtures

The compressive strength of non-autoclaved aerated concrete increased with sodium sulfonate dosage up to an optimum range, after which the strength began to decline. This trend is summarized in Table 3, where the reference mixture without an additive shows a 28-day compressive strength of 1.5-2.0 MPa, while mixtures with 0.10-0.15% sodium sulfonate reach 2.3-2.7 MPa; at 0.20% and above, the strength decreases, and the structure is reported to deteriorate at >0.25%.

Table 3 – Dependence of aerated concrete properties on sodium sulfonate dosage (laboratory series)

Sodium sulfonate dosage, % by cement mass	Compressive strength after 28 days, MPa	Note
0.00	1.5-2.0	Basic level
0.05	2.0-2.2	Slight improvement
0.10	2.3-2.5	Optimal structural improvement
0.15	2.5-2.7	Maximum positive effect
0.20	2.4-2.6	Slight decline due to overcompaction
>0.25	2.0-2.2	Structure deteriorates, overmoistening

The same direction of influence is reflected in the broader set of property changes attributed to sodium sulfonate (workability, pore size, density, thermal conductivity, and water absorption), indicating that the additive improves mixture plasticity and pore uniformity while lowering bulk density and thermal conductivity, with a slight increase in water absorption (Table 4).

Table 3. Changes in aerated concrete properties when sodium sulfonate is introduced

Property	Direction of change	Without additive	With additive	Comment
Plasticity of mixture	Increases	14–16 cm cone settlement	17–19 cm	Improved formability and homogeneity
Porosity uniformity	Increases	Pore size 1.2–1.8 mm	Pore size 0.8–1.2 mm	More stable pore structure due to foam stabilization
Bulk density (kg/m³)	Decreases	580–600	520–540	Material becomes lighter; thermal insulation improves
Compressive strength (MPa)	Increases (~5–10%)	2.8–3.0	3.1–3.3	Structure compaction and stronger bonding
Thermal conductivity (W/(m·°C))	Decreases	0.135–0.145	0.115–0.125	Lower density + better pore uniformity
Water absorption (% by mass)	Slightly increases	32–34	35–37	Increased open porosity

The strength-dosage relationship is also visualized in Figure 3, which indicates that the maximum strength occurs at approximately 0.10-0.15% sodium sulfonate.

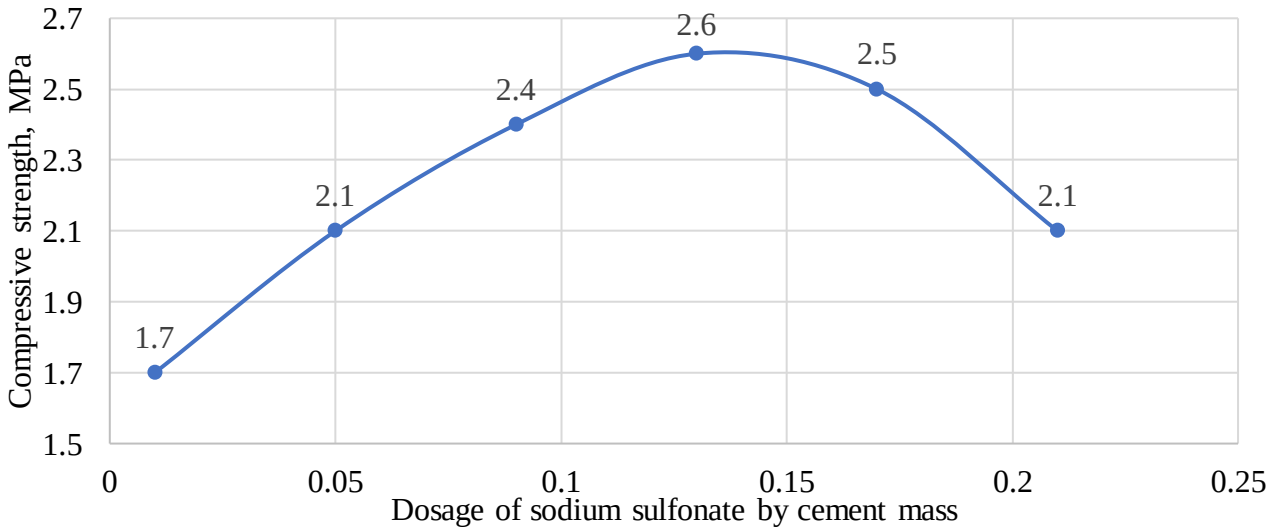

Figure 3 – Dependence of aerated concrete strength on sodium sulfonate content

3.2. Comparative performance of production compositions (GB1-GB4)

For the set of production compositions labeled GB1-GB4, the measured average density ranged from 610 to 740 kg/m^3, while compressive strength varied between 2.0 and 2.5 MPa (Table 4). The highest structural quality coefficient (SQC) among these compositions was reported for GB3 (0.034), indicating the best strength-to-density balance within this group.

Table 5 – Comparison of properties of aerated concrete compositions (GB series)

Sample	Average density, kg/m^3	Compressive strength, MPa	SQC
GB1*	610	2.0	0.020
GB2	740	2.3	0.025
GB3	700	2.5	0.034
GB4	650	2.2	0.023

** Reference sample*

A focused comparison between the reference and the best-performing composition again shows higher strength and SQC in GB3 than GB1.

3.3. Compressive strength of production samples

When compressive strength was reported for GB1-GB4 with reference to [9], the values were in the range of 5.81-6.72 MPa, with the maximum strength recorded for GB3 (6.72 MPa) (Figure 4).

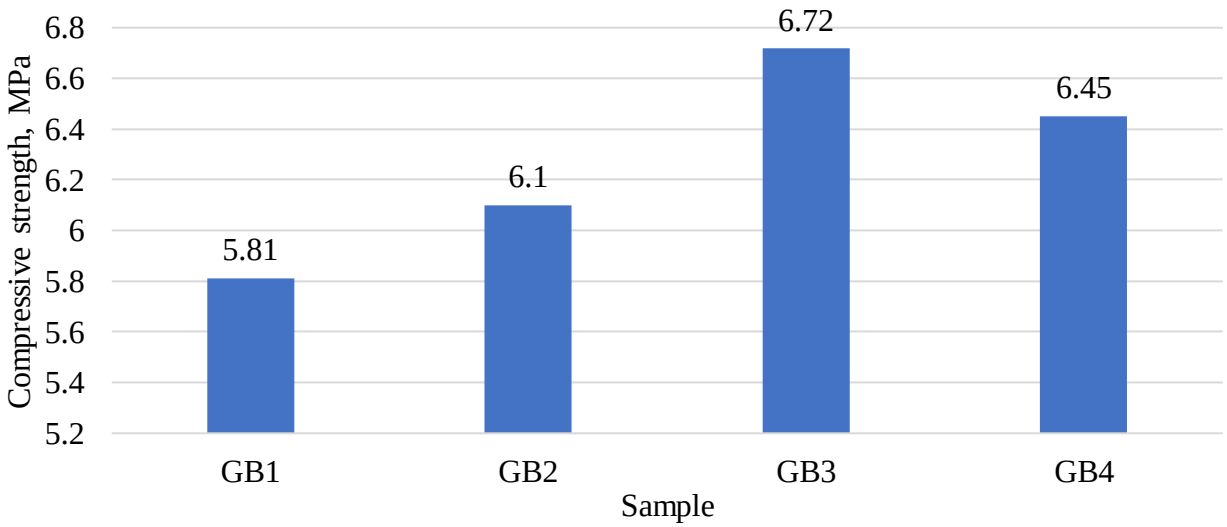

Figure 4 – Results of compressive strength tests on aerated concrete samples (GB series)

Overall, the abrasion results confirm a stable positive effect of sodium sulfonate on surface wear resistance across the modified compositions, with GB3 demonstrating the best performance in this set.

3.4. Abrasion resistance

Abrasion resistance results (mass-loss method) indicate that sodium sulfonate improves wear resistance by reducing the abrasion value from 0.84 g/cm² (GB1, grade G2) to as low as 0.71 g/cm² (GB3, grade G1) (Figure 5).

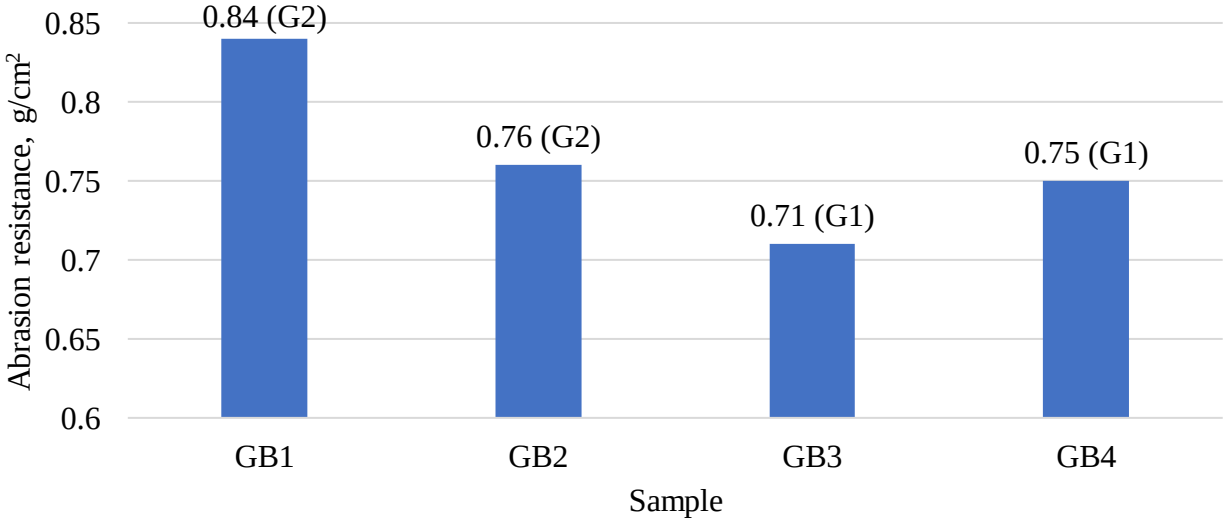

Figure 4 – Results of testing aerated concrete samples for abrasion resistance (GB series)

Overall, the abrasion results confirm a stable positive effect of sodium sulfonate on surface wear resistance across the modified compositions, with GB3 demonstrating the best performance in this set. Based on the data presented in Figure 4, we can conclude that the addition of sodium sulfonate

affects the abrasion resistance of aerated concrete samples. The control composition (GB1), which does not contain additives, showed abrasion resistance at the level of 0.84 g/cm^2, which corresponds to grade G2 according to [10]. The addition of sodium sulfonate to compositions GB2-GB4 led to a noticeable decrease in abrasion resistance. Thus, sample GB2 showed a decrease in abrasion resistance to 0.76 g/cm^2, which also corresponds to grade G2, but indicates a slight improvement compared to the control sample. The greatest reduction in abrasion was observed in sample GB3, where this indicator was 0.71 g/cm^2, which allowed it to be classified as grade G1, i.e., a higher class in terms of abrasion resistance. A similar effect is observed in composition GB4 (0.75 g/cm^2, grade G1), which confirms the stable positive effect of the additive on the wear resistance of the material. The results show that as the amount of sodium sulfonate increases, the abrasion resistance of aerated concrete decreases: from 0.84 g/cm^2 in the control sample to 0.71 g/cm^2 in composition GB3, which indicates an increase in the strength of the material.

4. Conclusion

This study evaluated sodium sulfonate as a structuring (surface-active) additive for non-autoclaved aerated concrete, focusing on how dosage affects strength development and performance indicators relevant to practical block production.

In the laboratory dosage series, the compressive strength increased with sodium sulfonate content up to an optimum range and then declined at higher dosages: the reference mixture (0.00%) reached 1.5-2.0 MPa at 28 days, while mixtures with 0.10-0.15% sodium sulfonate achieved 2.3-2.7 MPa; at 0.20% and above, the strength trend decreased and the structure was reported to deteriorate at >0.25%. The broader property trends attributed to sodium sulfonate indicate improved mixture plasticity and pore uniformity, reduced bulk density and thermal conductivity, and a slight increase in water absorption, which together reflect the additive's role in stabilizing the porous structure and enhancing thermal efficiency.

In the production verification series (GB1-GB4, designed density D700), the best overall balance of density and strength was obtained for GB3, which demonstrated the highest structural quality coefficient (0.034) among the tested compositions. Strength testing of GB-series samples also indicated values of 5.81-6.72 MPa, with the maximum recorded for GB3 (6.72 MPa). Importantly, sodium sulfonate improved wear resistance: abrasion decreased from 0.84 g/cm^2 (GB1, grade G2) to 0.71 g/cm^2 (GB3, grade G1), confirming a stable positive effect on surface durability for the modified compositions.

Overall, sodium sulfonate is an effective additive for improving the performance of non-autoclaved aerated concrete by enhancing strength (within an optimal dosage range) and reducing abrasion. Based on the dosage study, a sodium sulfonate content around 0.10-0.15% (by cement mass) can be recommended as a practical optimum to achieve the most favorable strength response while maintaining stable pore formation.

References

[1] R. Lukpanov, D. Dyussembinov, Z. Shakhmov, D. Bazarbayev, D. Tsygulyov, and S. Yenkebayev, "Influence of the technological foam concrete manufacturing process on its pore structure," *Magazine of Civil Engineering*, vol. 115, no. 7, p. 11513, 2022, doi: 10.34910/MCE.115.13.

[2] R. Lukpanov *et al.*, "Investigation of the influence of post-alcohol distillers' grains on the strength of concrete used in a two-component modified additive," *M&T*, no. 3, pp. 188–200, Sept. 2024, doi: 10.55956/ZSWL8979.

[3] M. Sypek, R. Latawiec, B. Łaźniewska-Piekarczyk, and W. Pichór, "Impact of Surfactant and Calcium Sulfate Type on Air-Entraining Effectiveness in Concrete," *Materials*, vol. 15, no. 3, p. 985, Jan. 2022, doi: 10.3390/ma15030985.

[4] R. E. Lukpanov, D. S. Dusembinov, S. B. Yenkebayev, and D. V. Tsygulyov, "Ratio of the ash concentration to the cement binder in the composition of concrete with the use of a modified additive," *Journal of Physics: Conference Series*, vol. 1926, no. 1, p. 012016, May 2021, doi: 10.1088/1742-6596/1926/1/012016.

[5] R. Lukpanov, D. Dyussembinov, A. Altynbekova, Z. Zhantlessova, and A. Smoljaninov, "Study of the pore structure of foam concrete using a two-stage foaming method," *tbus*, vol. 3, no. 4, p. 0047, Dec. 2022, doi: 10.54355/tbus/3.4.2023.0047.

[6] R. Lukpanov, D. Dyussembinov, A. Altynbekova, Z. Zhantlesova, and T. Seidmarova, "Research of foam concrete quality by two-stage foam injection method in comparison with classical foam concrete," *tbus*, vol. 4, no. 1, p. 0052, Mar. 2024, doi: 10.54355/tbus/4.1.2024.0052.
[7] "GOST 10178-85 Portland cement and portland blastfurnace slag cement. Specifications," Moscow, Russia: IPK, 1985, p. 8.
[8] "GOST 31359-2007 Cellular autoclave curing concretes. Specifications," Moscow, Russia: MNTKS, 2007, p. 15.
[9] "GOST 10180-2012 Concretes. Methods for strength determination using reference specimens," Moscow, Russia, 2012, p. 36.
[10] "GOST 13087-2018 Concretes. Methods of abrasion test," Moscow, Russia: Standardinform, 2018, p. 16.

Information about authors:

Nurlan Bekkaliev – Master of Technical Sciences, PhD Student, Department of Technology of Industrial and Civil Engineering, L.N. Gumilyov Eurasian National University, Astana, Kazakhstan, nurlan_b-90@mail.ru
Yerlan Sabitov – Candidate of Technical Sciences, Associate Professor, Dean, Faculty of Architecture and Civil Engineering, L.N. Gumilyov Eurasian National University, Astana, Kazakhstan, sabitov_yeye@enu.kz

Author Contributions:

Nurlan Bekkaliev – concept, data collection, drafting, analysis, testing, interpretation.
Yerlan Sabitov – resources, methodology, editing.

Conflict of Interest: The authors declare that there is no conflict of interest.

Use of Artificial Intelligence (AI): The authors declare that AI was not used.

Received: 18.11.2025
Revised: 25.12.2025
Accepted: 29.12.2025
Published: 31.12.2025